Master's thesis

NTNU
Norwegian University of Science and Technology
Faculty of Natural Sciences
Department of Chemical Engineering

Susanna Sprauten Uhre

The Effect of the Absorber Design and Operating Conditions on the MEA Emissions and Energy Consumption in an Absorption-Based Carbon Capture Plant

Master's thesis in Industriell kjemi og bioteknologi
Supervisor: Hanna Knuutila
Co-supervisor: Juliana G. Monteiro
June 2021

NTNU
Kunnskap for en bedre verden

Susanna Sprauten Uhre

The Effect of the Absorber Design and Operating Conditions on the MEA Emissions and Energy Consumption in an Absorption-Based Carbon Capture Plant

Master's thesis in Industriell kjemi og bioteknologi
Supervisor: Hanna Knuutila
Co-supervisor: Juliana G. Monteiro
June 2021

Norwegian University of Science and Technology
Faculty of Natural Sciences
Department of Chemical Engineering

NTNU

Kunnskap for en bedre verden

I hereby declare that the work done in this thesis is independent and in accordance with the exam regulations of the Norwegian University of Science and Technology.

Trondheim, 07.06.2021

Susanna Sprauten Uhre

Preface

This thesis was written during the spring semester of 2021 as the final part of my master's degree at the Department of Chemical Engineering at the Norwegian University of Science and Technology.

First, I would like to express my gratitude to my supervisor, Professor Hanna Knuutila and my co-supervisor, Juliana G. Monteiro for all the valuable guidance and support throughout the semester. Their dedication for the subject have been truly inspiring and brought many interesting discussions along the way. I would also like to thank Professor Hallvard F. Svendsen for help with the mist model and all of his useful advice, and PhD Candidate Lucas Braakhuis for always finding time to help me and never growing tired of all my questions.

I would also like to thank my friends and fellow students for making these five years in Trondheim so memorable. Last, but not least, I would like to thank my family for their invaluable support and encouragement.

Abstract

Industry is one of the largest anthropogenic sources for greenhouse gas emissions. Absorption-based CO_2 capture is an important mitigation strategy to reduce the CO_2 emissions and provide a sustainable future. One of the main challenges of carbon capture is the high energy requirement of the process. Energy is required to regenerate the solvent, which results in high operating costs. Another challenge is emissions of the solvent, as it have a negative impact on the environment and human health.

The main objective of this thesis was to investigate how the absorber design and operating conditions affected the MEA emissions and energy consumption of an absorption-based carbon capture plant. The capture process was simulated in CO2SIM, where 30 wt% MEA was used as solvent. The model was validated with experimental data. The model gave a good prediction of the experimental data. Five parameter studies was set up. The aim was to evaluate how the dimensions of the absorber column, the liquid flow rate, mass-transfer and effective mass-transfer area impacted the pressure drop, gas-phase and aerosol MEA emissions, capture rate, loadings and the reboiler duty. An in-house MATLAB model, the mist model, was then used to investigate aerosol formation and growth in the absorber column and water wash.

It was found that at a constant gas and liquid flow rate, an increase in absorber column diameter resulted in a reduced pressure drop. The results also showed that the reboiler duty could be reduced by an increase in diameter at the expense of a larger liquid flow. A clear trade-off was found between the energy consumption and emissions. The gas-phase emissions can be decreased by increasing the absorber diameter. This will in return result in a larger reboiler

duty due to lower lean and rich loading. It was found that the capture rate could be adjusted by changing the absorber column dimensions. More CO_2 can be captured at the expense of a larger absorber column.

The aerosol number concentration had a large impact on the results. A high aerosol number concentration resulted in the highest emissions. The aerosol emissions could be reduced by increasing the height of the absorber column or by increasing the diameter of the water wash. A lower liquid flow also resulted in lower aerosol emissions. It was seen that an isotherm absorber column resulted in both lower emissions and a lower energy consumption.

Sammendrag

Industri er en av de største kildene til menneskeskapte utslipp av klimagasser. Absorpsjons-basert CO_2-fangst er et viktig skadebegrensningstiltak for å redusere CO_2 utslippene og sikre en bærekraftig fremtid. En av hovedutfordringene med karbonfangst er det høye energiforbruket i prosessen. Energi er nødvendig for å regenerere absorbenten. Dette vil resultere i høye driftsutgifter. En annen utfordring er utslipp av absorbenten, som vil ha en negativ effekt på miljøet og menneskers helse.

Hovedmålet med denne avhandlingen var å undersøke hvordan designet og driftsforholdene av absorberen påvirker MEA utslippet og energiforbruket i et absorpsjons-basert karbonfangstanlegg. Prosessen ble simulert i CO2SIM hvor 30 vekt-% MEA-løsning ble brukt. Modellen ble validert med eksperimentell data. Modellen ga god prediksjon av den eksperimentelle dataen. Fem parameterstudier ble satt opp. Målet var å evaluere hvordan dimensjonene av absorber kolonnen, væskestrømmen, masseoverføringsarealet og det effektive masseoverføringsarealet påvirket trykkfallet i kolonnen, MEA utslippet, fangstraten, loading og energiforbruket i reboileren. En intern MATLAB modell, mist modellen, ble brukt for å undersøke aerosol dannelse og vekst i absorber kolonnen og vannvasken.

Det ble funnet at ved konstant gass- og væskestrøm vil en økning i absorber diameter resultere i en reduksjon i trykkfallet. Resultatene viste også at energiforbruket i reboileren kan reduseres ved å øke diameteren på absorberen på bekostning av en større væskestrøm. Det ble funnet et klart kompromiss mellom energiforbruk og utslipp. Gassfase utslipp kan reduseres ved å øke absorber diameteren, i gjengjeld vil dette resultere i et høyere energiforbruk. Det ble funnet at fangstraten kan justeres ved å endre absorber kolonne dimensjonene. Det kan

fanges mer CO_2 på bekostning av en større kolonne.

Konsentrasjonen av aerosol antallet hadde en stor innvirkning på resultatene. Høyere konsentrasjon ga størst utslipp. Aerosol utslippene kunne reduseres ved å øke høyden til absorberen eller ved å øke diameteren til vannvasken. Mindre væskestrøm resulterte i lavere aerosol utslipp. Det ble funnet at en isoterm absorpsjonskolonne vil gi lavere utslipp, og et lavere energiforbruk.

Contents

List of Figures

List of Tables

List of Symbols

Symbol	Unit	Description
A	m^2	Area
a	m^2/m^3	Specific geometric area
a_h	m^2/m^3	Effective interfacial area
C_h	Dimensionless	Hydraulic factor
C_N	droplets/cm^3	Aerosol number concentration
C_{px}	kJ/kgK	Heat capacity
C_x	mole/l	Concentration
D	m	Diameter
D_x	m^2/s	Diffusivity
g	m/s^2	Gravity
h	m	Height
$h_g^{d/f}$	$kW/m^2 \cdot K$	Heat transfer coefficient droplet/fluid
h_L	Dimensionless	Liquid hold-up
k	$W/m \cdot K$	Thermal conductivity
L	kg/h	Solvent flow rate
$N_{CO_2,abs}$	kg/h	Absorption rate
N_{Fr}	Dimensionless	Froude number
N_{Re}	Dimensionless	Reynolds number

N_x	kmole/m^2·s	Flux of any component
P	kPa	Pressure
R	m	Radius
r_x	kmole/m^3s	Rate of reaction
T	°C	Temperature
V	kg/h	Vapour flow rate

α	mole CO_2/ mole MEA	Loading
ν	m/s	Velocity
μ	Pa·s	Viscosity
ρ	kg/m^3	Density

Abbreviations

CAPEX	Capital expense
CCS	Carbon capture and storage
GGH	Gas-Gas heater
GPDC	Generalized pressure drop correlation
MEA	Monoethanolamine
MSW	Municipal solid waste
NTNU	Norwegian University of Science and Technology
OPEX	Operating expense
PCC	Post-combustion capture
WESP	Wet Electrostatic precipitator
WtE	Waste-to-energy
WW	Water wash

Chapter 1

Introduction

1.1 Motivation

Over the last century the concentration of CO_2 in the atmosphere has reached concerningly high values. Scientists are more certain than ever that this is strongly linked to human activities[5]. Greenhouse gases are components in the atmosphere that absorb radiation and thereby heat up the earth. CO_2 has been proven to be the main component which contributes to the greenhouse effect and long term climate changes[6]. Many counties have come to the conclusion that greenhouse gases like CO_2 need to be reduced in order to have a sustainable future. The Paris Agreement was the first binding agreement that aimed to reduce the greenhouse gases and limit global warming to below 2 °C.[7]

Industry is one of the largest anthropogenic sources of greenhouse gas emissions. Aside from combustion of fossil fuels, waste storage and treatment is a main source of CO_2 emissions. Due to a growing population and increased living standards the amount of municipal solid waste (MSW) also increases. The World Bank reports that by 2050 the waste generation in the world is expected to increase by 70% from 2016. This means 3.40 billion tonnes of waste each year.[8] The majority of the waste is either landfilled or dumped. Both methods release greenhouse gases like CO_2 and methane, which is not sustainable.[9] A key solution to this problem is energy recovery from waste, also called waste-to-energy (WtE). The energy is

recovered in the form of heat and electricity.[10] The most common method is to burn the waste in a mass-burn combustion plant. There are also challenges to face with WtE. One of them being CO_2 emissions. This problem can be solved with post-combustion carbon capture (PCC).

The most common PCC method is to remove CO_2 by chemical absorption. The burned waste will result in a flue gas. This flue gas will enter an absorption column where the CO_2 is absorbed by a solvent. The process is reversible and is driven by a thermal-swing separation. The rich solvent that leaves the absorber after CO_2 has been absorbed is heated up to reverse the reaction. The CO_2 is then released in a stripper where it is taken out. One of the main challenges of the process is the high energy requirement during the regeneration of the solvent, which can result in high operational costs. Another challenge is the emissions of the solvent. A small amount of the solvent may be released to the atmosphere together with the cleaned flue gas due to the volatility of the solvent. The emissions can occur as gas-phase emissions, liquid droplets or as aerosols. Gas-phase emissions and liquid droplets can be removed by implementing a water wash or a demister. The aerosols are small, which makes them difficult to capture. The solvent itself or degradation products have a negative impact on the environment and human health.[11] It is therefore important to understand how aerosols are formed and how they behave in the process.

1.2 Scope and Objective of the Thesis

The main objective of this thesis is to investigate how the absorber design and operating conditions affect the monoethanolamine (MEA) emissions and energy consumption of an absorption-based carbon capture plant.

30wt% MEA is used as solvent. MEA is a commonly used solvent and is a benchmark for post-combustion carbon capture.[12] The capture process is simulated in CO2SIM, which is a dedicated simulation tool for absorption-based CO2 capture. The simulation model will be validated with experimental data.

CO2SIM does not take aerosol formation into account. Further modeling is therefore nec-

essary. The aerosol formation and growth will be evaluated by the mist model. This is a in-house MATLAB model that shows the growth of droplets as well as internal composition change with respect to the position of the column. It will be investigated how the aerosol number concentration, liquid flow, absorber column dimensions and water wash diameters will affect the total MEA emissions.

Five parameter studies will be set up. The first parameter study will be performed at constant gas and liquid flow rate, reboiler duty and lean and rich loading. This will be used to evaluate how the pressure drop and gas-phase emissions are affected by a change in diameter.

The second parameter study will be performed at a constant height and gas flow, but with varying liquid flow, reboiler duty and diameter. This gives the opportunity to investigate how the liquid flow affect the reboiler duty, loadings and gas-phase emissions at different diameters.

The third parameter study will be performed at constant mass-transfer area, while the fourth will be performed at constant effective mass-transfer area. The liquid flow rate will be varied to find what liquid-gas ratio gives the lowest reboiler duty. When the lowest reboiler duty is found the gas-phase emissions and loadings will be evaluated. The parameter studies will then be compared to see if there are certain absorber column dimensions that provide lower emissions and reboiler duty than others.

The fifth parameter study will be performed to evaluate how the column dimensions affect the capture rate. An attempt to simulate an isotherm absorption column will also be made. Gas-phase emissions are strongly dependent on temperature. An isotherm column could possibly reduce the emissions.

1.3 Outline of the Thesis

An introduction and motivation of the thesis is given in Chapter 1. Chapter 2 describe the basic theory behind carbon capture and amine-based absorption. This chapter also include description of some of the most important process parameters, the design parameters for an absorption columns and theory of mass transfer inside a column.

Chapter 3 looks into available literature concerning aerosol growth and formation. In addition, available data for flow rate in a water wash is included.

Chapter 4 present the modelling tools that will be used. The chapter also includes how the base case, case 1-18, the isotherm column and the parameter studies are set up. It contains a water wash sensitivity analysis and the method of finding the pressure drop. A summary of the results from the validation of the simulation model is also included.

The results and discussion are presented in Chapter 5. The final conclusion can be found in Chapter 6. This chapter also includes recommendations for future work. Supplementary information can be found in Appendix A, B and C.

Chapter 2

Theory

2.1 CO_2 Capture and Storage

Carbon capture and storage (CCS) is a process where the CO_2 is removed from fuel or flue gas. After the CO_2 is removed, it is compressed, transported and stored. CCS makes it possible to lower the emissions from industrial processes.[13] The storage can be both onshore and offshore in geological formations. In 2020 there were 65 commercial CCS facilities worldwide, with 26 currently operating. These facilities capture and store around 40 Mt of CO_2 per year.[14]

In traditional power stations, fuel or waste is burned in order to make energy. This results in a flue gas. The flue gas consist mainly of N_2, H_2O, O_2, CO_2 and minor components like SOx and NOx. Post-combustion carbon capture (PCC) is a well established technology based on capturing the CO_2 from the flue gas after the fuel is burned.[13] There are many different techniques that can be used in PCC. However, the only one commercially available is absorption-based CO_2-capture.

Figure 2.1 describes a typical absorption-based carbon capture facility. The flue gas enters the bottom of the absorber, which is typically a packed column. A packed column is filled with porous packing material. The purpose is to improve the contact area between the gas and liquid phase.[13] The cold lean absorbent flow enters the top section of the column. At

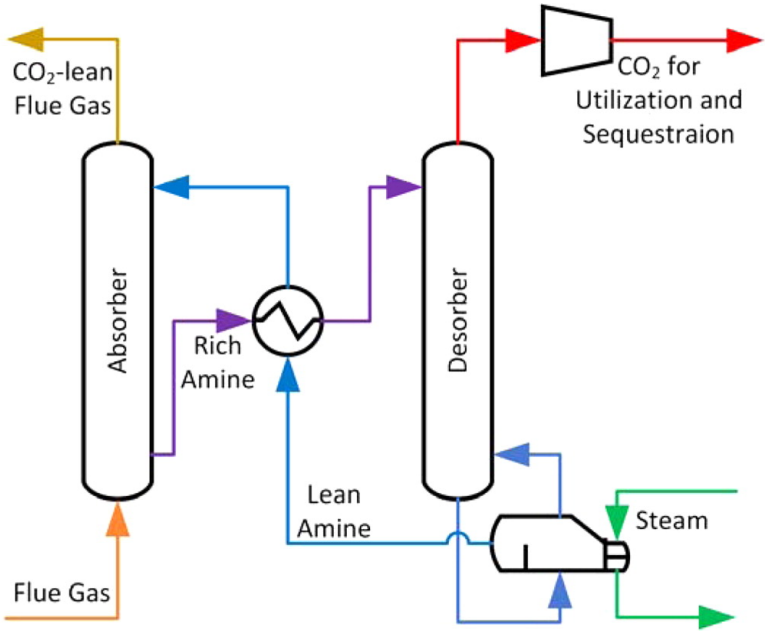

Figure 2.1: Typical absorption-based CO_2 capture facility[1]

this point, the absorbent is fresh and will absorb CO_2 in the gas. As the absorbent flows down the column, it will absorb an increasing amount of CO_2.[13] The rest of the cleaned gas mixture leaves the top of absorber. If the solvent is volatile, a small amount of solvent will be released to the atmosphere. A water wash can be placed on top of the absorber to reduce the emissions of solvent and volatile products.[15] This is usually also a packed column. Water is continuously recycled. The water will condense and absorb the volatile products.

The reactions between CO_2 and amine are reversible and driven by a thermal-swing separation. The solvent has a high affinity towards CO_2 at low temperatures and low affinity at high temperatures. The CO_2 is therefore absorbed by a cold amine. The CO_2-rich flow that leaves the bottom of the absorber is heated before it enters the desorber/stripper. The desorber is also commonly a packed bed. The heat will shift the equilibrium and CO_2 is released in the desorber.[13] The CO_2 is taken out at the top of the column. This stream can then be cooled down and stored. A reboiler is placed at the bottom of the desorber to regenerate the solvent. A fraction of the CO_2-lean stream is evaporated and re-enters the desorber. The rest of the lean stream is cooled down before it is sent back to the absorber.[13]

2.2 Implementation of CCS in the WtE Sector

Today, there are around 2,500 WtE plants operating around the world. These have the capacity to disposal approximately 400 million tons of waste per year.[16] There are different types of WtE systems and technologies. The most common and well established is the mass-burn combustion plant. These plants can burn waste with different composition and energy content.[17] The waste is biogenic and non-biogenic. The biogenic materials are plant-derived, so when incinerated the CO_2 that is produced will not lead to increased amount of atmospheric CO_2. Around 50-60% of the waste is usually biogenic, therefore, combined with CCS it can lead to negative emissions.[10]

The carbon capture plants for WtE plants are similar to those used for coal or gas-fired power stations. Less gas cleaning is required as the flue gas produced from MSW contain much less sulphur and less particulates are produced.[10] The WtE company AVR was the first to implement a large scale CO_2 capture facility. This have been operating since 2019, reducing the CO_2 emissions by 60,000 tonnes per year.[18] Twence in The Netherlands have a pilot plant where the plan is to capture 100,000 tonnes CO_2 per year by 2021.[10] Fortum in Norway is planning on implementing a full-scale capture plant to their WtE plant, which will capture 90% of the CO_2.[10]

2.3 Amine-Based Absorption

A number of different absorbents can be used in absorption-based post combustion CO_2 capture. Usually a chemical solvent is used to separate CO_2 from the other components in the gas.[13] The focus here will be on amine-based absorption, where CO_2 will react with an amine.

Amine-based absorption has high efficiency, mature technology and low cost.[19] Because of this, it has been shown to be a leading technology when it comes to carbon capture.[13] The desired properties of an amine are low volatility, high solubility and high selectivity for CO_2.[13] It is also desired that the amine has low propensity to degradate over time, high maximum loading, low lifetime cost and low enthalpy of absorption.[20]

The most commonly used absorbent is monoethanolamine (MEA). MEA has high affinity for CO_2 at low temperature, and low affinity at high temperatures, which makes it a good choice for a solvent[13]. It will also have a fast reaction with CO_2, which allows for smaller columns to be used in the absorption[19]. If the solvent reacts slow, taller columns are needed to capture the same amount of CO_2 because this would require a larger residence time. Other advantages include high capacity due to low molecular weight, and the fact that MEA is less volatile than many other amines. MEA is also relative inexpensive.[21] A disadvantage is that the limiting maximum loading is 0.5 mole CO_2 / mole MEA. It also have a high heat of reaction, which leads to high energy requirement in the reboiler. MEA is volatile and degradable, which means that fresh solution must be injected after some time and a water wash is needed to reduce the MEA emissions.[21]

Table 2.1: Reactions involved in absorption of CO_2 by MEA

Reaction	Stoichiometry
Water dissociation	$2\,H_2O \rightleftharpoons H_3O^+ + OH^-$
CO_2 hydrolysis	$CO_2 + 2\,H_2O \rightleftharpoons H_3O^+ + HCO_3{}^-$
Bicarbonate dissociation	$HCO_3{}^- + H_2O \rightleftharpoons H_3O^+ + CO_3{}^{2-}$
Carbamate hydrolysis	$MEACOO^- + H_2O \rightleftharpoons MEA + HCO_3{}^-$
Amine protonation	$MEA^+ + H_2O \rightleftharpoons MEA + H_3O^+$
Carbamate formation	$MEA + CO_2 + H_2O \longrightarrow MEACOO^- + H_3O^+$
Bicarbonate formation	$CO_2 + OH^- \longrightarrow HCO_3{}^-$

Table 2.1 shows the reactions involved in the absorption of CO_2 by MEA. MEA is not directly used in the water dissociation and CO_2 hydrolysis, but the presence of MEA in the solution might still influence their concentration. The protonation equilibria reactions are fast. Compared to these reactions the formation of carbamate (MEACOO-) and bicarbonate (HCO_3-) are slow. The carbonate formation reaction is the main mechanism to absorb CO_2.[13] MEA is a primary amine.[13]

The reaction between CO_2 and MEA is exothermic. Exothermic reactions will favor low temperatures in the absorption column and high temperatures in the desorption column to

reverse the reaction. When CO_2 is absorbed, heat is released.[21] The temperature in the absorber column will start to rise. The temperature is important as is has a direct influence on the reaction between CO_2 and MEA and the volatility of the compounds.[22]

2.4 Emissions from a PCC Plant

Solvent emission is one of the main challenges with absorption-based carbon capture. A small fraction of the solvent will be released to the atmosphere together with the cleaned flue gas. Loss of solvent will increase the operating cost of the plant and have a negative impact on the environment.[23]

In an amine-based CO_2-capture plant the emissions are typically in the form of the amine itself or degradation products. The degradation products can be ammonia, nitrosamines and nitramines.[24] It is possible to select an amine that does not form stable nitrosamines and nitramines in the capture process. However, these products can still be formed when the treated gas is released to the atmosphere.[24] These compounds pose a risk to human health as they can be highly carcinogenic.[11] Some countries have therefore proposed thresholds to how much amine emissions can be emitted.[25] The current threshold recommended for total nitrosamines and nitramines is 0.3 ng/m^3.[25][11]

The emissions can occur as liquid droplets, gas-phase emissions or as aerosols (mist). Droplets are large, and have typically a size above 10 μm. Gas-phase emissions depend on the volatility of the compound.[13] Volatility is temperature dependent. The gas-phase emissions are therefor highly affected by the temperature in the column.[26] MEA is a volatile compound, hence, emissions can occur in gas-phase. Aerosols are systems of particles suspended in gas[23]. Aerosols are small, and usually have a size below 2 μm. Liquid droplets can be removed by implementing a demister. The gas-phase emissions can be captured by implementing a water wash system. These are well established and understood methods.[13] The aerosol based emissions have in recent years been pointed out as a major problem. It is difficult to capture the aerosols due to their small size.[13] It has been reported that the amount of emissions from aerosols can be significant. Gas-phase emissions are typically in mg/Nm^3,

while aerosols emissions can be found in gram/Nm^3.[27]

Aerosols can be formed by spontaneous condensation or desublimation in a supersaturated gas-vapour mixture[23]. The system has to be supersaturated in order to form aerosols. The saturation has to exceed a critical barrier to reach nucleation and thus aerosol formation.[23] The aerosol formation can happen before the gas enters the absorber or in the absorber. In the absorber the liquid and the gas phases are in contact. Under ideal conditions there phases are commonly considered to be in thermodynamic equilibrium.[13] If an aerosol nuclei is present, this is considered to be a third phase. Volatile components in the gas phase can condense on the aerosol nuclei. The aerosols grow as they travel through the absorber by taking up condensed water, amine, and CO_2.[13]

There are several aspects that influence the aerosol emissions. The particle concentration can effect the emissions. Sulfuric acid or particulate matters like soot or ash can act as a nuclei in the aerosol formation.[23] The particle size distribution play an important role. The size and composition of the initial aerosol droplets have a large effect on the final size and composition. The reactivity of the amine and supersaturation have also been identified to have a large effect.[13]

2.5 Pressure Drop and Flooding

Pressure drop in the absorber column can be a significant factor for the operating cost, and therefore, important to consider when designing the column. A large pressure drop in the absorber column will require more energy for the fan that feeds the flue gas into the absorber, hence, the cost increases.[28]

Flooding is a condition that can occur if the gas or liquid flows are larger than the capacity of the column. It can be detrimental for the performance of the absorption. It is undesirable as it can lead to a large pressure drop in the column[29]. Flooding can be determined by changes in pressure or temperature differences[30]. This can be also be observed in the stripper. If flooding occur, the reboiled vapor can be hindered from rising, and the temperature at the bottom of the column will increase.[30] If the gas flow is held constant, an increase in the

liquid flow rate will lead to an increase in pressure drop. The pressure drop will increase until flooding occur. If flooding is achieved, the excess liquid will remain on top of the packing which can lead to the entire column being filled with liquid. This will increase the pressure drop even further.[29] Similarly, if the liquid flow is held constant, an increase in gas flow will also lead to an increase in pressure drop. When flooding occurs, the gas flow will hinder the liquid flowing downwards, and the liquid will accumulate at the top of the column. This will intensify the pressure drop even more.[29]

The gas velocity is important when determining the column diameter. The gas velocity in the absorber should promote good mixing between gas and liquid phase. A high gas velocity will provide a good contact between the gas and liquid, however, the resistance for the liquid flowing down in the column will increase. As a result, the pressure drop over the packing will be higher.[29] It should be a balance between good mixing and a low pressure drop when determining the gas velocity and column diameter. The gas velocity in an absorber column is typically in the range of 1-3 m/s.[28][31][32]

Liquid hold-up is defined as the volume of liquid contained per reactor volume[33]. It is common to use the void volume instead of the total volume of the reactor[33]. The hydrodynamic performance of the column is usually evaluated by both the pressure drop and the liquid hold-up[34]. Liquid hold-up will affect both the pressure drop and the mass-transfer inside the column. The liquid flowing through a column will wet the packing, leading to an improved mass-transfer. This will change the void fraction and bed structure causing a liquid-hold up. A liquid hold-up will in return increase the pressure drop.[35]

There are different methods of determining the pressure drop. In the literature, most of the pressure drops have been determined as the difference between outlet and inlet gas pressure, by simulating the process or by assumptions. Typical values for pressure drop in absorption columns are 0.2-1.2 kPa/m.[32][36][37][38][39]

2.6 Design of an Absorber Column

2.6.1 Dimensions of the Column

The capital expenditure (CAPEX) is one of the biggest cost contributions for CO_2 capture[32]. The column diameter and height are therefore important parameters to consider, together with the packing material. The column should be designed with a diameter large enough to avoid flooding.[40] Increasing the absorber diameter will reduce the gas velocity, and consequently the pressure drop. This is beneficial, as the operational expenses (OPEX) related to the pressure drop will be reduced.[32] However, a too large diameter will not favor the energy consumption.[40] The wetting of the packing can become too low at a large diameter, and the absorption will not be as effective. This would require high reboiler duty to achieve a high capture rate of CO_2. The diameter is usually specified to be at 70-80% of flooding[32]. The column diameter can be calculated when the maximum superficial gas velocity is determined[29]. The maximum superficial gas velocity depends on packing type.

In counter-current packed columns the fluids are in continuously contact through the column. This means that the liquid and gas composition will continuously change with the packing height.[40] Therefore, the amount of CO_2 absorbed strongly depend on the height of packing.

Columns are usually designed with the smallest diameter and lowest height possible to minimize the CAPEX.[41]

2.6.2 Energy Consumption in a CO_2 Capture Plant

A conventional CO_2 capture plant have two main energy sinks, which is represented in Figure 2.2. Heat is needed in the reboiler and stripper, while the compressor and circulation pumps require electrical energy.[2]

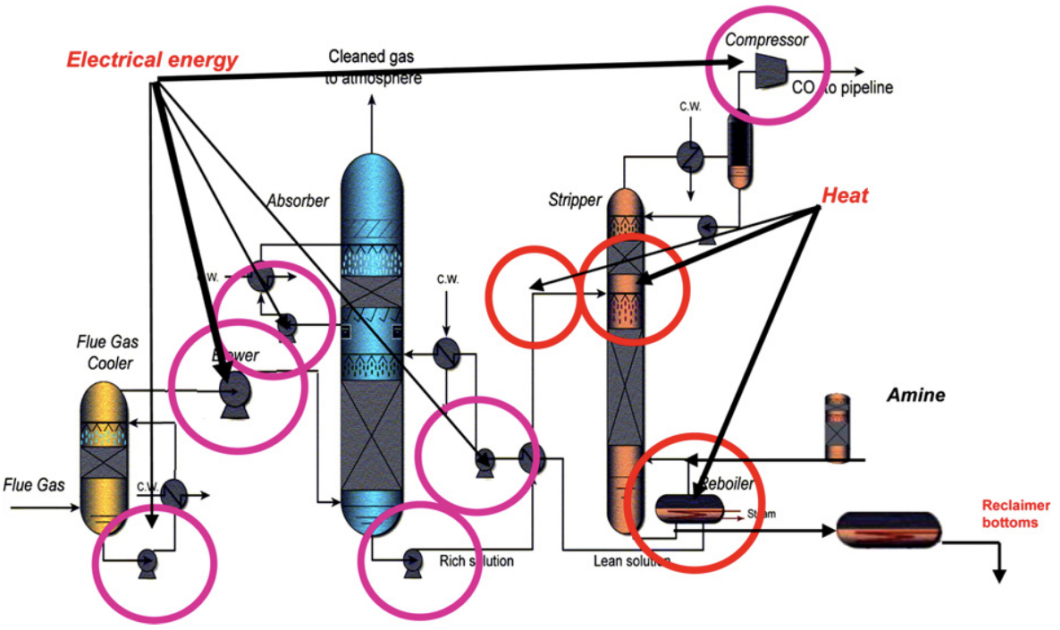

Figure 2.2: Energy sinks in a carbon capture plant[2]

The heat supplied to the reboiler has three different purposes[2]. The total heat requirement is the sum of the stripping heat, sensible heat and heat of desorption[42]. The reaction between CO_2 and amine is exotermic, and the heat required to reverse this reaction is the heat of desorption. Heat of desorption is dependent on the type of amine, and is therefore important to consider when choosing the absorbent.[42]

The CO_2-rich stream enters the stripper at the top section. As the solvent flows down, more CO_2 is stripped off. Heat is needed to generate vapour which will push the CO_2 up and out of the column. This heat is often referred to as the stripping heat.[2] This stripping heat is what maintain the driving force of the desorption. The driving force is the difference between the partial pressure of CO_2 in the gas phase ($p_{CO_2,gas}$) and the equilibrium partial pressure of CO_2, ($p_{CO_2,eq}$). Heat is also required to rise the temperature of the rich stream to the stripping temperature. The heat exchanger can not rise the temperature up to the reboiler temperature, and the temperature gap is refereed to as the sensible heat.

2.7 Column Internals

2.7.1 Packing Types

In an absorber column mass transfer occurs as a result of a chemical potential gradient between the gas and liquid phase. The separation is based on transferring one or more components from one phase to another. At the point where equilibrium is reached the mass transfer ends.[43] The rate the mass is transferred at is associated with the mass transfer coefficient.

The efficiency of the mass transfer is improved by contact devices like trays or packing.[44] Packed columns are typically preferred over tray towers as it offers a lower pressure drop and higher mass transfer.[29] The packing can be structured or random. Random packing have structural elements that are randomly dumped in a column.[44] Structured packings are typically made of metal sheets or wire mesh.[44] The main aspects to consider when choosing a packing type are the cost, pressure drop, corrosion resistance, specific area, design flexibility and structural strength.[29]

In this thesis a structural packing, Mellapak 250Y, will be used. This is made up of corrugated stainless steel sheets.[29] Structural packing are usually considered to be much more efficient than random packing. It offers lower pressure drop and a much more efficient mass transfer, however, at the expense of a higher cost.[44]

The column internals have a large impact on the efficiency and the size of the column.[41] The size of the column will determine the capacity and efficiency. With a structural packing a high capacity can be achieved with low surface area. This will in return give low absorption columns, but with a low efficiency. If a higher efficiency is desired, the surface area would have to be higher, and consequently result in much taller columns and a lower capacity. It is therefore a trade-off between capacity and efficiency.[41]

2.7.2 Effective Interfacial Area

The volumetric mass transfer coefficient will generally increase with increasing surface area[45]. However, there are other criteria to consider in order to achieve a higher mass transfer co-

efficient. The effective interfacial area is directly connected to mass and heat transfer rate between liquid and gas phase. It is therefore one of the most important parameters for determining the efficiency of the column and the absorption process.[29] The mass transfer area is also refereed to as the interfacial area.

The wetted surface area in the column is linked to the effective interfacial area. The mass transfer is only effective in the wetted area[46]. Unlike the definition of wetted area, the effective interfacial area does not only include the films on the packing surface but also the surface of drops and jets that flow through the voids of the packed bed.[29] [46]

Packing is said to have a specific geometric area (a) and an effective interfacial area (a_h). The effective interfacial area might in some cases be higher than the specific geometric area. This is a result of the droplets and jets in the free volume of the packing. The contribution of the effective area of these are then greater than its specific surface area.[29] A report from Wang et al. showed that a_h will increase with increasing liquid flow rate, and it is independent of the gas flow rate[47].

The specific geometric area is defined as

$$a = \frac{\text{interfacial area}}{\text{volume of packed bed}} \tag{2.1}$$

Equation 2.1 can be rewritten to find the interfacial area.

$$\text{interfacial area} = a \cdot \pi \cdot r^2 \cdot h \tag{2.2}$$

here r is the radius of the column and h is the height of the column.

Billet and Schultes developed expressions that can be used to find the effective interfacial area of a column.[3] This is calculated by

$$\frac{a_h}{a} = C_h \cdot N_{Re_L}^{0.15} \cdot N_{Fr_L}^{0.1} \qquad \text{for} \quad N_{Re_L} < 5 \tag{2.3}$$

$$\frac{a_h}{a} = 0.85 C_h \cdot N_{Re_L}^{0.25} \cdot N_{Fr_L}^{0.1} \quad \text{for} \quad N_{Re_L} \geq 5 \tag{2.4}$$

C_h is the hydraulic factor. This is a dimensionless factor specific for different packing types. N_{Re_L} is the liquid Reynolds number, and N_{Fr_L} is the liquid Froude number. These can be found by

$$N_{Re_L} = \frac{v_L \cdot \rho_L}{a \cdot \mu_L} \tag{2.5}$$

$$N_{Fr_L} = \frac{v_L^2 \cdot a}{g} \tag{2.6}$$

v_L is the liquid velocity, ρ_L is the liquid density, μ_L is the liquid viscosity and g is the gravity, which is 9.81 m/s^2. When the effective interfacial area, Reynolds number and Froude number have been found the liquid hold-up can be calculated. This is a dimensionless expression that was also developed by Billet and Schultes.[3]

$$h_L = \left(12\frac{N_{Fr_L}}{N_{Re_L}}\right)^{1/3} \cdot \left(\frac{a_h}{a}\right)^{2/3} \tag{2.7}$$

For Mellapak 250Y a_h is 250m^2/m^3 and C_h is 0.554.

Chapter 3

Literature Review

3.1 Aerosol Formation and Growth

The issue regarding aerosol-based emissions is a quite resent reported problem, and a field that needs more research. The papers that have been published are written with some different objectives. Most of the papers does not include all the data needed to simulate the process. The papers presented in this section will give some insight to the main findings of previous work regarding aerosol emissions. If available, the inlet composition and distribution are also included.

Majeed et al. (2017)[23] assessed the development of droplet size and composition by the use of a Matlab model. The droplet radius varied from 0.15-1.5μm with initial MEA concentration of 0.0001 M and 5 M. The focus was on internal characterization of the droplets, and no distribution or number concentrations were included. The article state that the droplet concentrations for small and larger droplets will become close to the bulk liquid phase. It also state that the initial size will influence the final size of the droplet.[23]

Majeed et al. (2017)[48] use the same Matlab model as the previous article to assess the droplet growth and internal composition. This article also includes the possible gas phase component depletion. Amine depletion in the gas phase can be created by aerosol formation and growth. Components in the gas will then be taken up by the aerosols. It is important, as gas phase amine depletion affect the aerosol droplet growth. The droplet radius varied from 0.15-1.5μm with initial MEA concentration of 0.0001 M and 5 M. The number concentration ranges from 1-10^7 droplets/cm^3. It was concluded that for large droplets (radius 1.5μm), with high number concentrations, gas phase depletion can occur. The depletion effect was seen to be strongest for the highest number concentration.[48]

Majeed et al. (2018)[49] modeled the development of a droplet through the absorber and a water wash. A droplet size distribution model was also developed. Two droplets were used with radii of 0.3 μm and 0.34 μm. The number concentrations used were 10^3, 10^5 and 10^7droplets/cm^3. The work showed that the flue gas CO_2 content affected the growth of the droplets as well as the outlet distribution. It was also found that an increased number concentration resulted in smaller droplets. Also here it was found that the depletion effect was strongest at the highest number concentrations.[49]

Majeed et al. (2018)[50] assessed the impact of initial CO_2 concentration and number concentration on the growth of the droplets. An inlet droplet size of 0.15 μm was used with the number concentration varying from 1-10^7 droplets/cm^3. It was found that the initial CO_2 content had a significant effect on the emissions. A higher CO_2 concentration in the inlet gas lead to higher emissions. This was because more carbamate was formed relative to free MEA. The water wash was then seen to be less effective, and the emissions increased. It was also found that the temperature profiles were unaffected by the number concentration and initial composition of the droplets. The water wash reduced the aerosol emissions significantly.[50]

Majeed et al. (2018)[51] assessed the impact of a water wash and demister on the aerosol composition and growth. The inlet droplet size used was 0.15 μm and 1.5 μm with the number concentrations varying between 1-10^7 droplets/cm^3. It was found that the water wash can be very effective when it comes to reducing the emissions from aerosols. The

aerosols enters the water wash with a significant amount of MEA, which is stripped out of the aerosols and removed by the water. The water wash section was also seen to have strong effect on the growth of the aerosols as water condense on the droplets. It was also found that if the droplets grow to a certain size, typically 3-8μm, implementing a demister can reduce the emissions.[51]

Mertens et al. (2016)[52] did not model the aerosol growth and development, but the size and number concentration were measured using an ELPI$^+$ device. This article show that aerosol formation can be prevented by removing the nuclei from a flue gas with a WESP. This method will only work if the flue gas does not contain any SO_2.[52]

Lombardo et al. (2016)[53] measured the aerosol and MEA emissions by the use of an ELPI$^+$ device. It was found that there was a strong relation between flue gas particle content, like sulfuric acid and dust, and the MEA aerosol emissions.

3.2 Water wash Section

A number of papers have been published where a water wash section have been included in the CO_2 capture process. The simulations in this thesis, excluding the validation of experimental data, were all performed with a water wash on top of the absorber. Adding a carbon capture system to a WtE-plant will generally increase the water use. A part of this water use is the make up water in the water wash.[54]

The water wash have a liquid water circulation flow. Some of the water is produced by condensation of the bottom liquid stream leaving the water wash. In a large number of the papers that have been published there is a lack of data regarding how big the liquid circulation flow usually is. This section present some of the articles that were found which includes the data for the water wash.

Kang et al. (2017)[55] have modeled aerosol growth in an absorber and water wash. It was reported that the water wash use the same L/G ratio as the absorber, which was 5.3 (mole/mole)

Madeddu et al. (2019)[56] report that the solvent flow used into the water wash was the water that was recovered in the stripper condenser

Notz et al. (2011)[57] report that the solvent flow used in the water wash was the condensed stream from the bottom of the water wash. Some fresh make-up water was added to avoid accumulation of amine in the water wash

Stec et al. (2015)[58] this article does not specify how large the liquid flow into the water flow was. It does mentions that a small flow of make-up water should be added into the water wash to avoid accumulation of MEA.

Chapter 4

Method

4.1 Modelling Tools

Two modelling tools were used, CO2SIM and the mist model. CO2SIM was used to model the absorber, stripper and water wash. The mist model was used to model the absorber and water wash. A demister was used in the mist model. This was a model of the Koch-Glitch demister, with a height of 15cm, a 200m^2m^{-3} surface, and 0.3mm wire thickness.

4.1.1 CO2SIM

CO2SIM is a flexible simulation tool used to solve processes related to CO_2-capture[59]. The software contains models which make detailed simulations of the thermodynamic vapour-liquid equilibrium, reaction kinetics and transport properties[59]. The equilibrium model used in this thesis was the e-NRTL model.

As mentioned, CO2SIM was used to simulate the absorber, stripper and water wash. The results from the simulations were the vapour and liquid phase compositions and temperature profiles in the columns. The vapour phase was used to investigate the MEA emissions in the gas phase. Aerosol formation and growth are not taken into account in CO2SIM. Further modeling was therefore necessary. This was done using the mist model.

4.1.2 Mist Model

The mist model is a MATLAB model used to describe aerosol formation and growth. The model shows how a droplet will grow or shrink as a result of mass transfer, as well as internal composition change with respect to the position in the column.[50]

The basis of the model is the liquid phase profiles for the MEA concentration, loading and temperature in the absorber and water wash from the CO2SIM simulation. The model also requires characterization of the inlet droplet composition, size and distribution.[50] The model is based on a system of equations. This includes differential balances for mass and energy inside an aerosol droplet and the gas phase. An equilibrium model and a kinetic model are also implemented.[48] The equilibrium model used was the e-NRTL model. Detailed description of the mist model has been published by Majeet et al. ([50],[48],[23]).

Several assumptions were made when developing the model. It was assumed that the liquid phase composition and temperature would not be affected by the aerosols. The assumption is based on the fact that the liquid phase have a much larger volume than the aerosol phase.[48] It was also assumed that the droplet size distribution could be modelled by a log-normal distribution. The model does not take into account breakage of droplets. The droplets are very small, and breakage of such small droplets would require very high energy. It was also assumed that coalescence is unlikely. The particles mainly follow the gas, and collisions are therefore unlikely.[50] Lastly, it was assumed that no reaction will take place in the gas phase.

$$\frac{\partial \mathrm{C}_x}{\partial \mathrm{t}} = \left(\frac{\mathrm{D}_x}{\mathrm{R}^2} \times \left[\left(\frac{2}{\xi} \cdot \frac{\partial \mathrm{C}_x}{\partial \xi} \right) + \frac{\partial^2 \mathrm{C}_x}{\partial \xi^2} \right] - \mathrm{r}_x \right) - \frac{3 \cdot \mathrm{C}_x}{\xi} \cdot \frac{\partial \xi}{\partial \mathrm{t}} \tag{4.1}$$

Equation 4.1 shows the concentration profile for the droplet phase. C_x is the concentration for any component x. r_x is the reaction rate, R is the droplet radius, D_x is the diffusivity, while ξ represent the dimensionless internal composition.[23]

$$\frac{\partial \mathrm{T}}{\partial \mathrm{t}} = \left(\frac{\mathrm{k}}{\rho_x \cdot \mathrm{C}_{\mathrm{p}x} \cdot \mathrm{R}^2} \times \left[\left(\frac{2}{\xi} \cdot \frac{\partial \mathrm{T}}{\partial \xi} \right) + \frac{\partial^2 \partial \mathrm{T}}{\partial \xi^2} \right] + \mathrm{r}_x \times \left(\frac{\Delta \mathrm{H}}{\rho_x \cdot \mathrm{C}_{\mathrm{p}x}} \right) \right) \tag{4.2}$$

Equation 4.2 shows the temperature profile for the droplet. The temperature is shown as T, ρ

is the density, C_p is the heat capacity, while k represent the thermal conductivity.[23].

The composition profile for the gas phase is calculated by

$$\frac{\partial n_x^g}{\partial t} = \dot{n}_x^f - \dot{n}_x^d \tag{4.3}$$

Here n is the number of moles in the gas volume, while $\dot{n}$ is the molar flow. f and d represent the bulk fluid and droplet respectively.[48]

The temperature profile for the gas phase is found by

$$\rho_g \cdot V_g \cdot C_p \frac{\partial T_g}{\partial t} = h_{lg}^f (T_f - T_g) - h_g^d (T_g - T_d) \tag{4.4}$$

Here, V_g is the gas volume, h_{lg}^f and h_g^d represent the bulk liquid side and droplet side heat transfer coefficient respectively. T_f is the bulk fluid temperature, T_g is the gas temperature, and T_d the droplet surface temperature.[48] Boundary conditions and solution procedures can be found in Majeed et al. (2017)[23],[48].

The results from the mist model show the size distribution. The size distribution is described by a log-normal distribution

$$f(R) = \frac{1}{R\sigma\sqrt{2\pi}} \exp\left(- \frac{(\ln R - \mu)^2}{2\sigma^2} \right) \tag{4.5}$$

Function 4.5 have two moments, σ and μ. The two moments are linked to two different droplets radii. The results of the model represent these moments as droplets, and show the development in size and concentration through the columns. Equations 4.6 and 4.7 show how the two moments are linked to the droplet radii.

$$\sigma = \sqrt{\ln \frac{\overline{R_2}}{\overline{R_1}}} \tag{4.6}$$

$$\mu = \ln \overline{R_1} - \frac{1}{2} \ln \frac{\overline{R_2}}{\overline{R_1}} \tag{4.7}$$

$$\frac{d\overline{R_1}}{dt} = \left\langle \frac{dR}{dt} \right\rangle = \langle \tilde{N}_1 \rangle = \tilde{N}_1 \tag{4.8}$$

$$\frac{d\overline{R_2}}{dt} = \frac{2}{\overline{R_1}} \langle R\tilde{N}_2 \rangle - \frac{\overline{R_2}}{\overline{R_1}} \langle \tilde{N}_1 \rangle = \frac{2}{\overline{R_1}} \tilde{N}_2 \langle R \rangle - \frac{\overline{R_2}}{\overline{R_1}} \tilde{N}_1 \tag{4.9}$$

The change in radius for droplet 1 and 2 with respect to time is calculated by equation 4.8 and 4.9 respectively. Here $\tilde{N}$ represents the volumetric flux into the droplet.

4.2 Validation of Simulation Model

A project was done during fall 2020, in the subject TKP4580 which is a preparation project for the master thesis. The project contained simulations of MEA emissions in an absorption-based CO_2 capture plant. CO2SIM was used as a simulation tool. In order to evaluate if the simulation model gave an accurate prediction, a validation was done with experimental data from Notz et al.[4]. The campaign was carried out by performing 47 experiments. These experiments were simulated in CO2SIM. The absorber and desorber were simulated separately. A detailed description of the pilot plant can be found in Appendix A. Appendix A also include a summery of the results from the validation.

In order to predict the accuracy of the simulation model, the percentage deviation in absorption and desorption rate between simulation and experimental data was found. The lean loading, rich loading and composition in each stream were also compared, together with the temperature profiles in the columns.

The validation showed that the absorber simulation both under- and over-predicted the temperature in the absorber and the absorption rate. Nothing stood out as a reason for this prediction. All deviations were under 20%, and it was decided that the simulation model of the absorber column gave reasonable results. The simulation results of the temperature in the desorber and the desorption rate were all under-predicted. Also here nothing stood out as the reason for this prediction. It was concluded that the deviations between simulated data and experimental data were acceptable, and that the model could be used for further modeling.

4.3 Defining a Base Case

The objective of this thesis was to investigate the MEA emissions in a full scale WtE-plant. Currently, there are no data available for sizing of a full-scale carbon-capture plants that capture CO_2 from a waste-to-energy plant. Due to lack of experimental data and data for sizing of the equipment some assumptions had to be made regarding the size of stripper and water wash. An e-NRTL rate based model with 30 wt% MEA as solvent was used as a basis for the simulations.

The flue gas composition and operating conditions used in the base case were gathered from in-house data. The flue gas consisted of 15.8 wt% CO_2, with a gas flow rate of $48\,\mathrm{kg\,s^{-1}}$. It enters the absorber column at 40°C at 105kPa.

There was no in-house or published data for the lean solvent liquid flow into the absorber. The composition was therefore calculated based on 30 wt% MEA and a desired lean loading of 0.19 $^{\text{mole CO}_2}/_{\text{mole MEA}}$. The lean solvent flow rate was calculated by

$$\mathrm{L} = \frac{\mathrm{N}_{CO_2,abs}}{\mathrm{C}_{MEA} \cdot (\alpha_{rich} - \alpha_{lean})} \tag{4.10}$$

L is the lean solvent flow in $\mathrm{kg\,h^{-1}}$, $\mathrm{N}_{CO_2,abs}$ is the absorption rate of CO_2, C_{MEA} is the molarity of MEA while α_{rich} and α_{lean} is the rich and lean loading. The rich loading was set to be 0.49 $^{\text{mole CO}_2}/_{\text{mole MEA}}$, and the capture rate was set to be 90%. A summery of lean solvent and flue gas flow can be found in Table 4.1

Table 4.1: Composition , total flow, temperature and pressure for flue gas and lean solvent flow in base case

Stream	H_2O [wt%]	CO_2 [wt%]	MEA [wt%]	O_2 [wt%]	N_2 [wt%]	Total flow [$\mathrm{kg\,s^{-1}}$]	T °C	P kPa
Flue gas	4.4	15.8	0	8.6	71.3	48.04	40	105
Lean flow	63.3	4.5	32.3	0	0	101.27	40	105

The superficial gas velocity had to be decided in order to calculate the diameter of the base case absorber column. Section 2.5 explained that the gas velocity in an absorber column is typically in the range 1-3 m/s. A superficial gas velocity of 2 m/s was therefore chosen. The column area is a function of the gas flow rate and the maximum velocity as shown in equation 4.11. A is the area, $\dot{V}_g$ is the gas flow rate, and v_g is the superficial gas velocity.

$$A = \frac{\dot{V}_g}{v_g} \tag{4.11}$$

Equation 4.11 can be rewritten to calculate the diameter (D) of the column. This is shown in equation 4.12.

$$D = \sqrt{\frac{4 \cdot \dot{V}_g}{\pi \cdot v_g}} \tag{4.12}$$

At a gas velocity of 2m/s the diameter of the absorber column was found to be 5.0m. It was decided that the base case should capture 90% CO_2. The height of the absorber column was adjusted until the wanted capture rate was achieved. The absorber was found to capture 90% CO_2 at a 25m height. The stripper was assumed to have a height of 15.0m, with 4.0m in diameter. The water wash was set to have a height of 3.0m with the same diameter as the absorber, 5.0m. There was also a lack of data considering the water wash specifications. It was therefore decided to use the same L/G ratio as the absorber column and add some make-up water to avoid amine build-up. The liquid flow rate into the water wash was 80 $\mathrm{kg\,s^{-1}}$.

Figure 4.1 shows the flow sheet from the simulation in CO2SIM. The flue gas enters the bottom of the absorber. The lean solvent is fed at the top of the absorber. The gas flow from the top of the absorber, P11, enters the bottom of the water wash. A small part of the bottom stream from the water wash is sent back to the absorber, while the rest is cooled down and recycled. Some fresh make-up water was added from stream P17 to the recycled water. The treated gas leaves the top of the water wash. The CO_2-rich stream leaves the bottom of the absorber and is heated in a flash. Typically a heat exchanger is used to heat up the rich flow and cool down the lean flow. This gave some simulation issues, so two flash tanks

were used instead. The warm rich liquid flow enters the top of the stripper, while the vapour from the flash is sent to a mixer together with the clean top stream of the stripper. The CO_2 is condensed, before it is taken out. The CO_2-lean flow leaves the bottom of the stripper. Part of the stream is evaporated in the reboiler and sent back to the stripper, while the rest of the stream is cooled down in a flash before it is sent back to the absorber. Control blocks were placed before the absorber and water wash liquid flow inlet. This was done to make it possible to keep the flow rates constant.

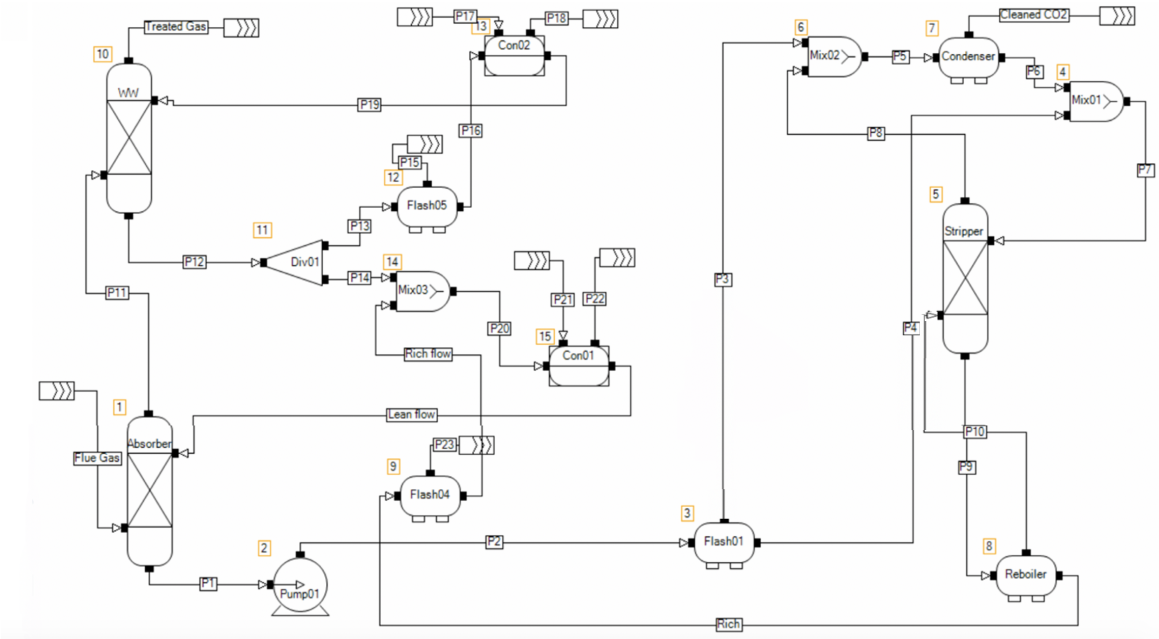

Figure 4.1: Flow sheet from the CO2SIM simulation of the absorber, water wash and stripper

4.4 Water wash Sensitivity Analysis

Water wash systems have usually been implemented to control the gas-phase emissions, but it has been reported to have an effect on aerosol emissions as well[51]. The operating conditions of the water wash have a significant effect on the emissions. A sensitivity analysis was performed in order to decide the operating parameters of the water wash.

First, the liquid flow entering the water wash was adjusted. The flow rate varied from $73.9\,\mathrm{kg\,s^{-1}}$ to $455.8\,\mathrm{kg\,s^{-1}}$. $73.9\,\mathrm{kg\,s^{-1}}$ was the lowest possible flow rate that could be used,

as the system would not converge at a lower flow rate. CO2SIM require a certain amount of MEA in the liquid flow into the water wash. The weight percentage of MEA was set to be constant at 1.31 wt%. It was found that the MEA vapour-phase emissions were highest at the lowest flow rate with 7.03ppm MEA. The emissions decreased as the flow rate increased. The vapour-phase emissions stabilized at a liquid flow of 202.6kg s^{-1}, with MEA emissions of 2.6ppm. Increasing the liquid flow even further did not decrease the emissions. The results can be found in Table B.1 in Appendix B. The emissions decreased quite a lot, from 7.03ppm to 2.6ppm. This required almost 3 times as much liquid as the lowest liquid flow possible. Even though the emissions decreased this will increase the cost of the plant as the energy requirement of the circulation pump and cooling of water will increase.

The amine concentration was then varied while the liquid flow was kept constant to investigate how it effected the vapour-phase emissions. The liquid flow was set to be 80.2kg s^{-1}, while the weight percentage of MEA varied from 0.54-1.83 wt%. The system would not converge at a lower weight fraction. It was found that the amine emissions increased from 3.2ppm to 9.4ppm with increasing amount of MEA. The emissions increased in a almost linear manner, and there was not one specific point where the emissions started to increase very fast. The results can be found in Table B.2 in Appendix B. It should also be mentioned that these are very low concentrations, and the model might not be as precise in this range.

The lowest liquid flow that could be used was 73.9kg s^{-1}. It was decided to add a small amount of fresh make-up water and use a liquid flow of 80.2kg s^{-1} in the further simulations. The weight percentage of MEA was set to be 1.31 wt%, which is approximately the middle point of the the varied MEA fractions. It was then decided that the water wash should have the same operating parameters and dimensions in all further simulations. That gives the opportunity to investigate more of the effect of the water wash. What goes into the water wash from the absorber might be different depending on the simulated case, but what happens in the water wash will be the same every time. The height of the water wash was set to 3.0m, with a 5.0m diameter. The height, diameter, liquid flow rate and MEA concentration will be constant unless something else is specified.

4.5 Defining the Cases and Parameter Studies

The parameters that were studied was the absorber column dimensions, mass transfer area, effective mass transfer area and liquid flow rate. The objective was to see the effect these parameters had on the pressure drop, MEA emissions, capture rate, reboiler duty and lean and rich loading. Five parameter studies were set up where the absorber column dimensions varied.

The base case was defined in Section 4.3. The absorber column had a 25.0m height with 5.0m diameter. It was decided all parameter studies should have cases were the diameter varied. All parameter studies had 5 cases with absorber column diameters that were 5.0m, 5.5m, 6.0m, 6.5m and 7.0m.

Parameter study 1 was set up to investigate the pressure drop and MEA emissions. In this study the liquid and gas flow rate were kept constant. As already mentioned in Section 4.3, the base case was set up with a lean loading of 0.19 $^{\text{mole CO}_2}/_{\text{mole MEA}}$ and a rich loading of 0.49 $^{\text{mole CO}_2}/_{\text{mole MEA}}$. As the diameter of the column in parameter study 1 increased, the height was adjusted to get the same lean and rich loading as the base case. Section 4.6 explain how the pressure drop was found.

Parameter study 2 was set up to investigate how the MEA emissions, reboiler duty, lean and rich loading were effected by increasing the diameter and varying the liquid flow rate. The same range of diameters for the absorber column were used. The base case with 5.0m in diameter was used as a starting point. The height of the base case was then adjusted to find the height that captured 90% CO_2, with the lowest reboiler duty. This height was found to be 21.5m. This height was then kept constant for the other cases where the diameter increased. The gas flow rate was also kept constant. The liquid flow rate was varied, and reboiler duty was adjusted until 90% CO_2 was captured. This was done to find the liquid-gas ratio that gave the lowest reboiler duty at a 90% capture rate.

Parameter study 3 was set up to investigate how the MEA emissions, reboiler duty, lean and rich loading were effected at a constant mass transfer area. Section 2.7.2 explains how the interfacial area can be found. The interfacial area depends on the specific geometric area of the packing. The simulations were performed with Mellapak 250Y, which have a specific area of 250 m^2/m^3 [3]. The height of each case was than calculated by Equation 4.13.

$$h = \frac{\text{interfacial area}}{a \cdot \pi \cdot r^2} \tag{4.13}$$

Where h is the packing height, a is the specific area and r is the radius of the absorber. The gas flow rate was kept constant. The liquid flow rate was varied, and the reboiler duty was adjusted to find the L/G ratio that gave the lowest reboiler duty at 90% capture rate.

Parameter study 4 was set up to investigate how the MEA emissions, reboiler duty, lean and rich loading were effected at a constant effective mass transfer area. Section 2.7.2 explains how the effective mass transfer area was found. The effective area was kept constant, while the diameters changed. The height for each case was calculated by Equation 4.14, where a_h is the effective area. The liquid flow rate was then varied at a constant gas flow rate, and the reboiler was adjusted to capture 90% CO_2.

$$h = \frac{\text{interfacial area}}{a_h \cdot \pi \cdot r^2} \tag{4.14}$$

It has now been explained how each case was set up for parameter study 1-4, and how the diameter, height and L/G ratio was found. A summery of this can be found in Table 4.2. The table shows which diameters were used, how the height and L/G ratio varied and the variation in loadings.

Table 4.2: Parameter study 1-4 with variations in column dimensions, L/G ratio and lean and rich loadings

	Study 1	**Study 2**	**Study 3**	**Study 4**
Diameter	5.0m, 5.5m, 6.0m, 6.5m, 7.0m	5.0m, 5.5m, 6.0m, 6.5m, 7.0m	5.0m, 5.5m, 6.0m, 6.5m, 7.0m	5.0m, 5.5m, 6.0m, 6.5m, 7.0m
Height	Adjusted to get same lean and rich loading	Constant at 21.5m	Calculated to get same mass transfer area	Calculated to get same effective mass transfer area
L/G	Constant at 2.11 kg/kg	Find L/G that gives the lowest reboiler duty	Find L/G that gives the lowest reboiler duty	Find L/G that gives the lowest reboiler duty
Lean and rich loadings	$\alpha_{\text{Lean}} = 0.19$ $^{\text{moleCO}_2}/_{\text{mole MEA}}$, $\alpha_{\text{Rich}} = 0.49$ $^{\text{moleCO}_2}/_{\text{mole MEA}}$	Result of simulation	Result of simulation	Result of simulation

Parameter study 5 was set up to investigate how the capture rate was effected by changing the absorber column dimensions. 9 cases were set up. For the first five cases the height was set to be constant at 21.5m, with the diameter varying from 5.0m to 7.0m. The mass transfer area for the column with 5m in diameter and 21.5m in height was calculated. This mass transfer area was then constant in the next four cases. The next four cases was set up with the diameter 5.5m, 6.0m, 6.5m and 7.0m. The height was calculated like in parameter study 3. The liquid and gas flow rate was set to be constant with a L/G ratio of 1.81 kg/kg. The reboiler duty was set to be constant at 73.6 $\text{GJ}\,\text{h}^{-1}$. The capture rate was then found.

4.6 Finding the Pressure Drop

There are different methods to find the pressure drop in a packed column. There are theoretical models as well as published correlations for different packing types. The packing used in these simulations were Mellapak 250Y from Sulzer. Sulzer report that the pressure drop can be found by the use of generalized pressure drop correlations (GPDC) with an accuracy of 20%.[60] Sulzer also provide pressure drop correlations for Mellapak 250Y, but these are dependent on the head pressure, which was out of range of the head pressure used in this thesis. A generalized pressure drop correlation was therefore used. This GPDC chart was developed by Leva, and is shown in Figure 4.2.[3]

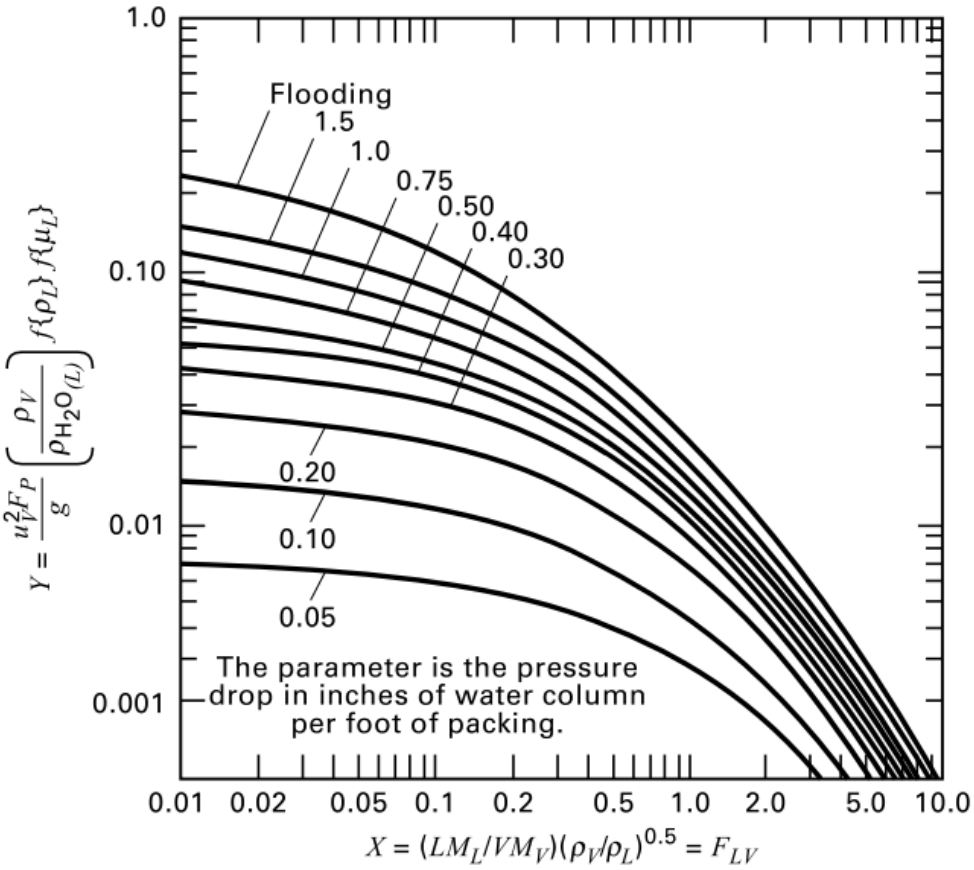

Figure 4.2: Generalized pressure drop correlation of Leva for packed columns[3]

F_{LV} is the liquid-to-gas kinetic-energy ratio which is calculated by

$$F_{LV} = \frac{LM_L}{VM_V} \cdot \left(\frac{\rho_V}{\rho_L}\right)^{0.5} \tag{4.15}$$

Where L is the liquid flow rate, V is the vapour flow rate, M_L and M_V is the total molar mass for liquid and vapour. ρ_L and ρ_V is the liquid and vapour density.

The pressure drop is found by calculating the F_{LV}, and finding the Y coordinate at flooding ($Y_{Flooding}$). The degree of flooding then have to be chosen to find the Y coordinate at that point. It was assumed to be 70% flooding in the column, as it is typical to operate in this region[3]. The Y coordinate at 70% flooding is then calculated by

$$Y_{70} = 0.70^2 \cdot Y_{Flooding} \tag{4.16}$$

The pressure drop is then found by locating the point at the x-axis that correspond to Y_{70} and the 70% flooding line. The pressure drop is given in inches H_2O/ft.

4.7 Investigation of Aerosol Emissions

As mentioned, the mist model was used to investigate the aerosol emissions, as CO2SIM only provide the gas-phase amine emissions. Also here there was a lack of data considering the inlet droplet composition, size and distribution. Therefore, assumptions had to be made. Literature sources as described in Section 3.1 provided inlet data that have been used previously. Similar inlet data were therefore used in these investigations. It was assumed that the inlet droplet had a sulfuric acid (H_2SO_4) concentration of 0.2 molL^{-1}, and a inlet gas water partial pressure of 5 kPa.

The inlet droplet distribution was characterized by two droplet sizes in the distribution model. The two droplets were 0.095 µm and 1.2 µm. Two number concentrations were used, 1.17· 10^7 droplets/cm^3 and 5.00· 10^7 droplets/cm^3. The inlet distribution of the aerosol model is important. The two droplet diameters will change in the column because of transfer of CO_2, water and MEA. The diameters to which the droplets have grown to at the top of the water

wash are what then forms the outlet distribution. The inlet distribution is shown in Figure 4.3.

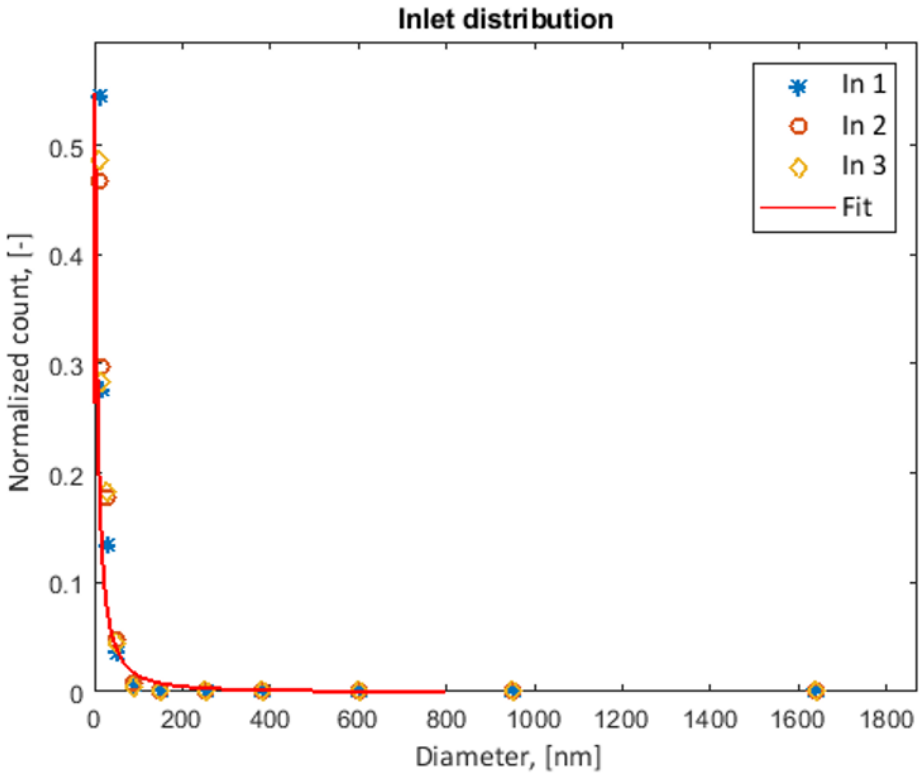

Figure 4.3: Inlet distribution used in aerosol modelling with the mist model

4.8 Isotherm Absorption Column

The amine composition in the gas phase along the column is strongly dependent on the temperature. CO_2 absorption with MEA favors low temperatures. It was therefore attempted to create an isotherm absorption column to investigate how it would affect both the gas-phase and aerosol emissions. An isotherm column is a column where the temperature is constant. It is not possible to create an isotherm column in CO2SIM. The absorption column was therefore divided into several sections, with intercooling in between. The intercooling push the temperature down after each column section, which prevent the temperature to rise as much as it would normally do.

The lowest absorber height from parameter study 4 was chosen. The absorber column was

4.36m tall, with a diameter of 7.0m. The column was then divided into 9, where each section was 0.484m tall. Figure 4.4 shows the flow sheet of the CO2SIM simulation.

The absorber columns is labeled Abs. The flue gas enters the bottom of the lowest absorber column, Abs 9. The lean flow enters the top of the top absorber column, Abs 1. The rich flow from the bottom of Abs 1 is taken out, cooled down to 40°C, before it enters the next absorber column. This procedure is repeated until the rich flow leaves Abs 9. The rich flow is then heated before it enters the stripper column. The rest of the system is the same as the base case, which was explained in Section 4.3.

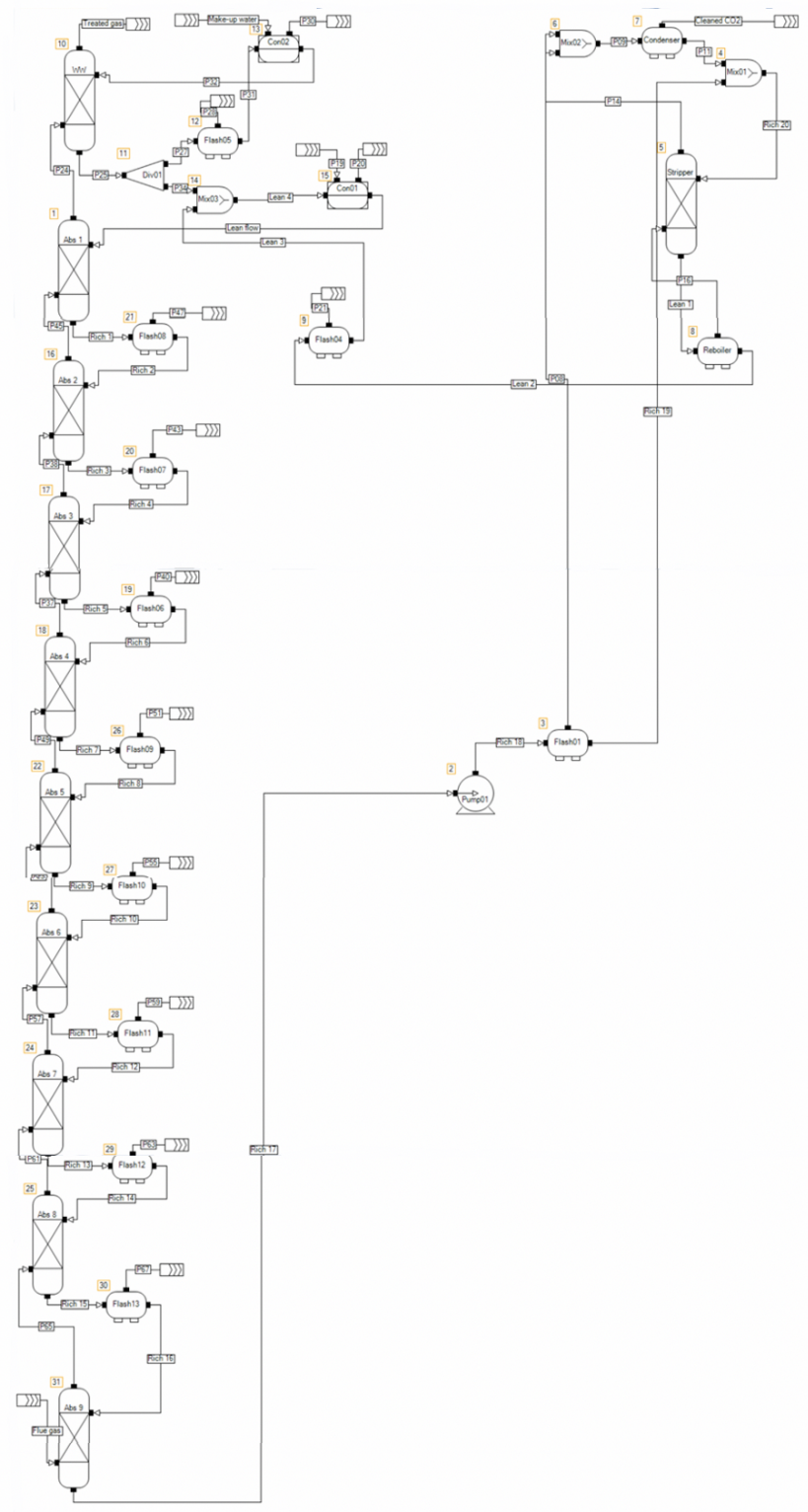

Figure 4.4: Flow sheet from the CO2SIM simulation of the isotherm absorber column with the water wash and stripper

Chapter 5

Results and Discussion

A summery of the different cases used in the five parameter studies with absorber column dimensions, capture rate, lean and rich loading, and liquid-gas ratio is shown in Table 5.1. Additional data can be found in Appendix C.3

Table 5.1: The different cases used in the parameter studies simulated in CO2SIM with corresponding diameter and height of absorber, lean and rich loading, L/G and capture rate

	Diameter [m]	Height [m]	Capture rate [%]	α_{Lean} $[\frac{\text{mole } CO_2}{\text{mole MEA}}]$	α_{Rich} $[\frac{\text{mole } CO_2}{\text{mole MEA}}]$	L/G $[\frac{\text{kg}}{\text{kg}}]$
Base case	5.0	25.0	90.0	0.19	0.49	2.11
Case 1	5.5	22.3	90.0	0.19	0.49	2.11
Case 2	6.0	20.6	90.0	0.19	0.49	2.11
Case 3	6.5	19.0	90	0.19	0.49	2.11
Case 4	7.0	17.6	90	0.19	0.49	2.11
Case 5	5.0	21.5	90.0	0.23	0.48	2.45
Case 6	5.5	21.5	90.0	0.23	0.48	2.53
Case 7	6.0	21.5	90.0	0.24	0.48	2.60
Case 8	6.5	21.5	90.0	0.25	0.48	2.66
Case 9	7.0	21.5	90.0	0.25	0.48	2.67
Case 5b	5.0	21.5	87.4	0.16	0.49	1.81

Case 6b	5.5	21.5	87.9	0.16	0.49	1.81
Case 7b	6.0	21.5	88.4	0.16	0.49	1.81
Case 8b	6.5	21.5	88.9	0.16	0.49	1.81
Case 9b	7.0	21.5	89.1	0.17	0.49	1.81
Case 10	5.5	17.8	90.0	0.24	0.48	2.67
Case 11	6.0	15.0	90.0	0.24	0.47	2.67
Case 12	6.5	12.8	90.0	0.24	0.47	2.67
Case 13	7.0	11.0	90.0	0.23	0.47	2.67
Case 10b	5.5	17.8	86.9	0.16	0.49	1.81
Case 11b	6.0	15.0	86.5	0.16	0.49	1.81
Case 12b	6.5	12.8	86.1	0.16	0.49	1.81
Case 13b	7.0	11.0	85.6	0.17	0.48	1.81
Case 14	5.0	8.5	90.0	0.19	0.45	2.38
Case 15	5.5	7.1	90.0	0.18	0.44	2.38
Case 16	6.0	5.9	90.0	0.17	0.43	2.38
Case 17	6.5	5.1	90.0	0.16	0.42	2.38
Case 18	7.0	4.4	90.0	0.15	0.40	2.38

5.1 Parameter Study 1

The gas velocity has a great impact on the size of the column as it affects the performance of the column. As discussed in Section 4.3, a superficial gas velocity of 2 m/s was chosen to calculate the diameter of the base case. The diameter was found to be 5.0m. Four cases were set up where the diameter increased with 0.5m from the base case.

The height for the base case was set to be 25m with a lean loading of 0.19 $^{\text{mol CO}_2}/_{\text{mol MEA}}$, and a rich loading of 0.49 $^{\text{mol CO}_2}/_{\text{mol MEA}}$. The capture rate was 90%. The main focus of parameter study 1 was to study the effect of pressure drop in the column and the effect on the MEA emissions. The reboiler duty, gas flow and lean flow were kept constant for the base case and case 1-4. The height for case 1, 2, 3 and 4 was then adjusted to get the same lean and rich loading as the base case. Table 5.2 shows the height and diameter for the base case, case 1, 2, 3, and 4. It also shows the rich loading, lean loading, reboiler duty and vapour phase MEA emissions before and after the water wash.

Table 5.2: The base case, case 1, 2, 3 and 4 in parameter study 1 with absorber column dimensions, the L/G ratio, reboiler duty, gas-phase MEA emissions at the top of the absorber and after the water wash, lean and rich loading, and cyclic capacity. All cases capture 90% CO_2

	Height	Diameter	L/G	Reboiler	Emissions top absorber	Emissions after WW	Lean loading	Rich loading	Cyclic capacity
	[m]	[m]	$[\frac{\text{kg}}{\text{kg}}]$	[GJ/t_{CO_2}]	[ppm]	[ppm]	$[\frac{\text{mol CO}_2}{\text{mol MEA}}]$	$[\frac{\text{mol CO}_2}{\text{mol MEA}}]$	$[\frac{\text{mol CO}_2}{\text{mol MEA}}]$
Base case	25.0	5.0	2.11	3.01	**880**	**9.16**	0.19	0.49	0.30
Case 1	22.3	5.5	2.11	3.01	**880**	**9.42**	0.19	0.49	0.30
Case 2	20.6	6.0	2.11	3.01	**880**	**9.72**	0.19	0.49	0.30
Case 3	19.0	6.5	2.11	3.01	**880**	**10.10**	0.19	0.49	0.30
Case 4	17.6	7.0	2.11	3.01	**880**	**10.40**	0.19	0.49	0.30

Table 5.2 shows that the vapour MEA emissions at the top of the absorber are the same for all the cases. Figure 5.1 shows the vapour temperature profile in the absorber for the base case, case 1, 2, 3, and 4. The temperature at the top of the absorber column is approximately the same for all the cases, as can be seen from the figure. The temperature bulge is quite close to the top of the column. The volatile emissions are strongly affected by the temperature. As a result of very similar temperature profiles for all the cases, the vapour MEA emissions are the same at the top of the absorber column.

The vapour MEA emissions after the water wash can also be found in Table 5.2. The emissions were also very similar after the water wash for all the cases. Figure 5.2 shows the vapour temperature profile in the water wash for the base case, case 1, 2, 3, and 4. In the water wash the vapour MEA emissions are only slightly increased as a result of very small variations in the temperature profiles.

When comparing the vapour MEA emissions at the top of the absorber and after the water wash it can also be observed that the water wash removed about 98.8% of the vapour emissions.

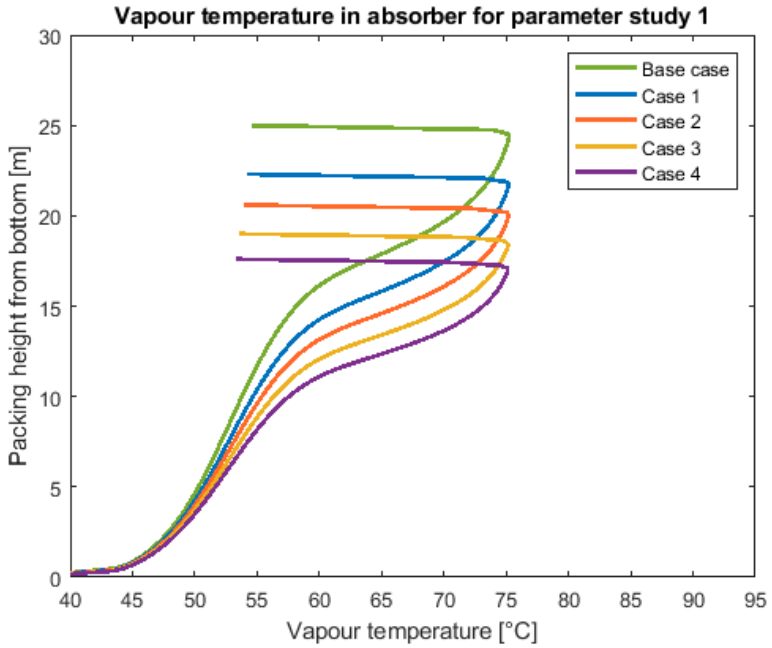

Figure 5.1: Vapour temperature profile in the absorber for base case, case 1, 2, 3, and 4 in parameter study 1

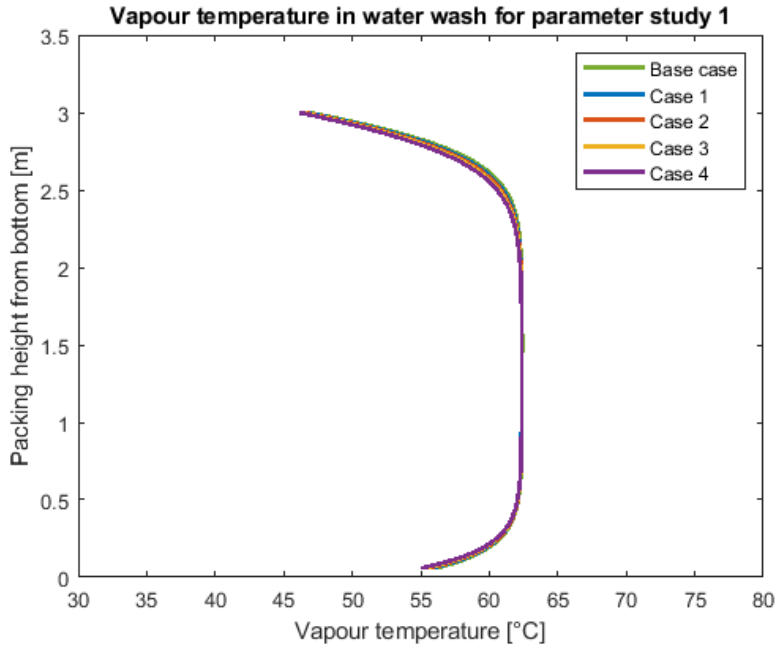

Figure 5.2: Vapour temperature profile in the water wash for base case, case 1, 2, 3, and 4 in parameter study 1

The gas velocity was calculated by equation 4.11. The pressure drop was calculated by the method described in section 4.6. Packing volume was calculated from equation 2.1. The calculation of the liquid hold-up is explained in Section 2.7.2. Every packing type have a specific void fraction. For Mellapak 250Y this void fraction is 0.97 m^3/m^3 [3]. The reduction in void fraction was found by subtracting the liquid hold-up from the void fraction. Table 5.3 shows the gas velocity, pressure drop and required packing volume, liquid hold-up and reduction in void fraction for the base case, case 1, 2, 3, and 4.

Table 5.3: Calculated gas velocity, pressure drop, required packing volume, liquid hold-up and reduction in void fraction for base case, case 1, 2, 3, and 4 in parameter study 1

	Gas velocity [m/s]	Pressure drop [kPa/m]	Packing volume [m^3]	Liquid hold-up [m^3/m^3]	Reduction in void fraction [%]
Base Case	2.00	1.23	492.84	0.058	6.0
Case 1	1.71	1.17	529.81	0.051	5.3
Case 2	1.44	1.07	582.45	0.046	4.7
Case 3	1.23	1.03	630.48	0.042	4.5
Case 4	1.06	0.97	677.25	0.038	3.9

Increasing the column diameter at constant gas and liquid flow results in decreased gas velocity. Consequently the pressure drop decreases, as can be seen from Table 5.3. As the diameter increases, the required packing height will go down. This does not mean that the required packing volume necessarily goes down. Table 5.3 shows that in these cases, an increase in diameter results in a larger the packing volume. The packing volume depend on the active area. The active area is affected by the liquid load.[32] Liquid load is defined as liquid flow rate per cross section area. As already mentioned in this parameter study, the liquid flow rate was kept constant, but as the diameter increases the cross section area increases. This means that the liquid load will decrease with increasing diameter. With a lower liquid loading the active area may go down, and the packing volume will increase accordingly.[32]

The results for gas velocity and pressure drop were compared to results from literature. It was found that at constant gas and liquid flow, an increase in diameter leads to a reduction in the pressure drop. This is in good agreement with what have been found in in published papers ([32],[61],[36]). The literature also showed that the pressure drop in an absorption column is typically in the range 0.2 - 1.2 kPa/m. Table 5.3 shows that the pressure drop is reduced from 1.23 kPa/m to 0.97 kPa/m. It is therefore in the typical range for pressure drops in an absorber column.

When designing an absorber column, both the CAPEX and OPEX are important parameters to consider. A higher pressure drop will lead to a higher energy demand. Reducing the pressure drop can therefore lead to a lower operating-cost as a result of a lower energy demand.

A consequence of an increase in diameter is a higher capital-cost. It is therefore a trade-off between OPEX and CAPEX that needs to be considered when designing the absorber column.[32]

The column diameter, liquid hold-up and gas velocity are closely related. The mass-transfer inside a column can be compromised by a high liquid hold-up. The liquid hold-up depend on the gas velocity. Table 5.3 show that the liquid hold-up decrease as the gas velocity decrease. The void fraction is defined as the ratio between the space occupied by the gas to the total volume. The table shows that a higher liquid hold-up result in a higher reduction in void fraction[62]. This will give a lower packing efficiency.

5.2 Parameter Study 2

The energy consumption needed for solvent regeneration is important to consider for both design and operation of a CO_2-capture system. The reboiler duty is connected to the quantity of CO_2 being stripped in the stripper column. Higher reboiler duty will result in more CO_2 stripped and a leaner solution leaving the stripper. The stripping column is one of the most energy-intensive part of the process, hence reducing the energy needed is important[13].

The main focus of parameter study 2 was to study the effect of the liquid-gas ratio on the reboiler duty, MEA vapour emissions and rich and lean loading.

As already discussed, the OPEX and CAPEX are important parameters to consider for an economical design. These costs can be reduced by reducing the height of the absorber column, and the reboiler duty. Case 5 with a diameter of 5.0m was used to find the lowest height of the absorber column with the lowest reboiler duty that capture 90% of the CO_2. The lowest height was found to be 21.5m, with a reboiler duty of 2.95 GJ/t_{CO_2} (72.6 GJh^{-1}).

The height that was found for case 5 was then kept constant for all the cases in parameter study 2. The gas flow rate was also kept constant. The liquid flow rate was then varied, and the reboiler duty was adjusted so that 90% CO_2 was captured. The L/G ratio that gave the lowest reboiler duty was then found. Table 5.4 shows the height, diameter, L/G, reboiler duty, MEA vapour emissions at the top of the absorber and after the water wash, the lean and rich

loading and the cyclic capacity at a 90% capture rate.

Table 5.4: Case 5, 6, 7, 8 and 9 in parameter study 2 with absorber column dimensions, the L/G ratio and corresponding lowest reboiler duty, gas-phase MEA emissions at the top of absorber and after water wash, lean and rich loading, and cyclic capacity. All cases capture 90% CO_2

	Height	Diameter	L/G	Reboiler	Emissions top absorber	Emissions after WW	Lean loading	Rich loading	Cyclic capacity
	[m]	[m]	$[\frac{kg}{kg}]$	$[GJ/t_{CO_2}]$	[ppm]	[ppm]	$[\frac{\text{mol } CO_2}{\text{mol MEA}}]$	$[\frac{\text{mol } CO_2}{\text{mol MEA}}]$	$[\frac{\text{mol } CO_2}{\text{mol MEA}}]$
Case 5	21.5	5.0	2.45	2.95	891.37	8.856	0.227	0.480	0.251
Case 6	21.5	5.5	2.53	2.91	892.43	8.755	0.234	0.480	0.240
Case 7	21.5	6.0	2.60	2.88	892.67	8.645	0.241	0.480	0.237
Case 8	21.5	6.5	2.66	2.85	892.70	8.556	0.247	0.480	0.232
Case 9	21.5	7.0	2.67	2.83	893.00	8.536	0.250	0.480	0.230

It can be observed from Table 5.4 that the L/G ratio increases with increasing diameter. The cross-section area will increase as the diameter increases. The wetting will then not be as sufficient. The liquid flow rate is a key parameter in the absorption/desorption process. It will influence the mass transfer in both the absorber and the stripper. In order to improve the wetting, and hence the mass transfer, the liquid flow needs to increase when the diameter increases.

The lean loading is important, as it directly influence the equilibrium partial pressure, and hence the driving force for mass transfer.[63] When the lean loading is lower, the equilibrium partial pressure of CO_2 is lower. This results in a higher amount of water vapour required to achieve the equilibrium CO_2 partial pressure, and the reboiler duty will therefore increase. This can be seen from Table 5.4. Case 5 has the lowest lean loading and the highest reboiler duty. As the diameter of the absorber column increases, the lean loading increases, and correspondingly the reboiler duty decreases.

As the lean loading, the rich loading is also related to the equilibrium partial pressure of CO_2, and will therefore affect the reboiler duty. The rich loading is affected by the height of the

column. If the column is tall enough, the residence time will be large enough for the rich loading to reach equilibrium at the bottom of the column. This is why the rich loadings are approximately the same in this parameter study. Of course, if more significant digits were included, the rich loading would not be exactly the same. Because the optimal L/G ratio has small variations, and the height is the constant, the rich loading is therefore equal in all the cases.

Cyclic capacity is defined as the difference between the rich and lean loading. The cyclic capacity is strongly related to the energy performance of the process. A high cyclic capacity is beneficial. The sensible heat loss from when the rich and lean flows are heat exchanged, is reduced at a high cyclic capacity[64]. A high cyclic capacity could also result in a reduction of the dimensions of the plant and a smaller liquid circulation flow.[64] Table 5.4 shows that case 5 with the highest cyclic capacity have the lowest liquid to gas ratio, which is expected at a constant capture rate.

Figure 5.3 shows a plot of reboiler duty versus L/G for case 5-9. It can be observed that the reboiler duty starts decreasing as the liquid flow increases. It reaches a minimum at the optimum L/G ratio. After that point, the reboiler duty starts to increase again. It can also be observed that the reboiler duty decreases with increasing diameter.

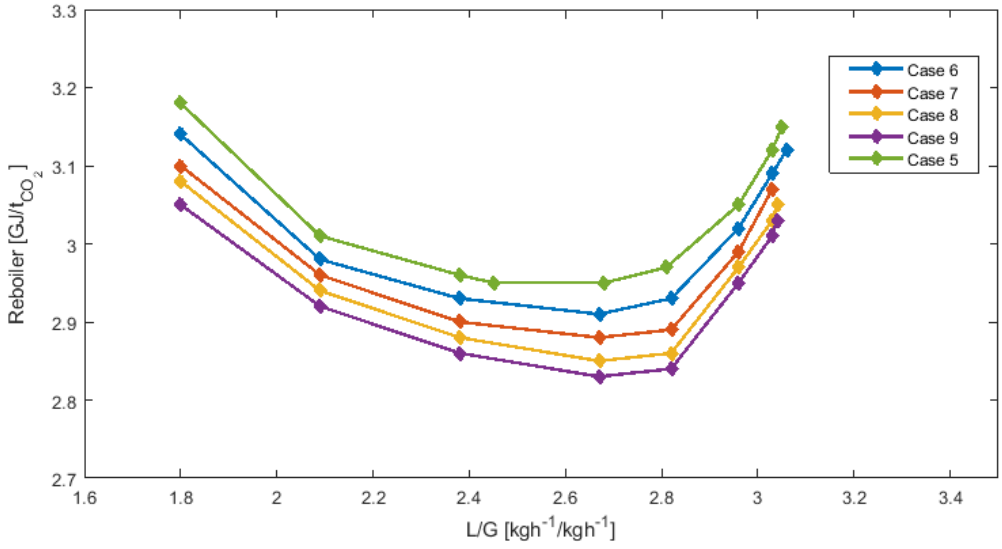

Figure 5.3: Reboiler duty versus L/G ratio for case 5, 6, 7, 8 and 9 in parameter study 2

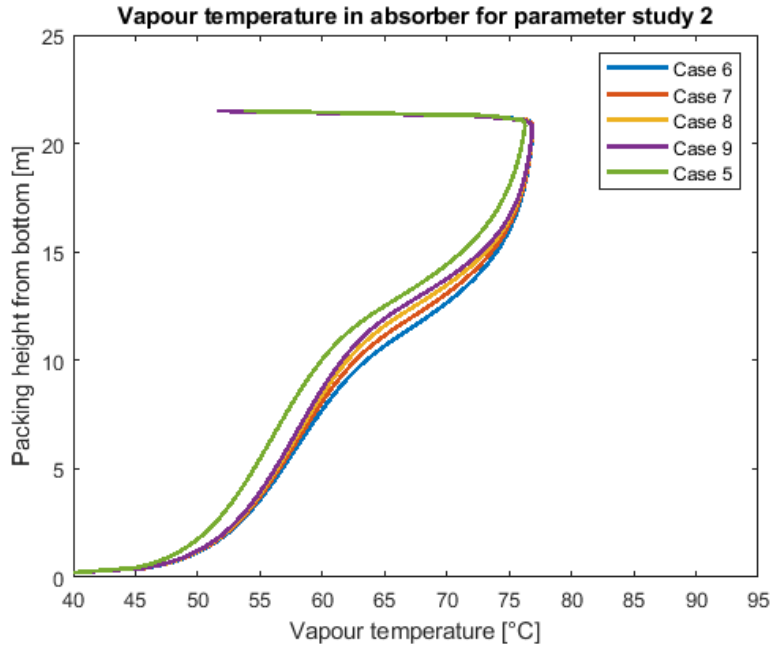

Figure 5.4: Vapour temperature profile in the absorber case 5-9 in parameter study 2

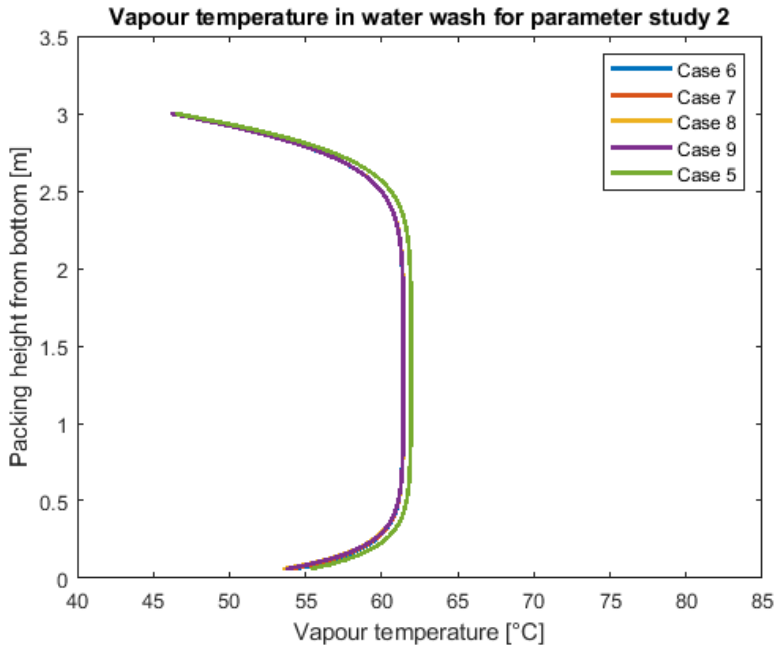

Figure 5.5: Vapour temperature profile in the water wash for case 5-9 in parameter study 2

Table 5.4 shows the vapour MEA emissions at the top of the absorber column and after the water wash. It can be observed that all the cases have very similar emissions. Figure

5.4 shows the vapour temperature profiles inside the absorber column for all 5 cases. As the graph shows, the temperatures does not deviate much from each other, which results in similar emissions at the top of the absorber. Figure 5.5 shows the vapour temperature profiles inside the water wash. Also here, the temperature has very small deviations in all the cases, and the emissions after the water wash are very similar.

5.3 Parameter Study 3

The area at which mass-transfer occurs is important for the capacity and efficiency of the column. One main characteristic of a packing is the specific surface area (a). This is the total interfacial area per unit volume of packing.[65] The specific surface area for Mellapak 250Y is 250 m^2/m^3 [3]

In parameter study 2 case 5 was used to find the lowest height with the lowest reboiler duty. This case had a diameter of 5.0m, with a 21.5m height. These dimensions were used to calculate the interfacial area with equation (2.2). The interfacial area was found to be 105961m^2.

The objective of parameter study 3 was to investigate how the vapour MEA emissions, reboiler duty and lean and rich loading behaved when the interfacial area was kept constant. With an interfacial area of 105961m^2, new heights were calculated for the other cases with equation (4.13). The heights are shown in Table 5.5 together with diameter, L/G, reboiler duty, MEA vapour emissions at the top of absorber and after water wash, lean and rich loading, and cyclic capacity.

To keep the interfacial area constant, the height decreases as the diameter increases as Table 5.5 shows. The gas flow rate was kept constant, while the liquid flow rate was varied. The reboiler duty was adjusted to ensure that 90% of the CO_2 was captured. The L/G ratio that gave the lowest reboiler duty was found. The results in Table 5.5 are all at a 90% capture rate.

Table 5.5: Case 5, 10, 11, 12 and 13 in parameter study 3 with absorber column dimensions, the L/G ratio and corresponding lowest reboiler duty, gas-phase MEA emissions at the top of the absorber and after water wash, lean and rich loading, and cyclic capacity at 90% capture rate

	Height	Diameter	L/G	Reboiler	Emissions top absorber	Emissions after WW	Lean loading	Rich loading	Cyclic capacity
	[m]	[m]	$[\frac{kg}{kg}]$	[GJ/t_{CO_2}]	[ppm]	[ppm]	$[\frac{\text{mol } CO_2}{\text{mol MEA}}]$	$[\frac{\text{mol } CO_2}{\text{mol MEA}}]$	$[\frac{\text{mol } CO_2}{\text{mol MEA}}]$
Case 5	21.5	5.0	2.45	2.95	891.37	8.86	0.227	0.478	0.251
Case 10	17.84	5.5	2.67	2.97	887.4	8.46	0.240	0.471	0.231
Case 11	15.00	6.0	2.67	3.01	883.6	8.40	0.238	0.470	0.232
Case 12	12.77	6.5	2.67	3.04	877.6	8.32	0.237	0.468	0.231
Case 13	11.01	7.0	2.67	3.07	871.1	8.23	0.235	0.466	0.231

As already discussed, the lean and rich loading are important parameters, as they have a large effect on the reboiler duty . The loading will effect the equilibrium partial pressure and therefore the mass transfer driving force. A lower lean loading require a higher amount of water vapour to achieve the equilibrium CO_2 partial pressure, and the reboiler duty will therefore increase. This can be observed in Table 5.5. As the diameter increases, the rich loading and lean loading decrease. This results in a higher reboiler duty.

Table 5.5 shows that the optimal L/G ratio was 2.67 $^{kg}/_{kg}$ for case 10-13. The liquid-gas ratio is affected by the cyclic capacity. It can be observed that the cyclic capacity has very small deviations and is approximately the same for all the cases. This results in the same optimal L/G ratio. Case 5 have a optimal L/G ratio at 2.45 $^{kg}/_{kg}$ with a reboiler duty of 2.95 GJ/t_{CO_2}. The reboiler duty stays constant for a certain range of liquid-gas ratios. When case 5 was operated with a L/G ratio of 2.67 $^{kg}/_{kg}$, the reboiler duty did not increase, and was constant at 2.95 GJ/t_{CO_2}. The cyclic capacity was then 0.231 $^{\text{mol } CO_2}/_{\text{mol MEA}}$ for case 5, which correspond to the cyclic capacities of the other cases.

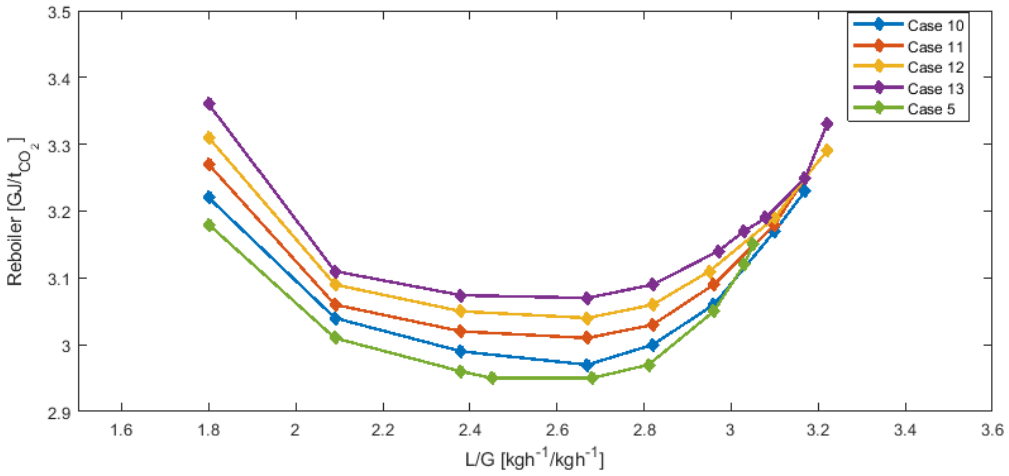

Figure 5.6: Reboiler duty versus L/G ratio for case 5, 10, 11, 12 and 13 in parameter study 3

Figure 5.6 shows a plot of reboiler duty versus L/G for case 5, 10, 11, 12 and 13. It can be observed that the trend is the same as in parameter study 2. The reboiler duty decreases until it reached a minimum. After that point is starts increasing. The figure shows that a larger diameter results in a higher reboiler duty. Case 13 has the highest reboiler duty with a diameter of 7.0m. It should be noted that that this is the opposite of what was found in parameter study 2. In parameter study 2 the case with 7.0m in diameter had the lowest reboiler duty. This is a result of different rich/lean loadings and cyclic capacity. A shorter column will be more beneficial for the capital expenses, but the energy demand is higher.

The vapour phase MEA emissions can be found in Table 5.5. It can be observed that the emissions at the top of the absorber as well as the emissions after the water wash decrease with increasing diameter. Figure 5.7 shows the vapour temperature in the absorber plotted against packing height. Case 5 has the highest top temperature of 54.5°C which leads to the highest emissions. Figure 5.8 shows the vapour temperature profile in the water wash. Also here case 5 has the highest top temperature and the highest emissions after the water wash.

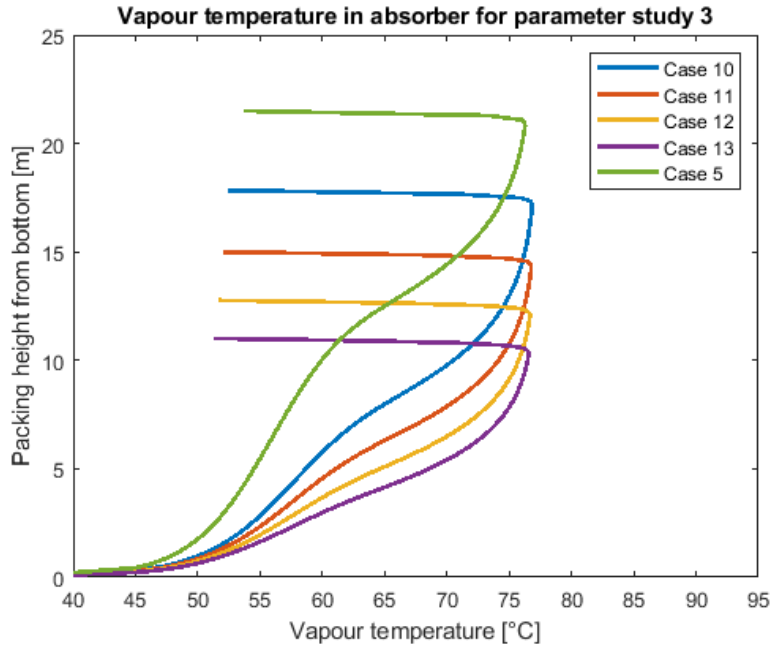

Figure 5.7: Vapour temperature profile in the absorber for case 5, case 10, 11, 12 and 13 in parameter study 3

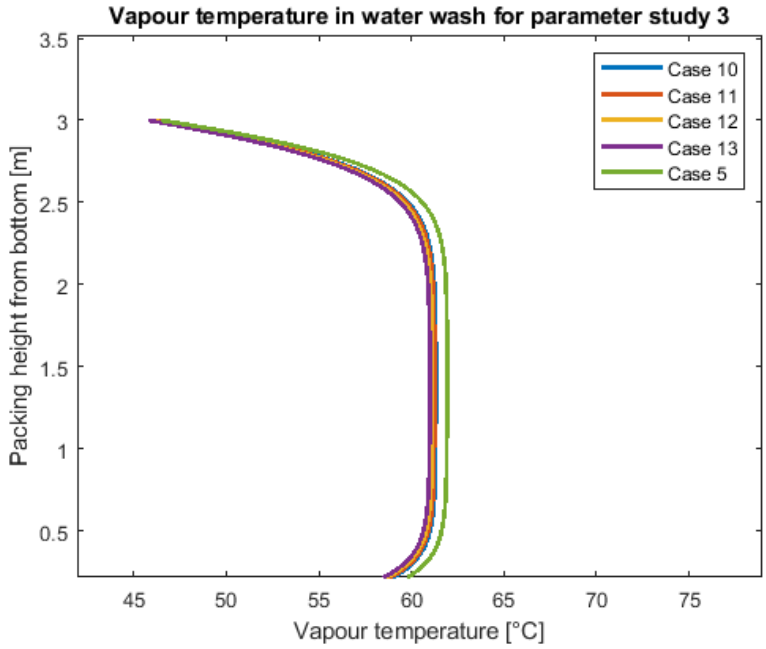

Figure 5.8: Vapour temperature profile in the water wash for case 5, 10, 11, 12 and 13 in parameter study 3

5.4 Parameter Study 4

The effective interfacial mass transfer area is one of the most important efficiency parameters in absorption columns as it is directly connected to the mass transfer between liquid and gas phase. Parameter study 3 was conducted by keeping the interfacial area constant. In parameter study 4, the effective interfacial area was kept constant.

Section 2.7.2 gives an explanation on how the effective interfacial area was calculated. Case 5 from parameter study 3 was used to find the Froude number and Reynolds number. The Reynolds number was found to be 9.53, hence equation 2.4 was used. The effective interfacial area was found to be 41973 m^2. This is around 2.5 times lower than the interfacial area that was found to be 105961 m^2 An advantage of using the effective interfacial area is that the necessary heights of the columns are lower. This means a reduction in the CAPEX.

The objective of parameter study 4 was to investigate how the vapour MEA emissions, reboiler duty, lean and rich loading behaved at constant effective interfacial area. Table 5.6 shows the heights calculated from the effective interfacial area for case 14-18. It can be observed that the new heights are much lower than the heights in parameter study 3. Table 5.6 also shows the diameter, L/G, reboiler duty, MEA vapour emissions at the top of the absorber and after the water wash, lean and rich loading and cyclic capacity.

As the diameter increases for each case, the height decreases to keep the effective interfacial area constant. It should be mentioned that the packing heights that were found are very low. It might not be very realistic, but can still be used to see the trends in the results.The flue gas into the absorber was kept constant. The liquid flow rate was then varied to find the L/G ratio that gave the lowest reboiler duty. Every case in Table 5.6 capture 90% CO_2.

Table 5.6: Case 14-18 in parameter study 4 with absorber column dimensions, the L/G ratio and corresponding lowest reboiler duty, gas-phase MEA emissions at the top of the absorber and after the water wash, lean and rich loading, and cyclic capacity. All cases capture 90% CO_2

	Height	Diameter	L/G	Reboiler	Emissions top absorber	Emissions after WW	Lean loading	Rich loading	Cyclic capacity
	[m]	[m]	$[\frac{kg}{kg}]$	$[GJ/t_{CO_2}]$	[ppm]	[ppm]	$[\frac{\text{mol } CO_2}{\text{mol MEA}}]$	$[\frac{\text{mol } CO_2}{\text{mol MEA}}]$	$[\frac{\text{mol } CO_2}{\text{mol MEA}}]$
Case 14	8.52	5.0	2.38	3.46	847.62	8.32	0.189	0.447	0.258
Case 15	7.07	5.5	2.38	3.57	826.36	8.02	0.182	0.440	0.258
Case 16	5.94	6.0	2.38	3.70	798.86	7.63	0.174	0.432	0.258
Case 17	5.06	6.5	2.38	3.92	769.10	7.23	0.162	0.420	0.258
Case 18	4.36	7.0	2.38	4.35	741.55	6.87	0.146	0.404	0.258

Table 5.6 shows that the optimal L/G ratio was 2.38 $^{kg}/_{kg}$ for all the cases. The cyclic capacity was the same in all the cases, which lead to the same L/G ratio. At a constant L/G ratio, an increased diameter will lead to less wetting of the packing because the liquid has to be distributed over a larger diameter. As a result of this, the rich loading decreases when the diameter increases. The lean loading also decreases at a larger diameter. A lower lean loading makes the stripping in the reboiler more difficult, and a higher reboiler duty is necessary to achieve a capture rate at 90%. This can be seen in the table, where case 18 have the highest reboiler duty at 4.35 GJ/t_{CO_2}, with the lowest lean loading at 0.146 $^{\text{mol } CO_2}/_{\text{mol MEA}}$.

Figure 5.9 shows a plot of the reboiler duty versus L/G for case 14-18. Like in the other parameter studies, the reboiler duty decrease as the L/G increases. It reaches a minimum at 2.38$^{kg}/_{kg}$ before it increases again. Also here it can be observed that a larger diameter result in a higher reboiler duty. The same trend was found in parameter study 3.

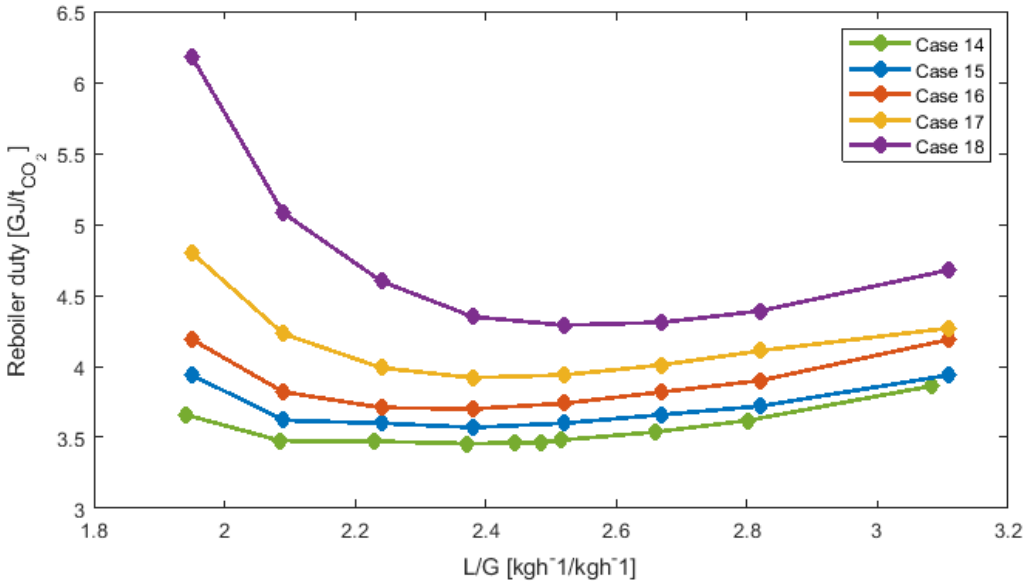

Figure 5.9: Reboiler duty versus L/G ratio for the case 14, 15, 16, 17 and 18 in parameter study 4

The vapour phase MEA emissions can be found in Table 5.6. The emissions both at the top of the absorber and after the water wash decrease with an increasing diameter. Figure 5.10 shows the vapour temperature profile for all the cases in the absorber, and Figure 5.11 shows the vapour temperature profile in the water wash. It can be observed that the top temperature in the absorber varies from 53.3°C for case 18 to 50.3°C for case 14. This shows how large effect the temperature have on the volatile emissions. A 3°C temperature difference leads to a difference of 106.1ppm MEA emissions after the absorber.

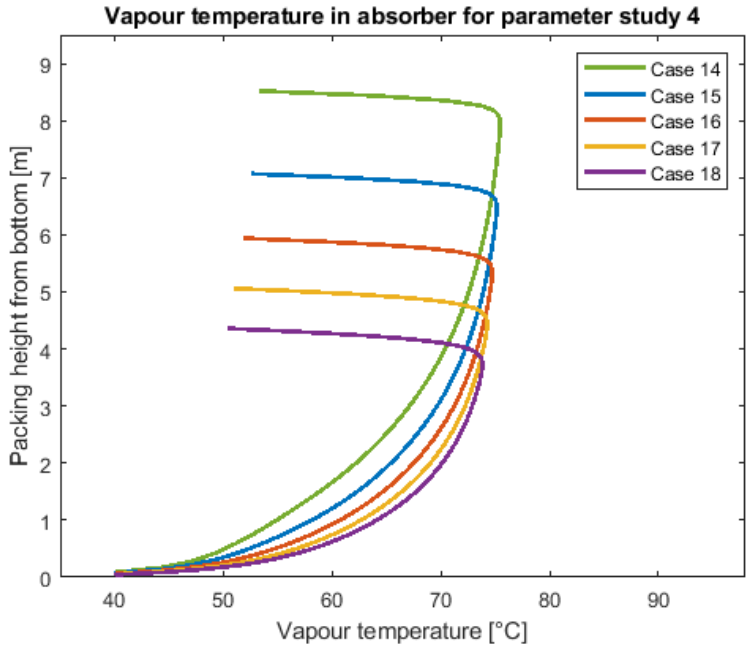

Figure 5.10: Vapour temperature profile in the absorber for case 14, 15, 16, 17 and 18 in parameter study 4

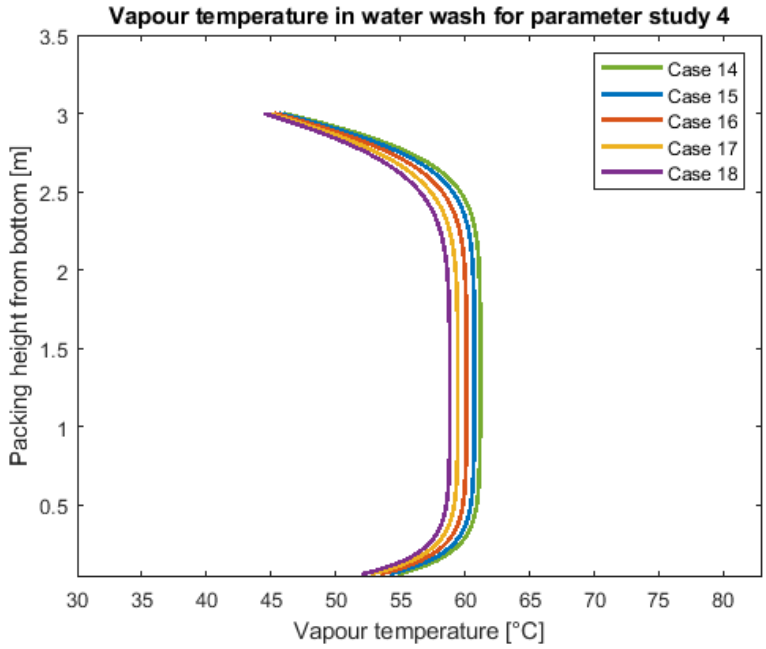

Figure 5.11: Vapour temperature profile in the water wash for case 14, 15, 16, 17 and 18 in parameter study 4

5.5 Parameter Study 5

Up-until now, all the cases have captured 90% CO_2. One of the objectives in this thesis was to evaluate how the capture rate was effected by changing the absorber column dimensions. Table 5.7 show the different column dimensions that were used. The liquid and gas flow rate was set to be constant with a L/G ratio of 1.81 kg/kg. The reboiler duty was set to be constant at 73.6 GJ/h.

Table 5.7: Height, diameter, L/G, reboiler, capture rate, lean and rich loading and cyclic capacity for case 5b-13b at constant L/G ratio and constant reboiler duty in parameter study 5

	Height	Diameter	L/G	Reboiler	Capture rate	Lean loading	Rich loading	Cyclic capacity
	[m]	[m]	$[\frac{kg}{kg}]$	$[GJ/t_{CO_2}]$	[%]	$[\frac{\text{mol } CO_2}{\text{mol MEA}}]$	$[\frac{\text{mol } CO_2}{\text{mol MEA}}]$	$[\frac{\text{mol } CO_2}{\text{mol MEA}}]$
Case 5b	21.5	5.0	1.81	3.08	**87.44**	0.16	0.49	0.33
Case 6b	21.5	5.5	1.81	3.06	**87.94**	0.16	0.49	0.33
Case 7b	21.5	6.0	1.81	3.05	**88.40**	0.16	0.49	0.33
Case 8b	21.5	6.5	1.81	3.03	**88.79**	0.16	0.49	0.33
Case 9b	21.5	7.0	1.81	3.02	**89.14**	0.17	0.49	0.32
Case 10b	17.84	5.5	1.81	3.10	**86.96**	0.16	0.49	0.33
Case 11b	15.00	6.0	1.81	3.11	**86.51**	0.16	0.49	0.33
Case 12b	12.77	6.5	1.81	3.13	**86.06**	0.16	0.49	0.33
Case 13b	11.01	7.0	1.81	3.15	**85.63**	0.17	0.48	0.31

Table 5.7 shows the height, diameter, L/G, reboiler, capture rate, lean and rich loading and cyclic capacity for the cases in parameter study 5. It can be seen that at constant height, the capture rate will increase as the diameter increases. Parameter study 1 showed that as the diameter increases the gas velocity goes down. At a lower gas velocity the gas will have more time to react with the solvent. The packing area will also increase with increasing diameter

at constant height. This results in more CO_2 captured.

Case 5b was used to calculate the mass transfer area. This was set to be constant for case 10b-13b, and the height was calculated based on that. It can be observed that at constant mass transfer area the capture rate will decrease slightly as the diameter increases. The total mass transfer area is constant, but as the diameter increases the cross section area increases. The liquid flow is constant, but at a larger diameter the liquid has to be distributed over a larger cross section area. This leads to poor wetting of the packing, and the capture rate decreases.

This shows that the capture rate can be adjusted by changing the absorber column dimensions. The best option would be to increase the active area.

5.6 Summery and Comparison of the Parameter Studies

Parameter study 1 showed that at constant liquid and gas flow, an increase in column diameter results in a lower gas velocity. Consequently the pressure drop decreases. A low pressure drop is favorable for the energy requirement in the column and to avoid potential flooding. The study also showed that at similar temperature profiles, the volatile MEA emissions will approximately be the same.

Parameter study 2 was performed at a constant height and flue gas flow rate. The diameter was increased, and the L/G ratio that gave the lowest reboiler duty was found. The study showed that the reboiler duty is strongly dependent on the rich and lean loading. At a larger diameter, the L/G increased, hence, the cyclic capacity decreased which lead to a decrease in reboiler duty. The vapour MEA emissions had small variations as a result of close top temperatures in the absorber and water wash.

Parameter study 3 was performed at constant interfacial area and constant flue gas flow rate. It showed that when the interfacial area is constant, the cyclic capacity will have very small variations even though the diameter increases. This leads to the same optimal L/G ratio. The reboiler duty increased as the diameter increased. Case 13 with 7.0m in diameter had the highest reboiler duty and the largest diameter. This was the opposite of parameter study 2, where the case with 7.0m in diameter had the lowest reboiler duty. This was a result of differences in lean and rich loading. It shows that the energy demand is higher in a shorter column, even though it is beneficial for the capital expenses. The volatile MEA emissions decreased with increasing diameter as a result of lower top temperature in the column.

Parameter study 4 was performed at constant effective interfacial area with constant flue gas flow rate. The effective interfacial area was found to be smaller than the interfacial area, which resulted in shorter columns. At constant effective interfacial area the cyclic capacity was also the same for all the cases, which lead to the same optimum L/G ratio for the lowest reboiler duty. As for parameter study 3, the reboiler duty increased with increasing diameter. The volatile MEA emissions decreased with increasing diameter.

Parameter study 5 was performed to evaluate how the capture rate was affected by changing

the absorber column dimensions. It was found that more CO_2 can be captured at the expense of larger column dimensions.

All the parameter studies showed that there is a trade off between energy consumption and volatile MEA emissions. The case with the lowest MEA emissions was case 18 in parameter study 4. The vapour MEA emissions after the water wash in case 18 were found to be 6.87ppm, with a reboiler of 4.35GJ/t_{CO_2}. The lowest reboiler duty was found for case 4 in parameter study 1. The reboiler duty was 2.83GJ/t_{CO_2}, which resulted in vapour MEA emissions of 8.54ppm. Between the case with the lowest vapour-phase emissions and the case with the lowest reboiler duty there is not a large difference in emissions. Choosing dimensions of the absorber column based on vapour-phase emissions is therefore probably not the best approach. The next sections evaluate how the aerosol based emissions are effected by the absorber column dimensions and operating conditions. Aerosol based emissions have been reported to have a large contribution on the total MEA emissions and should be taken into account.

5.7 Aerosol Emissions at Different Number Concentrations

Up until now, only the volatile MEA emissions have been discussed. The aerosol emissions are an important factor as it can lead to emissions higher than the emissions limit of a post-combustion carbon capture plant. The aerosol growth and composition change were modeled with the mist model as discussed in Section 4.1.2. The results of bulk liquid phase loading, MEA mass fraction and temperature as a function of the position in the column from the CO2SIM simulation were used as model inputs together with inlet droplet composition, number concentration and size distribution.

The first aerosol simulation was performed with case 18 from parameter study 4. The absorber column had a height of 4.36m, and 7.0m in diameter. The liquid phase H_2O and MEA composition and temperature profile can be found in Appendix C.2. The inlet gas had a water partial pressure of 5kPa, and a temperature of 40°C. The inlet droplets were simulated with 0.2molL^{-1} H_2SO_4 with a distribution of 95nm and 1200nm. The mist model simula-

tions were done at two different number concentrations, 1.17· 10^7 droplets/cm^3 and 5.00· 10^7 droplets/cm^3.

As the aerosols travel through the absorber and water wash they undergo changes in terms of size and internal composition. In the columns they are exposed to the bulk liquid. As already mentioned, it is assumed that the liquid phase is not affected by the aerosols. The volume of the liquid phase is much larger than the aerosols.[48] Aerosols will have a fast uptake and release because of their small size, while the transport in the liquid phase will be much slower. The droplets leave the water wash together with the treated gas.

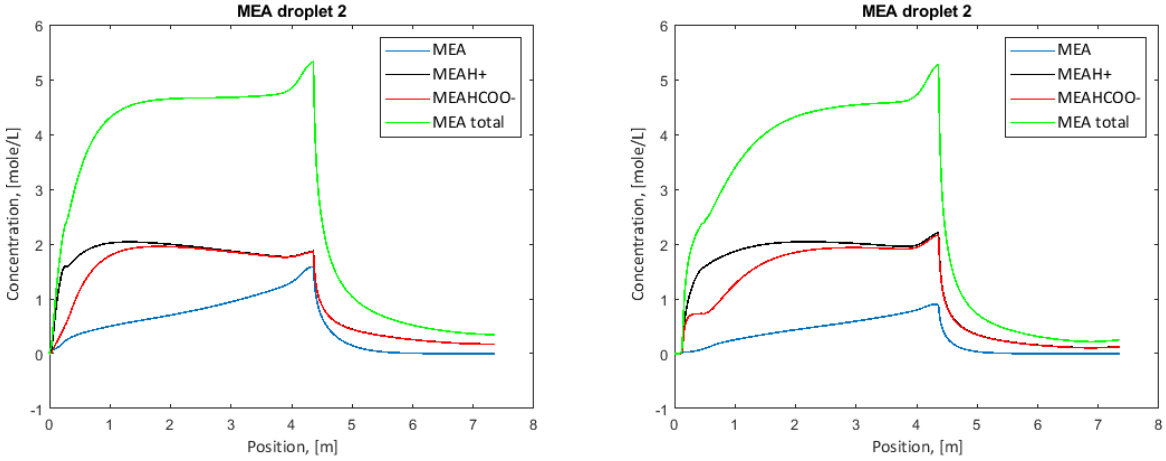

Figure 5.12: (a) MEA concentration at 1.17· 10^7 droplets/cm^3 (b) MEA concentration at 5.00· 10^7 droplets/cm^3

Figure 5.12 shows the MEA concentration in droplet 2 as a function of position in the column at 1.17· 10^7 droplets/cm^3 and 5.00· 10^7 droplets/cm^3. The figure also shows the carbamate (MEAHCOO-) concentration. The flue gas enters the absorber at a relative low temperature. The inlet aerosol droplet does not contain MEA. As the droplet moves up the absorber column MEA is transferred into the droplet. The MEA concentration in the gas phase increase further up in the column. This leads to an increase in driving force towards the droplet, and the MEA concentration inside the droplet starts to build up. Figure 5.13 shows the concentration of bound CO_2 and 1000 times free CO_2 for droplet 1 and 2 and the water partial pressure profile at 1.17· 10^7 droplets/cm^3. At the bottom of the absorber column the concentration of free CO_2

is high. The driving force for absorption is large at this point because of the low temperature in the flue gas. As Figure 5.13 (a) shows, the free CO_2 concentration rapidly decreases at the bottom of the column, and the bound CO_2 concentration increase. Carbamate is formed in the reaction between CO_2 and MEA, and Figure 5.12 shows that the carbamate concentration increase at this point. The lean solvent enters the top of the absorber at a low temperature. At this point the MEA concentration in the droplet increase rapidly. The droplet enters the water wash at 4.36m. The MEA concentration drastically decreases in the water wash. The MEA concentration at the top of the absorber is slightly higher for the lowest number concentration.

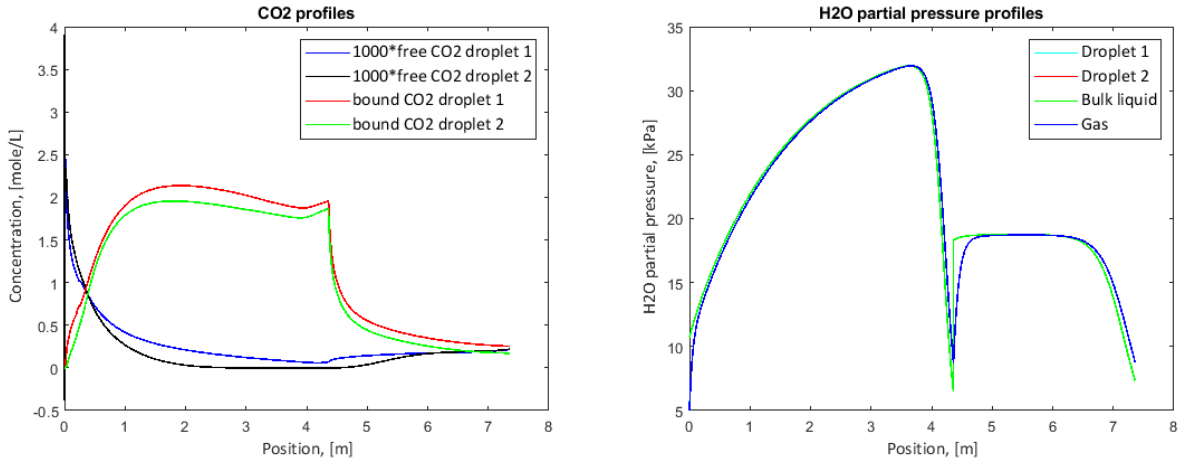

Figure 5.13: (a) Concentration of bound CO_2 and 1000 times free CO_2 for droplet 1 and 2 at $1.17 \cdot 10^7$ droplets/cm^3 (b) Partial pressure of H_2O at $1.17 \cdot 10^7$ droplets/cm^3

Figure 5.12 (a) shows a slight bump in the curve for MEAH+ at approximately 0.2m. This is a result of the equilibrium models used in the mist model. The mist model is built of two equilibrium models, one for sulfuric acid with a correction for MEA and CO_2, and a NRTL-model with correction for sulfuric acid. When the molar ratio of MEA and two times sulfuric acid reach 1 there is a switch between one equilibrium model to another. The switch between the models is what gives a bump in the figure. It does not affect the partial pressure of water. Water is the determining component when it comes to the size of the droplets and thereby also concentration. This bump at the switch in equilibrium model is therefore assumed not to effect the outcome of the results.

The CO_2 profiles and partial pressure of water have only been included for $1.17 \cdot 10^7$droplets/cm^3 as the profiles for $5.00 \cdot 10^7$droplets/cm^3 are very similar. The focus will mainly be on the MEA profiles. CO_2 and water partial pressure profiles will only be included if there are significant differences.

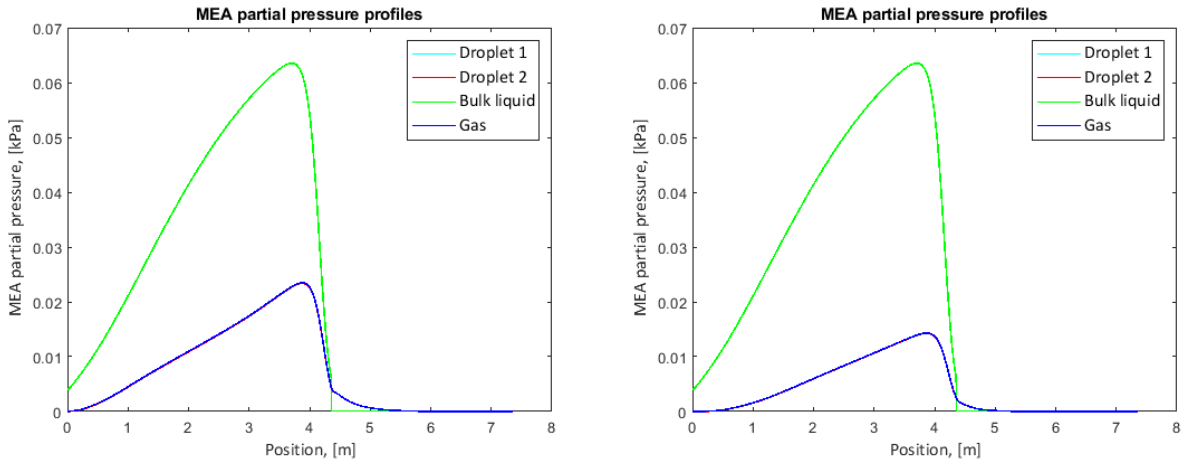

Figure 5.14: (a) Partial pressure of MEA at $1.17 \cdot 10^7$ droplets/cm^3 (b) Partial pressure of MEA at $5.00 \cdot 10^7$ droplets/cm^3

Figure 5.14 shows the partial pressure of MEA at $1.17 \cdot 10^7$ droplets/cm^3 and $5.00 \cdot 10^7$ droplets/cm^3. It can be observed that the depletion effect is stronger for the highest number concentration. Increasing the number of droplets will give a larger interfacial area and droplet volume. For $1.17 \cdot 10^7$ droplets/cm^3, MEA in the gas phase is zero up to around 0.2m in the absorber column. For $5.00 \cdot 10^7$ droplets/cm^3 it is zero up until 0.6m. Because of a larger interfacial area the uptake of MEA will be faster from the gas phase to the aerosols. The partial pressure of MEA in the gas phase will then be approximately 0 for a longer period for the highest number concentration. Further up in the absorber the transfer of MEA to the aerosols slows down. The transfer from bulk liquid is than able to keep up with the transfer to the droplets, and MEA partial pressure in the gas phase starts to build up again as the figure shows. The MEA concentration depends on the depletion of MEA. At the largest number concentration the depletion is stronger, and the build up of MEA in the droplets is slower. The figure shows that the MEA partial pressure in the gas phase increases much faster for $1.17 \cdot 10^7$ droplets/cm^3 than for $5.00 \cdot 10^7$ droplets/cm^3 It can also be observed from Figure

5.14 that the bulk liquid is not affected as it is the same for each number concentration. This is in good agreement with what have been found in published papers.

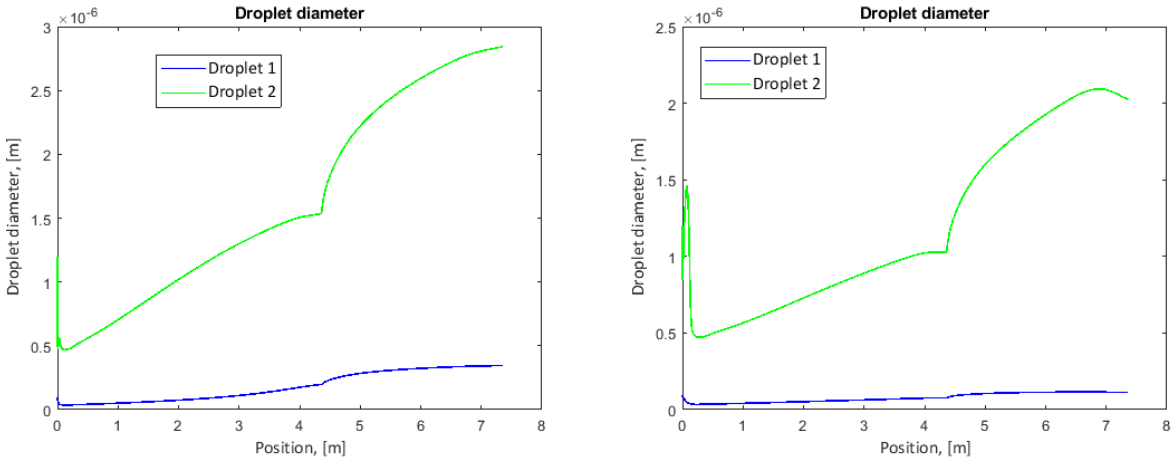

Figure 5.15: (a) Droplet diameter at 1.17· 10^7 droplets/cm^3 for droplet 1 and 2 (b) Droplet diameter at 5.00· 10^7 droplets/cm^3 for droplet 1 and 2

Figure 5.15 shows the droplet diameter for both number concentrations. The droplet growth is a very important aspect. A demister can be implemented, but it will not be able to remove the smallest droplets. The figure shows that the droplet growth for both number concentrations. This indicates that MEA and water have been taken up by the aerosols. Section 3.1 shows some results from previous work on aerosol emissions. Some of these articles showed that the bulk gas phase was affected by the aerosol phase. It have also been seen that a larger aerosol number concentration have a greater impact on the gas phase than a lower number concentration.[48] [66] This is in good agreement with the result found here. The figures show a very rapid drop in size at the bottom of the absorber. This is caused by water evaporating rapidly because of the high water vapour pressure in the inlet gas. As MEA and CO_2 are transferred to the droplet and carbamate is produced, the water vapour pressure is reduced. Water is then absorbed by the droplets, resulting in an increase in size. It can be observed that the lowest number concentration results in the largest droplets. The transport of water to the aerosols has a large impact on the growth, but when moving up the absorber, the transport of MEA will have a big impact as well. A higher concentration of MEA inside the droplet will result in a larger driving force for water transport to the droplet. The MEA concentration

is higher inside the droplet for 1.17· 10^7 droplets/cm^3. This leads to a faster droplet growth. The droplets enter the water wash at 4.36m. The water flowing into the water wash has a low temperature. This causes water to condense on the droplet, resulting in a drastically increase in size.

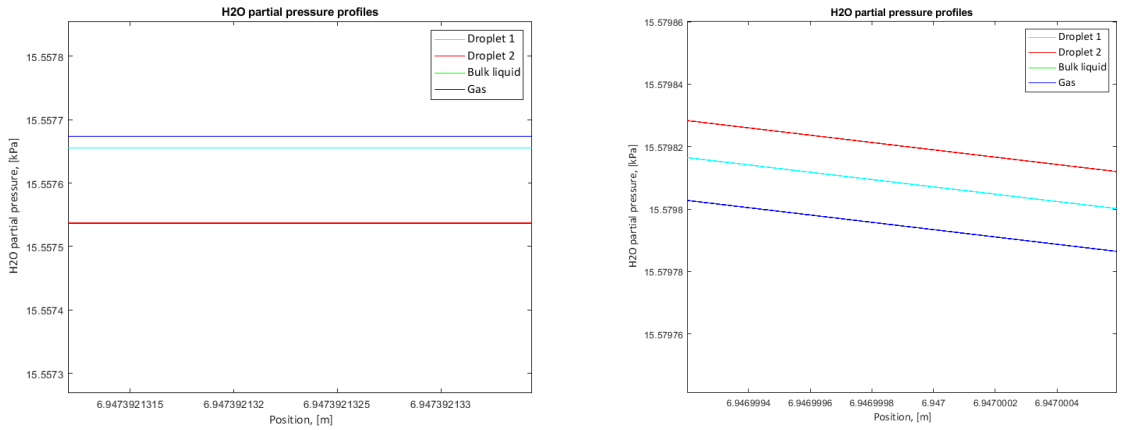

Figure 5.16: (a) A zoomed in look at the water partial pressure at 1.17· 10^7 droplets/cm^3 for droplet 2 (b) A zoomed in look at the water partial pressure at 5.00· 10^7 droplets/cm^3 for droplet 2

Figure 5.15 (b) shows a decrease in size at the top of the water wash for droplet 2 at 5.00· 10^7 droplets/cm^3. This can be explained by the partial pressure of water. The MEA concentration is lowest for the high number concentration as a result of strong depletion of MEA to the gas phase. At a low MEA concentration, the partial pressure of water is higher, and the evaporation of water is stronger. Figure 5.16 shows a zoomed in look at the water partial pressure for both number concentrations around 6.9m in the column. This is the point where the decrease in size occur for 5.00· 10^7 droplets/cm^3. The figure shows that for 1.17· 10^7 droplets/cm^3 the water partial pressure in the gas is higher than the two droplets, which gives a mass transfer from the gas to the droplets. At 5.00· 10^7 droplets/cm^3 the water partial pressure in droplet 2 is higher. This gives a mass transfer from droplet 2 to the gas, and the droplet shrinks.

Figure 5.17 shows the outlet distributions for the two number concentrations before and after the demister. The largest droplets have been removed. This is beneficial, as the largest

droplets have the most significant effect for the emissions. As discussed, the lowest number concentration had the largest droplets at the top of the water wash. This results in a lower droplet distribution as Figure 5.17 shows, as the demister has removed the largest droplets. At a inlet number concentration of $1.17 \cdot 10^7$ droplets/cm^3 the MEA emissions after the water wash was found to be 265ppm (661 mg/Nm^3), with a number concentration of $1.15 \cdot 10^7$ droplets/cm^3. For the high number concentration the MEA emissions after the water wash were 340ppm (848 mg/Nm^3) with a number concentration of $4.98 \cdot 10^7$ droplets/cm^3. The number concentration is only slightly lower than the inlet. Even though the droplets were smaller for the high number distribution the total MEA emissions were higher as a result of more droplets.

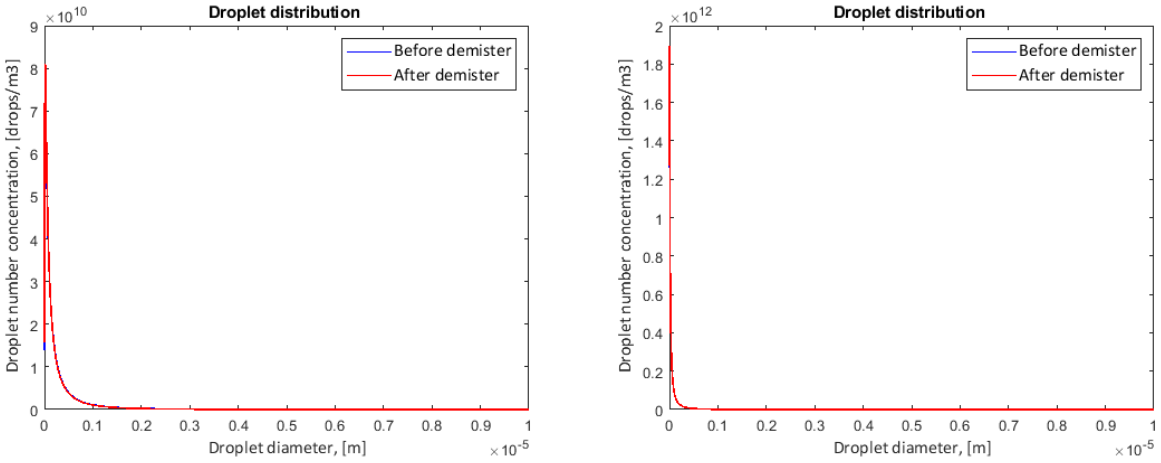

Figure 5.17: (a) Outlet distribution at $1.17 \cdot 10^7$ droplets/cm^3 (b) Outlet distribution at $5.00 \cdot 10^7$ droplets/cm^3

5.8 Aerosol Emissions at Different Absorber Column Dimensions

Parameter study 3 and 4 showed that the volatile MEA emissions varied very little as the column dimensions varied. In both studies the volatile emissions decreased as the diameter of the absorber increased as a result of lower top temperature in the column. This does not necessarily mean that the aerosol emissions will follow the same trend.

Two cases from parameter study 4 were chosen to investigate how the aerosol emissions behaved. Case 15 with a height of 7.07m and 5.5m diameter and case 18 with a height of 4.36m and 7.0m in diameter were used. Case 15 will be referred to as tall, and case 18 will be referred to as low. Case 18 was used in section 5.7 to discuss the effect of different number concentrations. The focus here will be on the effect of different absorber column dimensions. The liquid phase composition of H_2O and MEA and temperature profile can be found in Appendix C.2. Also here the inlet gas had a water partial pressure of 5kPa and a temperature of 40°C. The inlet droplets were simulated with 0.2molL^{-1} H_2SO_4 with a distribution of 95nm and 1200nm. The mist model simulations were performed at two different number concentrations, 1.17· 10^7 droplets/cm^3 and 5.00· 10^7 droplets/cm^3. Only the figures for 1.17· 10^7 droplets/cm^3 are included, as the trends were the same for both number concentrations.

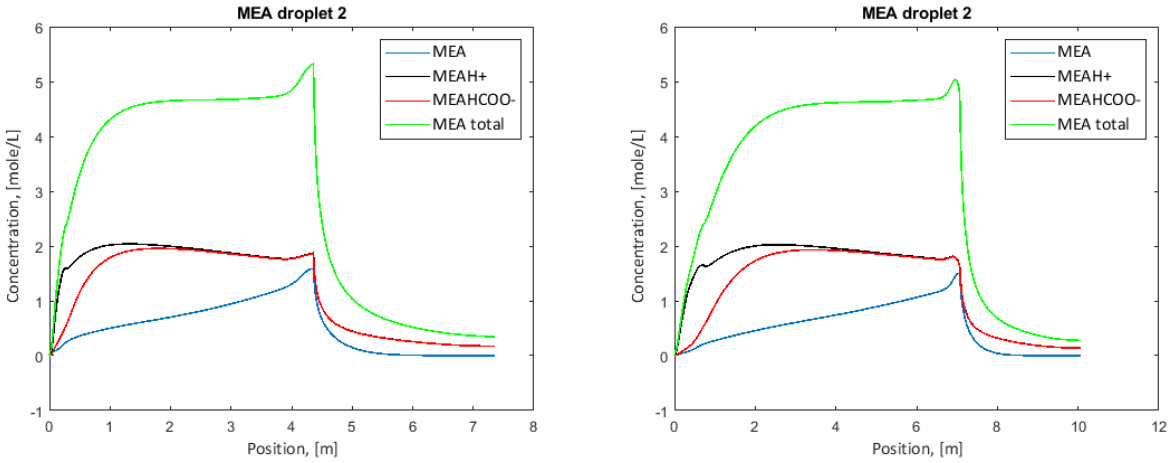

Figure 5.18: (a) MEA concentration for case 18 with the low absorber column at 1.17· 10^7 droplets/cm^3 (b) MEA concentration for case 15 with the tall absorber column at 1.17· 10^7 droplets/cm^3

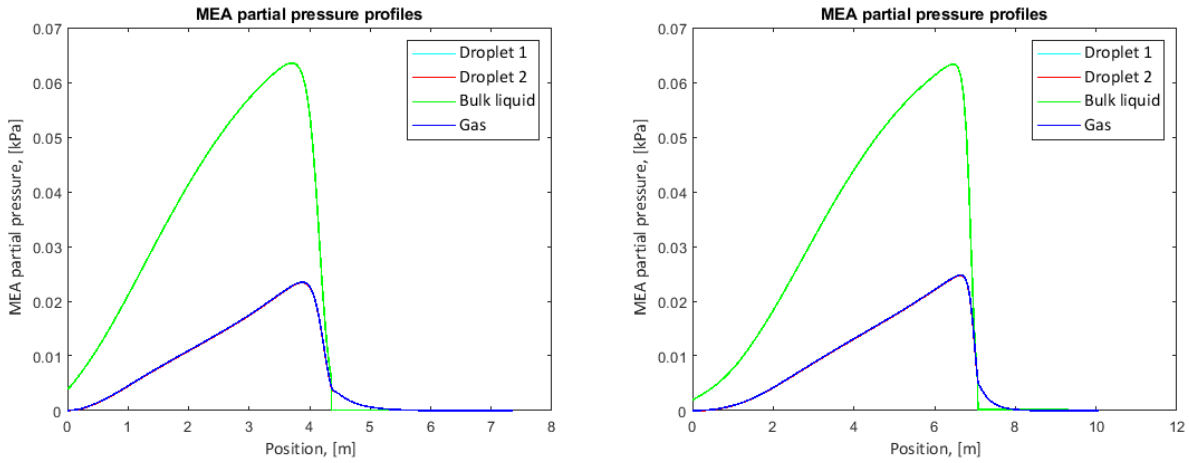

Figure 5.19: (a) MEA partial pressure profile for case 18 with the low absorber column at $1.17 \cdot 10^7$ droplets/cm^3 (b) MEA partial pressure profile for case 15 with the tall absorber column at $1.17 \cdot 10^7$ droplets/cm^3

Figure 5.18 shows the MEA concentration in droplet 2 for the low and tall column at $1.17 \cdot 10^7$ droplets/cm^3. It can be observed that the MEA concentration at the top of the water wash is only slightly higher for the low absorber column. Figure 5.19 shows the MEA partial pressure profile for both the low and tall column. As the figure shows, the partial pressure profiles are very similar for both columns. Both columns have depletion of MEA to the gas phase, and the MEA concentration drops drastically in the water wash. The effective mass transfer area is the same in both cases. Both cases also capture 90% CO_2, and are operated at the same cyclic capacity and liquid-gas ratio. This result in very similar MEA concentrations and partial pressure for the tall and low column.

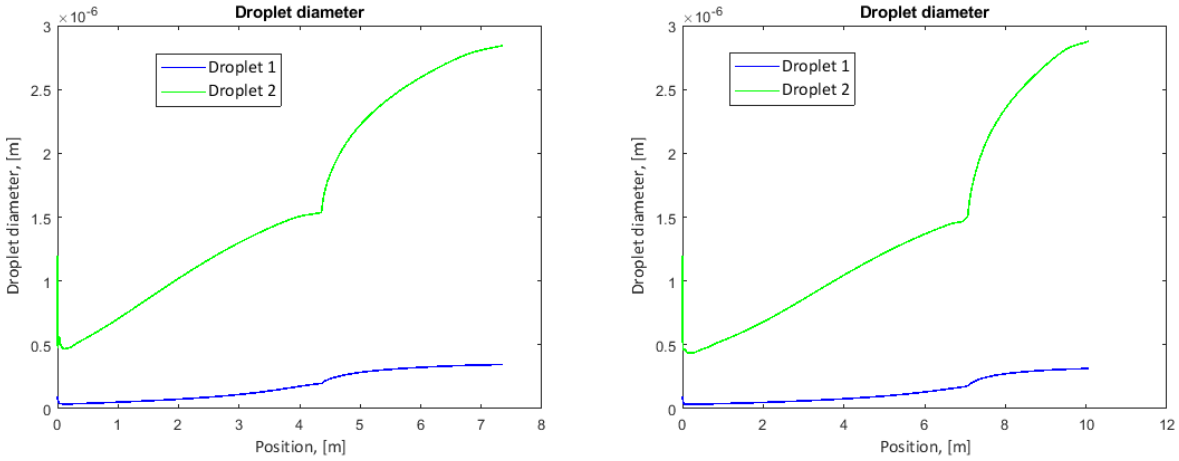

Figure 5.20: (a) Droplet diameter for case 18 with the low absorber column at $1.17 \cdot 10^7$ droplets/cm^3 (b) Droplet diameter for case 15 with the tall absorber column at $1.17 \cdot 10^7$ droplets/cm^3

The droplet diameters for low and tall column are shown in Figure 5.20. The diameter for droplet 2 is slightly larger in the tall column. There is not a big difference. It can also be observed that the diameter for droplet 1 is slightly smaller for the tall column than for the low column. The large droplets have the most significant effect when it comes to the MEA emissions. The desire is therefore to remove the large droplets. As already mentioned, the mist model has a demister implemented. Demisters will remove droplets of a certain size depending on the type of demister. The point is therefore not to get the largest aerosol droplets possible, but to have droplets large enough to be removed by the demister.

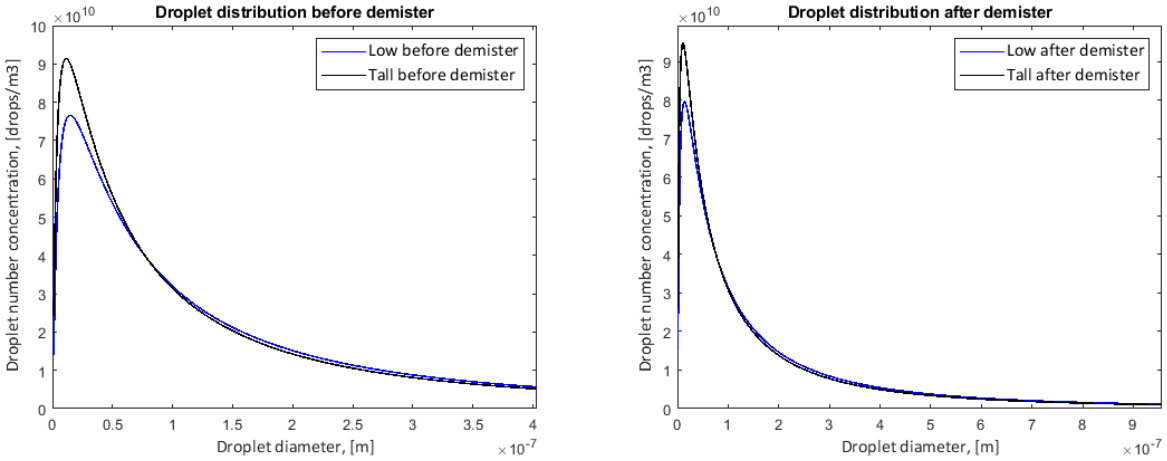

Figure 5.21: (a) Outlet distribution for low and tall absorber column at 1.17· 10^7 droplets/cm^3 before demister(b) Outlet distribution for low and tall absorber column at 1.17· 10^7 droplets/cm^3 after demister

The droplet distribution for the low and tall column before the demister are shown in Figure 5.21 (a), Figure 5.21 (b) show the distribution after the demister. The droplet distribution indicates that there are more small droplets for the tall column. The tall column had a slightly larger droplet 2 and a slightly smaller droplet 1. When the difference between the large and small droplets increases the distribution curve is pushed towards the smaller droplets. It is also clear that the demister remove the larger droplets, as the curves in Figure 5.21 (b) is pushed towards the left and the smaller droplet size.

Table 5.8 shows the MEA emissions after the absorber, before the demister, after the demister and the number concentration for the tall and low column at 1.17· 10^7 droplets/cm^3 and 5.00· 10^7 droplets/cm^3. The tall column results in the lowest MEA emissions for both number concentrations. In parameter study 4 it was found that the tall column had slightly higher gas-phase MEA emissions, but here it can be seen that when including the aerosols the total MEA emissions are lower. This is a result of the largest droplets being removed in the demister. The outlet distribution shows that the tall column has most small droplets, resulting in the lowest MEA emissions. It is also clear that the water wash and demister have an effect on the aerosol emissions, as the emissions are lower both after the water wash and after the demister. This is in good agreement with what have been found in published papers. Previous work

presented in Section 3.1 have also shown that implementing a water wash or demister can reduce the aerosol emissions.

Table 5.8: Absorber configurations tall and low at $1.17 \cdot 10^7$ droplets/cm^3 and $5.00 \cdot 10^7$ droplets/cm^3 with corresponding aerosol-based MEA emissions after the absorber, before demister, after demister and number concentration at the inlet and after demister. Inlet partial pressure of water was 5kPa with a inlet concentration of H_2SO_4 of 0.2mol L^{-1}

	C_N inlet [droplets/cm^3]	MEA after absorber [ppm]	MEA before demister [ppm]	MEA after demister [ppm]	C_N after demister [droplets/cm^3]
Tall	$5.00 \cdot 10^7$	856	303	289	$4.98 \cdot 10^7$
Tall	$1.17 \cdot 10^7$	**668**	**262**	**224**	$1.15 \cdot 10^7$
Low	$5.00 \cdot 10^7$	978	357	340	$4.98 \cdot 10^7$
Low	$1.17 \cdot 10^7$	**771**	**314**	**265**	$1.15 \cdot 10^7$

5.9 MEA Emissions at Different Water wash Diameters

In all five parameters studies and investigations of the aerosol emissions up until now the dimensions of the water wash have been constant. The water wash has had a height of 3.0m with a 5.0m diameter. Case 15 and case 18 have been used to investigate the aerosol emissions, these have a diameter of 5.5m and 7.0m respectively. This means that the gas velocity has been different in the absorber and the water wash. By keeping the dimensions of the water wash constant it gave the opportunity to see more of the effect of what happens in the water wash. What goes in from the absorber is a bit different, but what happens in the water wash is the same for all the cases. New simulations were performed where the absorber and water wash had the same diameter.

Table 5.9 shows the vapour phase MEA emissions after the water wash for case 15 and 18 when the water wash had the same diameter as the absorber and at 5.0m. It can be observed that the volatile emissions are only slightly effected. The difference in top temperature for

case 15 with the two different diameters in the water wash is 0.16°C. The top temperature has barely changed, which is why the emissions are so close. The same goes for case 18. The temperature profiles can be found in Appendix C.1. The liquid-phase composition and temperature profiles used in the mist model can be found in Appendix C.2. The emissions at the top of the absorber have not been included as these were not affected by changing the water wash diameter.

Table 5.9: Case 15 and 18 with corresponding vapour MEA emissions after the water wash when water wash have the same diameter as the absorber and at 5.0m

	Absorber diameter [m]	Water wash diameter [m]	Vapour MEA emissions after water wash [ppm]
Case 15	5.5	5.0	8.02
Case 15	5.5	5.5	8.20
Case 18	7.0	5.0	6.87
Case 18	7.0	7.0	7.01

The aerosol-based MEA emissions after the absorber, before demister and after demister for the tall and low absorber column when the water wash had the same diameter as the absorber and at 5.0m is shown in Table 5.10. The table also shows the number concentration at the inlet and after the demister. As already mentioned, the vapour phase emissions at the top of the absorber were not affected by changing the water wash diameter. The table shows that the aerosol MEA emissions at the top of the absorber were also not affected.

Table 5.10 shows that the aerosol-based emissions are higher for both the tall and low column at a smaller diameter in the water wash. The active area depends on the diameter. A smaller diameter leads to a lower active area, which result in higher MEA emissions. It should also be noted that the difference in emissions is largest for the low column with the largest diameter. For the tall column, a decrease in diameter from 5.5m to 5.0m increase the emissions after the demister with approximately 5%. For the low column, decreasing the diameter from 7.0m to 5.0m increase the emissions with 19%. A smaller diameter in the water wash means lower retention time. The difference in retention time with 7.0m and 5.0m in diameter is larger than

5.5m and 5.0m in diameter. This means that the droplets have less time to loose MEA in the water wash, resulting in high emissions.

Table 5.10: Absorber configurations tall and low at $1.17 \cdot 10^7$ droplets/cm^3 and $5.00 \cdot 10^7$ droplets/cm^3 with corresponding aerosol-based MEA emissions after the absorber, before demister, after demister and number concentration after demister when the water wash have the same diameter as the absorber and at 5.0m. Inlet water partial pressure in gas was 5kPa, with an inlet H_2SO_4 concentration of 0.2mol L^{-1}

Absorber configuration	Water wash diameter [m]	C_N inlet [droplets/cm^3]	MEA after absorber [ppm]	MEA before demister [ppm]	MEA after demister [ppm]	C_N after demister [droplets/cm^3]
Tall	5.5	$5.00 \cdot 10^7$	856	286	275	$4.98 \cdot 10^7$
Tall	5.0	$5.00 \cdot 10^7$	856	303	289	$4.98 \cdot 10^7$
Tall	5.5	$1.17 \cdot 10^7$	668	250	212	$1.15 \cdot 10^7$
Tall	5.0	$1.17 \cdot 10^7$	668	262	224	$1.15 \cdot 10^7$
Low	7.0	$5.00 \cdot 10^7$	978	289	275	$4.98 \cdot 10^7$
Low	5.0	$5.00 \cdot 10^7$	978	357	340	$4.98 \cdot 10^7$
Low	7.0	$1.17 \cdot 10^7$	771	262	217	$1.15 \cdot 10^7$
Low	5.0	$1.17 \cdot 10^7$	771	314	265	$1.15 \cdot 10^7$

5.10 The Effect of Liquid flow on the MEA Emissions

The solvent flow is, as already mentioned, a key parameter in absorption. An increase in the liquid solvent flow will enhance the wetting and consequently the mass transfer in the absorption. If the solvent flow is too large on the other hand, the residence time of the solvent in the absorber will be short, and it is not able to capture enough CO_2.[63]

Parameter study 3 and 4 showed that there is a trade-off between energy consumption of the process and amine emissions. The cases with the highest reboiler duty resulted in the lowest MEA emissions. The vapour phase MEA emissions are dependent on the vapour temperature in the column. There is a significant concern regarding the amount of amine emitted to the

atmosphere from carbon capture. Degradation products like nitrosamines and nitramines can be carcinogenic and purpose a risk to the human health. As some countries have proposed thresholds to how much amine emissions can be emitted, carbon capture companies might have to increase the energy consumption in order to limit the amine emissions and obtain these thresholds.[25]

A study was done to investigate how the MEA emissions were effected by increasing the liquid flow and thereby the reboiler duty. Case 15 from parameter study 4 was chosen, which capture 90% CO_2. In parameter study 4 it was found that the lowest reboiler duty was 3.57 GJ/t_{CO_2} at a L/G ratio of 2.38 $^{kg}/_{kg}$. The L/G ratio was then increased to 3.51 $^{kg}/_{kg}$, which resulted in a reboiler duty of 4.23 GJ/t_{CO_2} at a 90% capture rate. The liquid-phase profiles for composition and temperature used in the mist model can be found in Appendix C.2.

Table 5.11: Case 15 from parameter study 4 with the L/G ratio that gives the lowest reboiler duty with the corresponding vapour phase MEA emissions after the water wash, and case 15 with an increased L/G ratio with corresponding reboiler duty and vapour phase MEA emissions. Both capture 90% CO_2

	Absorber diameter [m]	Height [m]	L/G [$\frac{kg}{kg}$]	Reboiler [GJ/t_{CO_2}]	Vapour MEA emissions after water wash [ppm]
Case 15	5.5	7.07	2.38	3.57	8.02
Case 15	5.5	7.07	3.51	4.23	4.81

Table 5.11 shows the original case 15 from parameter study 4 with the L/G ratio that gave the lowest reboiler duty and the case at an increased L/G ratio with the corresponding vapour phase MEA emissions after the water wash. The table shows that the vapour-phase MEA emissions have significantly decreased at a higher L/G ratio. The vapour temperature profile in the water wash can be found in Figure 5.22. Only the water wash temperature profile was included, as the trend was the same for the absorber. As the figure shows the temperature in the water wash is lower for the high L/G ratio through the whole column. As already mentioned, the vapour phase emissions are strongly dependent on the temperature, and a lower vapour temperature results in lower vapour emissions.

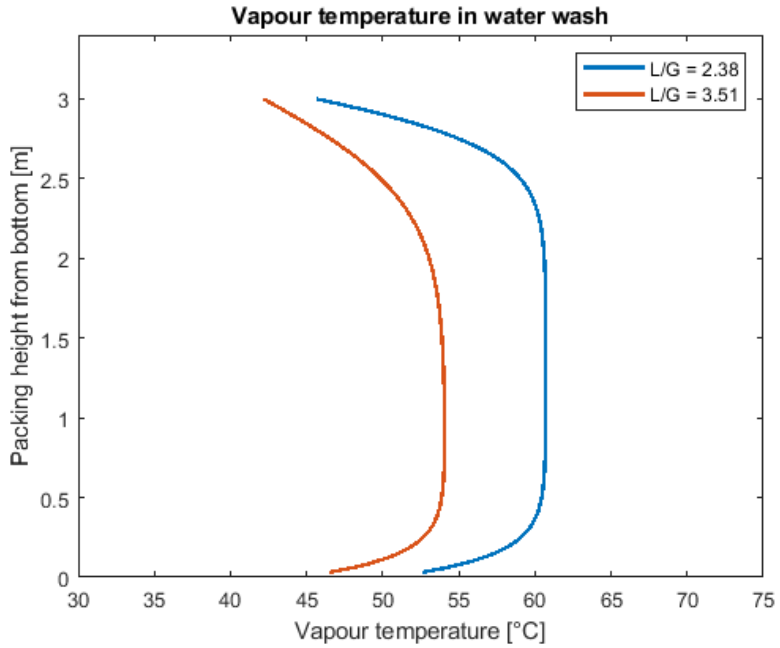

Figure 5.22: Vapour temperature profile in the water wash. Blue line represent L/G = 2.38 $^{kg}/_{kg}$ and orange line L/G = 3.51 $^{kg}/_{kg}$

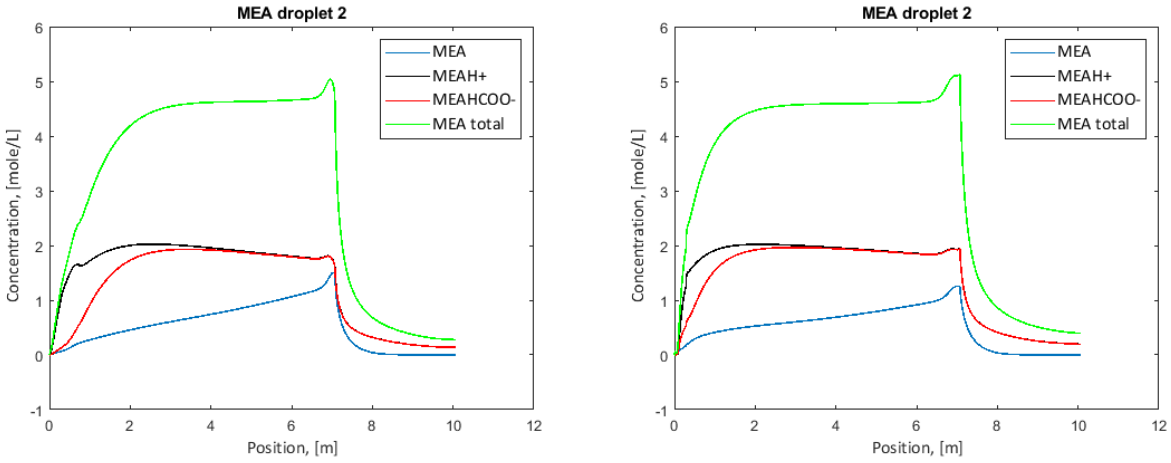

Figure 5.23: (a) MEA concentration for case 15 with a L/G ratio of 2.38 $^{kg}/_{kg}$ at 1.17· 10^7 droplets/cm^3 (b) MEA concentration for case 15 with a L/G ratio of 3.51 $^{kg}/_{kg}$ at 1.17· 10^7 droplets/cm^3

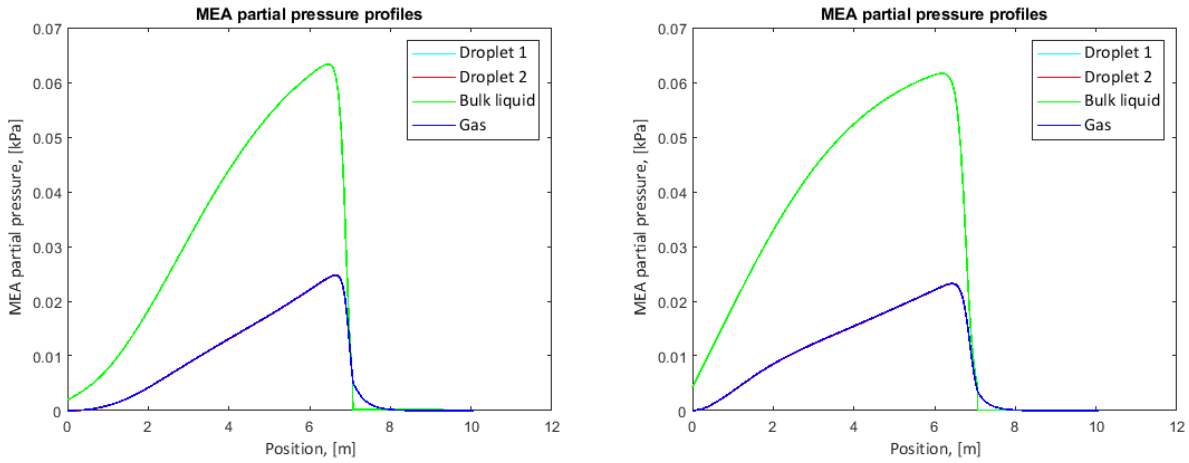

Figure 5.24: (a) MEA partial pressure for case 15 with a L/G ratio of 2.38 $^{kg}/_{kg}$ at 1.17· 10^7 droplets/cm^3 (b) MEA partial pressure for case 15 with a L/G ratio of 3.51 $^{kg}/_{kg}$ at 1.17· 10^7 droplets/cm^3

Figure 5.23 shows the MEA concentration in droplet 2 at a L/G ratio of 2.38 $^{kg}/_{kg}$ and 3.51 $^{kg}/_{kg}$ at 1.17· 10^7 droplets/cm^3. The figure shows that the MEA concentration at the top of the water wash is highest for the case with the highest L/G ratio. The MEA partial pressure profile for both cases are represented in Figure 5.24. It can be observed in two different MEA partial pressure curves that below 5m the partial pressure of MEA is higher for the case with the high L/G ratio. The rich loading when L/G was 3.51 $^{kg}/_{kg}$ was 0.404$^{\text{mole } CO_2}/_{\text{mole MEA}}$, while at 2.38$^{kg}/_{kg}$ the rich loading was 0.440$^{\text{mole } CO_2}/_{\text{mole MEA}}$. The rich loading is lowest for the high L/G ratio, which means that there are more free MEA resulting in a higher partial pressure of MEA in the bulk liquid phase at the bottom of the column. Towards the top of the column the partial pressure becomes approximately the same.

Figure 5.25 showes the droplet diameter for droplet 1 and 2 for case 15 with a L/G ratio of 2.38$^{kg}/_{kg}$ and 3.51$^{kg}/_{kg}$ at 1.17· 10^7 droplets/cm^3. The droplet distributions are shown in Figure 5.26. It can be observed that the difference in droplet diameter is small. This results in very similar droplet distribution, where the larger droplets have been removed for both L/G ratios.

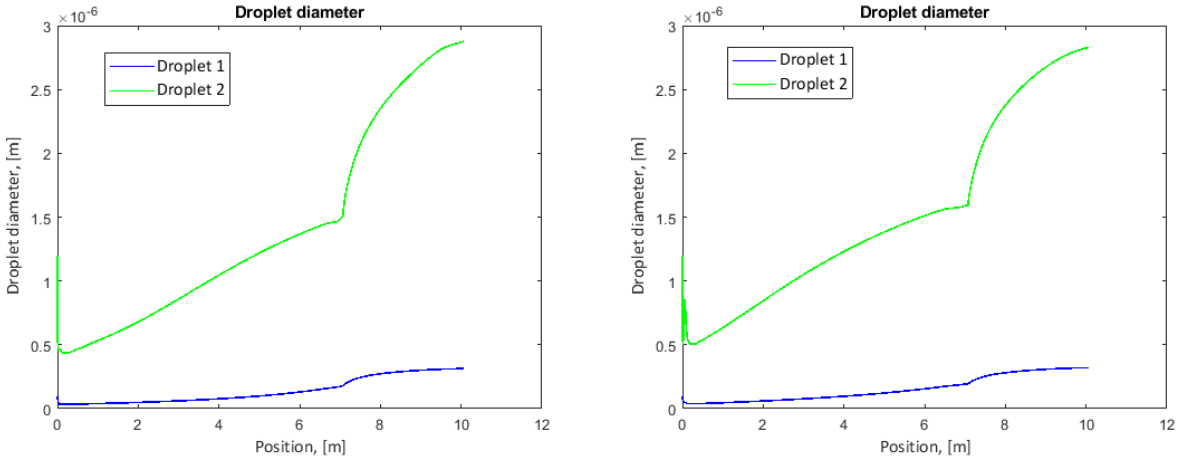

Figure 5.25: (a) Droplet diameter for case 15 with a L/G ratio of 2.38 at 1.17· 10^7 droplets/cm^3 (b) Droplet diameter for case 15 with a L/G ratio of 3.51 at 1.17· 10^7 droplets/cm^3

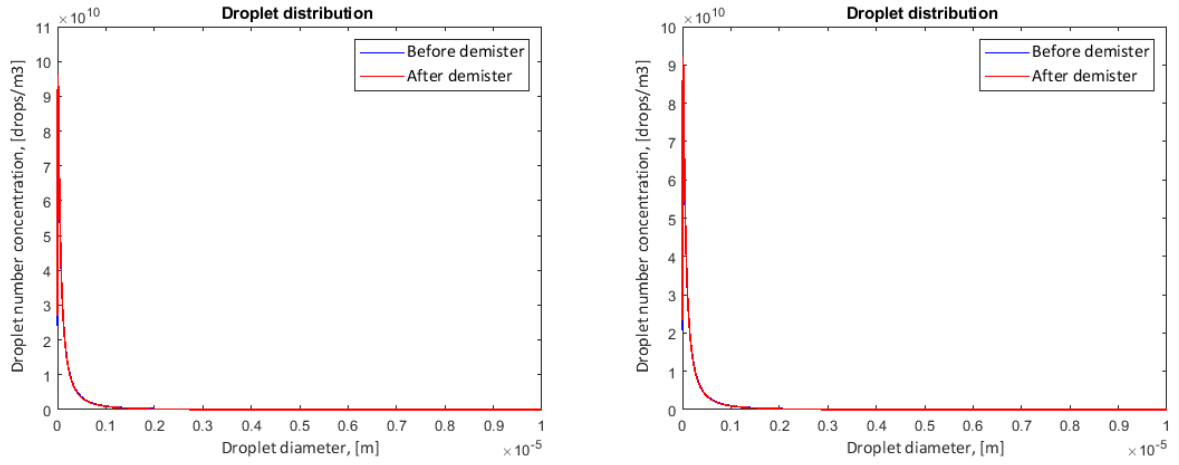

Figure 5.26: (a) Droplet distribution for case 15 with a L/G ratio of 2.38 at 1.17· 10^7 droplets/cm^3 (b) Droplet distribution for case 15 with a L/G ratio of 3.51 at 1.17· 10^7 droplets/cm^3

Table 5.12: Case 1 with L/G ratio of 2.38 $^{kg}/_{kg}$ and 3.51 $^{kg}/_{kg}$ with inlet number concentration, aerosol MEA emissions after the absorber, before the demister and after the demister, and outlet number concentration. Both capture 90% CO_2

	L/G $[\frac{kg}{kg}]$	C_N inlet [droplets/cm^3]	MEA after absorber [ppm]	MEA before demister [ppm]	MEA after demister [ppm]	C_N after demister [droplets/cm^3]
Case 1	2.38	1.17· 10^7	668	262	224	1.15· 10^7
Case 1	3.51	1.17· 10^7	829	353	301	1.15· 10^7

Table 5.12 shows the MEA emissions after the absorber, before the demister and after the demister for the two different L/G ratios. It also includes the inlet and outlet distribution of droplets. Table 5.11 showed that the vapour phase MEA emissions after the water wash were lower for the largest L/G ratio as a result of lower temperature. In table 5.12 is can be observed that the aerosol MEA emissions are actually higher for the largest L/G ratio. The partial pressure of MEA in the liquid bulk phase at the bottom was higher for $3.51^{kg}/_{kg}$ as a result of lower rich loading. This could indicate that the effect of free MEA is more important than the temperature for the increased amount of MEA in the aerosols in this case. It should also be noted that a very short column was used in this study. The absorber column is only 4.36m. That means that there might be some limitations as a result of the low height because the rich loading is a function of the lean loading. The residence time is not large enough in a short column to reach equilibrium at the bottom of the column. Parameter study 2 was performed at a constant height of 21.5m in the absorber column. It was then observed that the rich loading was not affected by increasing the liquid flow, but the lean loading increased. In that case, the aerosol results might be different.

5.11 MEA Emissions with an Isotherm Absorber Column

One problem to overcome for carbon capture technologies is the high energy consumption. A strategy to reduce the energy consumption is to implement intercooling systems. In an intercooled absorber column, a fraction of the liquid is withdrawn, cooled down and sent back into the absorber. Cooling the liquid down enables a shift in the equilibrium, which increases the mass transfer driving force and more CO_2 will be absorbed.[13]

An isotherm column is a column where the temperature is constant. If the temperature of the absorber is kept constant it could possibly decrease the amine emissions of the process. The idea was therefore to simulate an isotherm absorber column to investigate how it effected the MEA emissions. The shortest column from parameter study 4, case 18 was chosen. The absorber was 4.36m tall, with a 7.0m diameter. It is not possible to simulate an isotherm column in CO2SIM. The absorber was therefore split into 9 sections, each of 0.484m. Intercooling was implemented in between each column to keep the temperature as constant as

possible. This case will be referred to as the isotherm column. The liquid-phase profiles for temperature and H_2O and MEA composition can be found in Appendix C.2.

Figure 5.27 shows the liquid and vapour temperature profile in the absorber and water wash for the original case 18 and the isotherm case. It can be observed that the temperature in the absorber for the isotherm case is not completely constant. It varies from 40°C to 45°C. This is a small variation, as the temperature in the original column reaches 74°C at the warmest.

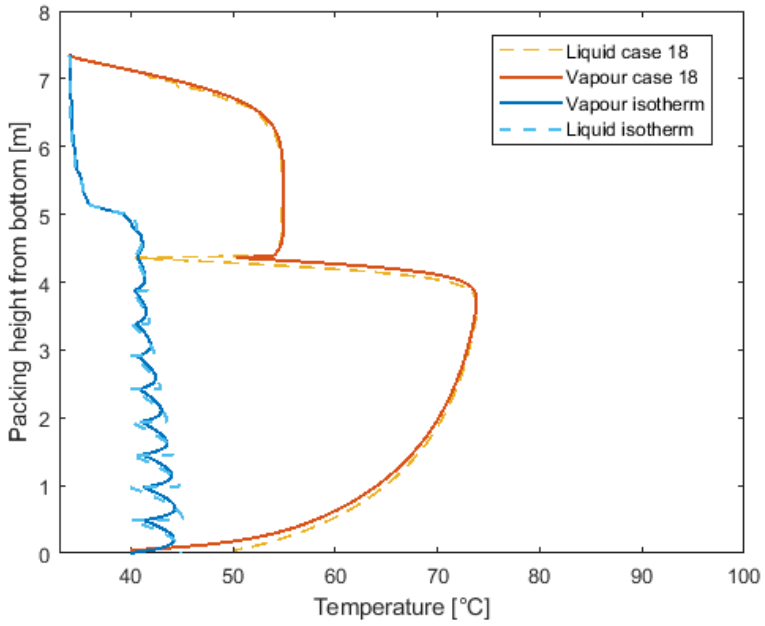

Figure 5.27: Vapour and liquid temperature profile in the absorber and water wash for case 18 and the isotherm case

Table 5.13: Case 18 and isotherm column with corresponding reboiler duty, lean and rich loading, cyclic capacity and vapour phase MEA emissions after the water wash. Both at a 90% capture rate

	Reboiler [GJ/t_{CO_2}]	α_{Lean} [$\frac{\text{mole } CO_2}{\text{mole MEA}}$]	α_{Rich} [$\frac{\text{mole } CO_2}{\text{mole MEA}}$]	Cyclic capacity [$\frac{\text{mole } CO_2}{\text{mole MEA}}$]	Vapour MEA emissions after water wash [ppm]
Case 18	4.35	0.146	0.404	0.258	6.87
Isotherm	3.99	0.151	0.425	0.274	3.55

Table 5.13 shows both cases with reboiler duty, lean and rich loading, cyclic capacity and vapour phase MEA emissions after the water wash. Both cases capture 90% CO_2. The reaction between CO_2 and MEA is exothermic, which result in high temperatures in the absorber column. MEA has high affinity for CO_2 at low temperatures. Decreasing the temperature will consequently increase the CO_2 capture capability. The rich loading is higher for the isotherm case, which means that more CO_2 have been absorbed in the absorber. The cyclic capacity is also higher in the isotherm column which in return results in a lower reboiler duty. The vapour phase MEA emissions at the top of the water wash are lower for the isotherm column. This is a result of the low temperature. The results from the CO2SIM simulation were used in the mist model to investigate if the results were similar for the aerosol emissions. The liquid-phase profiles can be found in Appendix C.2.

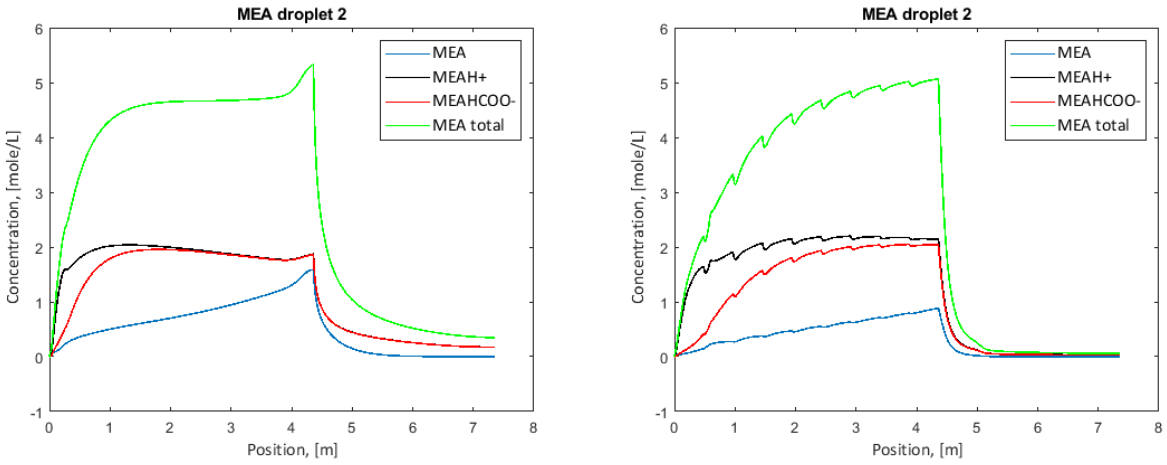

Figure 5.28: (a) MEA concentration in droplet 2 for case 18 at 1.17· 10^7 droplets/cm^3 (b) MEA concentration in droplet 2 for the isotherm column at 1.17· 10^7 droplets/cm^3

Figure 5.28 shows the concentration of MEA in droplet 2 for case 18 and the isotherm column at 1.17· 10^7 droplets/cm^3. It can be observed that the concentration of MEA is much lower at the top of the water wash for the isotherm case. The concentration drops much faster in this case and reaches approximately 0 not far into the water wash. The temperature profiles showed that the temperature is lower in both the absorber and water wash for the isotherm case. For case 18, the MEA in gas phase at the top of the absorber was 42ppm, while for the isoterm case it was 14ppm. This means that there are more MEA in case 18 that is able

to react with the remaining CO_2 and release heat, which results in higher temperatures. In the isotherm case there is a very small amount of MEA entering the water wash, and the concentration of MEA inside the droplet drops fast.

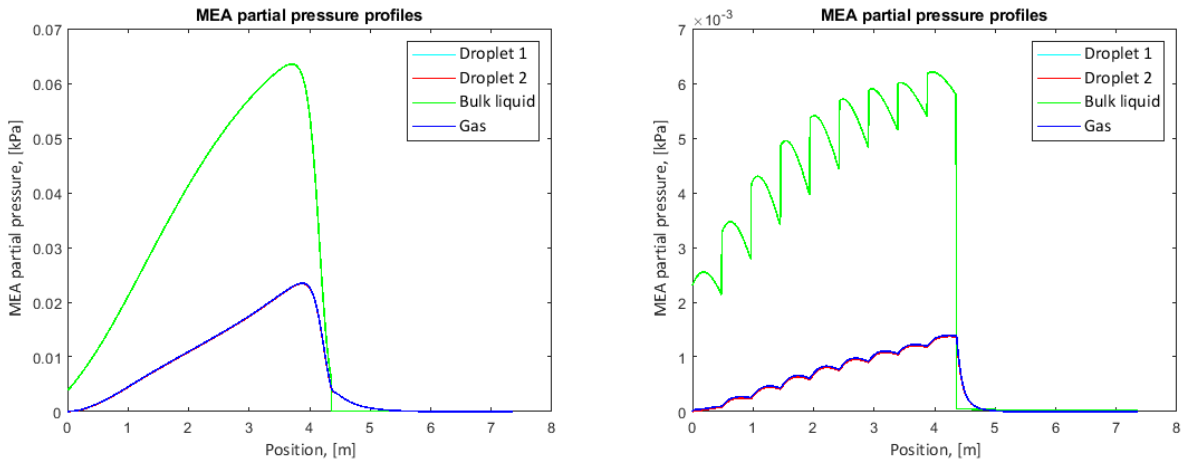

Figure 5.29: (a) MEA partial pressure profile for case 18 at 1.17· 10^7 droplets/cm^3 (b) MEA partial pressure profile for the isotherm column at 1.17· 10^7 droplets/cm^3

The MEA partial pressure profile can be found in Figure 5.29 for both cases. Because of the low temperature, more MEA has been used to capture CO_2. The rich loading was higher in the isotherm case. This means that there is less free MEA in the gas phase. It can be seen that the MEA partial pressure is about 10 times lower for the isotherm column.

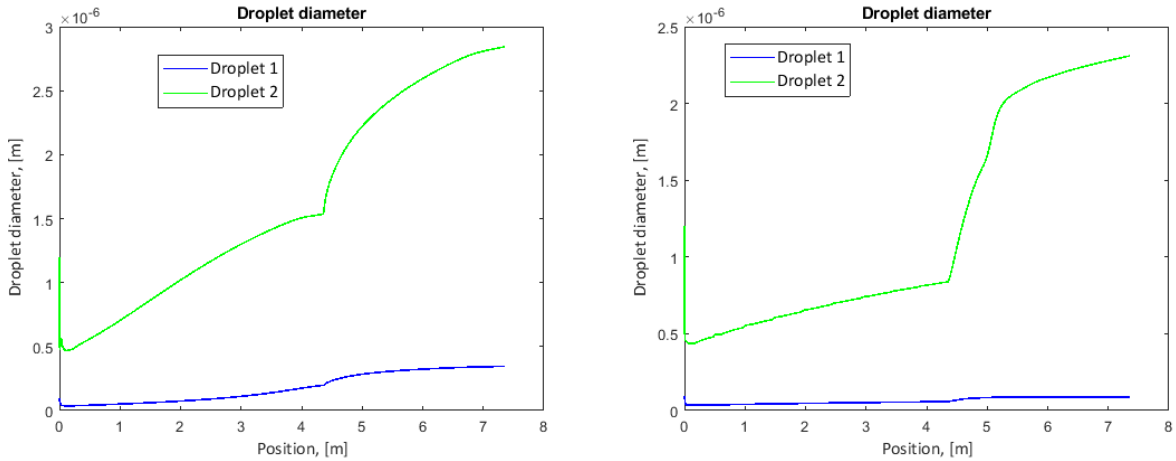

Figure 5.30: (a) Droplet diameter for case 18 at 1.17· 10^7 droplets/cm^3 (b) Droplet diameter for the isotherm column at 1.17· 10^7 droplets/cm^3

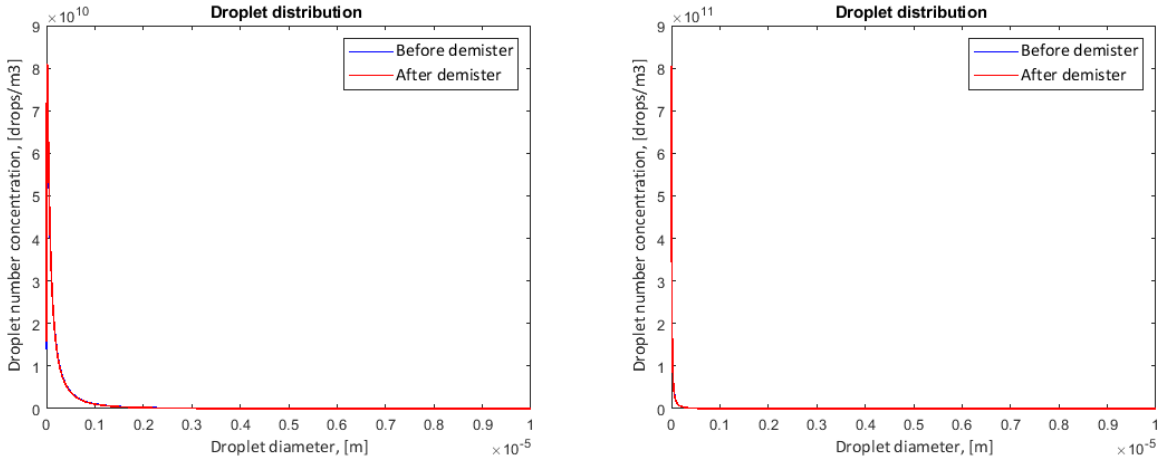

Figure 5.31: (a) Droplet distribution for case 18 at 1.17· 10^7 droplets/cm^3 (b) Droplet distribution for the isotherm column at 1.17· 10^7 droplets/cm^3

Figure 5.30 shows the droplet diameter for both cases. As the figure shows, the droplet diameter is lower for both droplet 1 and 2 in the isotherm case. The droplet distribution is shown in Figure 5.31. It can be observed that in the isotherm case, the distribution is shifted towards very small droplets. Case 18 has much more larger droplets. The inlet and outlet number concentration and MEA emissions after the absorber, before the demister and after demister are shown in Table 5.14. The aerosol MEA emissions are much lower in the isotherm case, almost 10 times lower. In the isotherm case, the concentration of MEA in the gas phase is so low that the transfer of MEA into the droplets from the gas phase is very difficult. The emissions in the non-isotherm case are therefore much higher.

Table 5.14: Case 18 and isotherm column with inlet number concentration, aerosol MEA emissions after the absorber, before the demister and after the demister, and outlet number concentration. Both capture 90% CO_2

	C_N inlet [droplets/cm^3]	MEA after absorber [ppm]	MEA before demister [ppm]	MEA after demister [ppm]	C_N after demister [droplets/cm^3]
Case 18	1.17· 10^7	771	314	265	1.15· 10^7
Isotherm	1.17· 10^7	118	27	26	1.17· 10^7

5.12 Summery of Aerosol Emissions

It has now been shown how the aerosol emissions are affected by different number concentrations, the absorber column and water wash dimensions, different liquid flow rates and in the case of an isotherm column.

It was found that the number concentration have an impact on the final aerosol emissions. A higher number concentration will have a stronger depletion effect as a result of a larger interfacial area and droplet volume. It was also found that the gas-phase was affected by the aerosols while the liquid-phase was unaffected. The highest number concentration resulted in the highest MEA emissions as a result of more droplets. This is in good agreement with what have been found in literature.

Two cases with the same effective mass transfer area were compared. One tall column with a small diameter, and a low column with a larger diameter. It was found that the tall column resulted in lowest total MEA emissions. The droplets were slightly larger in the tall column. The large droplets have the most significant effect for the emissions. As the demister is able to remove the largest droplets, it resulted in the lowest emissions. It was also seen that the water wash and demister were capable of removing aerosols. This is also in agreement with what has been found in published papers. It was also found that the diameter of the water wash, and consequently the gas velocity, had an impact on emissions. The same two cases were used in simulations where the water wash had the same diameter as the absorber, and a smaller diameter. It was found that the gas-phase emissions were only slightly affected by a change in water wash diameter. When including the aerosol emissions, it was found that a smaller diameter led to higher emissions as a result of a lower active area.

Parameter study 3 and 4 showed that increasing the liquid flow at a constant gas flow rate decreased the gas-phase MEA emissions. When including the aerosols it was found that increasing the liquid flow actually resulted in higher emissions. This indicated that free MEA had a larger impact than the temperature on the emissions. An isotherm absorber column was simulated to investigate if it could reduce the emissions. It was found that the isotherm column resulted in the lowest energy consumption and the lowest emissions.

Chapter 6

Conclusion

The main objective of this thesis was to investigate how the absorber design and operating conditions affected the MEA emissions and energy consumption in an absorption-based carbon capture plant. The work involved performing five parameter studies, in which the dimensions of the absorber column, liquid flow rate, mass-transfer area and effective-mass transfer area were adjusted. CO2SIM was used to create a simulation model. This model was used to investigate the vapour-phase MEA emissions, capture rate, loadings and reboiler duty. The pressure drop was found by a generalized pressure-drop correlation. CO2SIM did not take aerosols into account. A mist model was therefore used to investigate the aerosol formation and growth.

It was found that at a constant gas and liquid flow rate, an increase in column diameter results in a reduction in pressure drop. This is the result of a lower gas velocity at a larger diameter. A low pressure drop is beneficial for the energy consumption of the fan that feeds the flue gas into the absorber. The gas-phase emissions were only slightly increased.

Parameter study 2 showed that at a constant height, an increase in the diameter will reduce the reboiler duty at the expense of a larger liquid flow. The reboiler duty depend on the rich and lean loadings. At a constant height the rich loading was unaffected by a change in diameter. The lean loading, on the other hand, increased. This resulted in a lower cyclic capacity. A higher lean loading requires a lower amount of water vapour to achieve an equilibrium CO_2

partial pressure, which means that the reboiler requires less energy. The gas-phase emissions were only slightly decreased.

The work showed that there is a clear trade-off between energy consumption and emissions. Parameter study 3 and 4 showed that the gas-phase MEA emissions can be reduced by increasing the absorber diameter. The gas-phase emissions are strongly dependent on temperature. Increasing the diameter resulted in lower temperature inside the column, which in return results in lower gas-phase emissions. These parameter studies were performed at constant mass-transfer and constant effective mass-transfer area. Increasing the diameter resulted in a lower lean loading which in return increases the reboiler duty. So, vapour amine emissions can be addressed by increasing the absorber diameter at the cost of an increased reboiler duty.

The capture rate was found to decrease with a larger diameter at a constant mass-transfer area because of poor wetting of the packing. If the height was kept constant, an increase in diameter resulted in higher capture rates because the active area increased. This shows that more CO_2 can be captured at the expense of larger absorber column dimensions.

It was found that the aerosol number concentration had a large impact on the final aerosol emissions. The large number concentration resulted in the smallest droplets. Large droplets can be an advantage, as these can possibly be removed by the demister. The large number concentration with many small droplets resulted in the highest MEA emissions.

Both the absorber and water wash dimensions affected the MEA emissions. It was found that a taller absorber column will grow the droplets to a larger size. The large droplets are removed in the demister. In return the total MEA emissions were lower. The demister removed a good amount of the aerosols. Simulations were performed where the water wash had the same diameter as the absorber and a smaller diameter. This showed that the gas-phase emissions were barely affected by a change in the water wash diameter. The aerosol emissions on the other hand were lowest when the diameter were the same in absorber and water wash. This was a result of a higher active area.

Operating at a larger liquid flow will reduce the temperature in the columns. In return, the

gas-phase emissions decrease. The total MEA emissions were found to be higher at a larger liquid flow, as a result of large aerosol emissions. This showed that even though the gas-phase emissions are strongly dependent on the temperature, the amount of free MEA have a large impact as well. Choosing dimensions and operating conditions of the absorber column should therefore be based on both gas-phase and aerosol MEA emissions, as the aerosol have a large contribution on the total MEA emissions.

Finally, an isotherm absorber column was simulated. The simulation showed that an isotherm column will strongly reduce the emissions, and at the same time result in a lower energy consumption.

6.1 Future Work

None of the results, apart from the validation of the model, were compared to experimental data. It is therefore difficult to say how accurate the simulations results were. In the future the results should be backed up by pilot-plant operations and experimental testing.

The simulations that were performed with an increased liquid flow showed that the gas-phase emissions decreased, but the aerosol MEA emissions increased. The simulations were performed with a very low absorber column. The height might be a limitation, and it would be interesting to investigate if these results were different at a more realistic absorber column height.

It was found that an isotherm absorption column will be beneficial for both the MEA emissions and energy consumption. More work should therefore be done to see if this could be a possibility in the reality. If not, an alternative could be to use intercooling at certain points in the absorber. The OPEX and CAPEX for an isotherm column would also be interesting to look into.

The liquid flow, MEA fraction and dimension of the water wash were seen to have a strong effect on the emissions. Studies on the water wash should be performed to optimize the operating conditions of the water wash.

References

[1] B. Dutcher, M. Fan, and A.G. Russell. Amine-based CO_2 capture technology development from the beginning of 2013—a review. *ACS Appl. Mater. Interfaces*, 7(4): 2137–2148, 2015.

[2] H.F. Svendsen, E.T. Hessen, and T. Mejdell. Carbon dioxide capture by absorption, challenges and possibilities. *Chemical Engineering Journal*, 171(2011):718–724, 2010.

[3] J.D. Seader, E.J. Henley, and D.K. Roper. *Separation Process Principles*. New York: Wiley, 1998.

[4] R. Notz, H.P. Mangalapally, and H. Hasse. Post combustion CO_2 capture by reactive absorption: Pilot plant description and results of systematic studies with mea. *International Journal of Greenhouse Gas Control*, 6(2012):84–112, 2011.

[5] I.P.C.C. Climate change 2014 synthesis report summary for policymakers. Technical report, IPCC, 2014.

[6] IEA. Energy technology perspectives 2012; pathways to clean energy system. Technical report, IEA, 2012.

[7] European Commission. Paris agreement. URL `https://ec.europa.eu/clima/policies/international/negotiations/paris_en`.

[8] S. Kaza, L. Yao, P. Bhada-Tata, and F. Van Woerden. *What a Waste 2.0 : A Global Snapshot of Solid Waste Management to 2050*. Washington, DC, USA: World Bank Group, 2018.

[9] P. Wienchol, A. Szle, and M. Ditaranto. Waste-to-energy technology integrated with carbon capture - challenges and opportunities. *Energy*, 198(1):117352, 2020.

[10] David T. Kearns. Waste-to-energy with ccs: A pathway to carbon-negative power generation. Technical report, Global CCS Institute, 2019.

[11] Norwegian Institute of Public Health. CO_2 capture: Health effects of amines and their derivatives. From `https://www.fhi.no/en/publ/2011/co2-capture-health-effects-of-amine/`, 2016.

[12] P. Feron, A. Cousins, K. Jiang, R. Zhai, and M. Garcia. An update of the benchmark post-combustion CO_2-capture technology. *Fuel*, 273(1):117776, 2019.

[13] G. Puxty and M. Maeder. *Absorption-Based Post-Combustion Capture of Carbon Dioxide*. Woodhead Publishing Series in Energy, 2016.

[14] B. Page, G. Turan, A. Zapantis, J. Burrows, C. Consoli, J. Erikson, I. Havercroft, D. Kearns, H. Liu, D. Rassool, E. Tamme, A. Townsend, and T. Zhang. Global status of ccs. Technical report, Global CCS institute, 2020.

[15] T. Spietz, T. Chwola, A. Krótki, A. Tatarczuk, L. Wieclaw-Solny, and A. Wilk. Ammonia emission from co2 capture pilot plant using aminoethylethanolamine. *International Journal of Environmental Science and Technology*, 15(2018):1085–1092, 2017.

[16] Ecoprog. Waste to energy 2020/2021- technologies, plants, projects, players and backgrounds of the global thermal waste treatment business. Technical report, ecoprog GmbH, 2020.

[17] P. Breeze. *Traditional Waste Combustion Technologies*. Academic Press, 2018.

[18] TNO. CO_2 capture: Health effects of amines and their derivatives. URL `https://www.tno.nl/en/focus-areas/energy-transition/roadmaps/towards-co2-neutral-industry/reducing-co2-emissions-through-capture-use-and-storage/co2-capture-with-avr/`.

[19] X. Wu, Y. Yu, Z. Qin, and Z. Zhang. The advances of post-combustion CO_2 capture with

chemical solvents: Review and guidelines. *Energy Procedia*, 63(2014):1339–1346, 2014.

[20] E. A. van Nierop, S. Hormoz, K.Z. House, and M.J. Aziz. Effect of absorption enthalpy on temperature-swing CO_2 separation process performance. *Energy Procedia*, 4(2011): 1783–1790, 2011.

[21] T. Witzøe. Simulation of pilot data with aspen plus. Master's thesis, The Norwegian University of Science and Technology, 2015.

[22] H. Rashid, N. Hasan, M. Nor, and M. Iskandar. Temperature peak analysis and its effect on absorption column for CO_2 capture process at different operating conditions. *Chemical Product and Process Modeling*, 9(2):105–115, 2014.

[23] H. Majeed, H.K. Knuutila, M. Hillestad, and H.F Svendsen. Characterization and modelling of aerosol droplet in absorption columns. *International Journal of Greenhouse Gas Control*, 58(2017):114–126, 2017.

[24] O.M. Bade, J.N. Knudsen, O. Gorset, and I. Askestad. Controlling amine mist formation in CO_2 capture from residual catalytic cracker (rcc) flue gas. *Energy Procedia*, 63 (2014):884–892, 2014.

[25] Scottish Environment Protection Agency. Review of amine emissions from carbon capture systems. Technical report, Scottish Environment Protection Agency, 2013.

[26] N. Yi, M. Fang, W. Di, Z. Xia, T. Wang, and Q. Wang. Aerosol emissions of amine-based CO_2 absorption system: Effects of condensation nuclei and operating conditions. *Environmental Science & Technology*, 55(8):5152–5160, 2021.

[27] P. Khakharia, L. Brachert, J. Mertens, C. Anderlohr, A. Huizinga, E.S. Fernandez, B. Schallert, K. Schaber, T.J.H. Vlugt, and E. Goetheer. Understanding aerosol based emissions in a post combustion CO_2 capture process: Parameter testing and mechanisms. *International Journal of Greenhouse Gas Control*, 34(2015):63–74, 2015.

[28] A. Menon, M. Duss, and C. Bachmann. Post-combustion capture of CO_2. *Petroleum Technology Quarterly*, 14(3):115–121, 2009.

[29] M. Amaratunga. Optimization of gas velocity, pressure drop and column diameter in CO_2 capture. Master's thesis, Telemark University College, 2013.

[30] B.K. Ajibola. Optimization of flooding in an absorption-desorption unit. Master's thesis, Central Ostrobothnia University of Applied Sciences, 2010.

[31] S. Hussain, S. Dayarathna, A. Mathisen, M.C. Melaaen, H. Sørensen, and M. Zarsav. Simulation of CO_2 capture from an aluminium production plant. *WIT Transactions on Ecology and the Environment*, 181(2014):729 – 739, 2014.

[32] N. Razi, H. F. Svendsen, and O. Bolland. Cost and energy sensitivity analysis of absorber design in CO_2 capture with mea. *International Journal of Greenhouse Gas Control*, 19(2013):331–339, 2013.

[33] I.O.A Hodgson. Pressure drop, liquid hold-up and mass transfer in a graphite fibre bed with upward co-current gas-liquid flow. Master's thesis, The University of British Columbia, 1993.

[34] P. Alix and L. Raynal. Liquid distribution and liquid hold-up inmodern high capacity packings. *chemical engineering research and design*, 86(2008):585–591, 2008.

[35] A. Zakeri, A. Einbu, and H.F. Svendsen. Experimental investigation of pressure drop in structured packings. *Chemical Engineering Science*, 73(2012):285–298, 2012.

[36] H. Leifsen. Post-combustion co2 capture using chemical absorption. Master's thesis, The Norwegian University of Science and Technology, 2007.

[37] U. Desideri and A. Paolucci. Performance modelling of a carbon dioxide removal system for power plants. *Energy Conversion and Management*, 40(18):1899–1915, 1999.

[38] O.B. Kallevik. Cost estimation of CO_2 removal in hysys. Master's thesis, Telemark University College, 2010.

[39] L.E. Øi. Aspen hysys simulation of co2 removal by amine absorption from a gas based power plant. Technical report, SIMS2007 Conference, 2007.

[40] H. Leifsen. Post-combustion CO_2 capture using chemical absorption. Master's thesis, The Norwegian University of Science and Technology, 2007.

[41] M. Pilling and D.R. Summers. Be smart about column design. Technical report, American Institute of Chemical Engineers, 2012.

[42] I.R. Krokvik. Screening of aqueous solvent systems for post-combustion co2 capture by chemical absorption. Master's thesis, The Norwegian University of Science and Technology, 2016.

[43] M. Afkhamipour and M. Mofarahi. Review on the mass transfer performance of CO_2 absorption by amine-based solvents in low- and high-pressure absorption packed columns. *RSC Advances*, 1(19):17577–18177, 2017.

[44] L. Hegely, J. Roesler, P. Alix, D. Rouzineau, and M. Meyer. Absorption methods for the determination of mass transfer parameters of packing internals: A literature review. *AIChE Journal*, 63(8):3246–3275, 2018.

[45] L.S. Tana A.M. Shariff K.K. Lau T. Tsuji. Modification of effective surface area correlation for structured packed absorption column at elevated pressures. *Materials Today: Proceedings*, 5(10):22085–22092, 2018.

[46] G. Q. Wang, X. G. Yuan, and K. T. Yu. Review of mass-transfer correlations for packed columns. *nd. Eng. Chem. Res.*, 44(23):8715–8729, 2005.

[47] C. Wang. Mass transfer coefficients and effective area of packing. Master's thesis, The University of Texas at Austin, 2015.

[48] H. Majeed, H.K. Knuutila, M. Hillestad, and H.F Svendsen. Gas phase amine depletion created by aerosol formation and growth. *International Journal of Greenhouse Gas Control*, 64(2017):212–222, 2017.

[49] H. Majeed, H.K. Knuutila, M. Hillestad, and H.F Svendsen. Predicting aerosol size distribution development in absorption columns. *Chemical Engineering Science*, 192 (2018):25–33, 2018.

[50] H. Majeed and H.F Svendsen. Characterization of aerosol emissions from co2 capture

plants treating various power plant and industrial flue gases. *International Journal of Greenhouse Gas Control*, 74(2018):282–295, 2018.

[51] H. Majeed and H.F Svendsen. Effect of water wash on mist and aerosol formation in absorption column. *Chemical Engineering Journal*, 333(2018):636–648, 2017.

[52] J. Mertensa, P. Khakharia, P. Rogiers, J. Blondeau, H. Lepaumier, E. Goetheer, B. Schallert, K. Schaber, and I. Moretti. Prevention of mist formation in amine based carbon capture: field testing using a wet electrostatic precipitator (wesp) and a gas- gas heater (ggh). *Energy Procedia*, 114(2017):987 – 999, 2017.

[53] G. Lombardo, B.F. Fostaas, M.I. Shah, A.K. Morken, O.A. Hvidsten, J. Mertens, and E.S. Hamborg. Results from aerosol measurement in amine plant treating gas turbine and residue fluidized catalytic cracker flue gases at the co2 technology centre mongstad. *Energy Procedia*, 114(2017):1210 – 1230, 2017.

[54] G. Magneschi, Z. Zhang, and R. Munson. The impact of co2 capture on water requirements of power plants. *Energy Procedia*, 114(2017):6337 – 6347, 2017.

[55] J.L. Kang, Y. Zhang, S. Fulk, and G.T. Rochelle. Modeling amine aerosol growth in the absorber and water wash. *Energy Procedia*, 114(2017):959–976, 2017.

[56] C. Madeddu, M. Errico, D. Porcu, and R. Baratti. Solvent recovery system for a CO_2-mea reactive absorption-stripping plant. *Chemical Engineering Transactions*, 74(2019): 805–810, 2019.

[57] R. Notz, H.P. Mangalapally, and H. Hasse. Post combustion CO_2 capture by reactive absorption: Pilot plant description and results of systematic studies with mea. *International Journal of Greenhouse Gas Control*, 6(2012):84–112, 2011.

[58] M. Stec, A. Tatarczuk, L.W. Solny, A. Krótki, T. Spietz, A. Wilk, and D. Spiewak. Demonstration of a post-combustion carbon capture pilot plant using amine-based solvents at the Łaziska power plant in poland. *Clean Techn Environ Policy*, 18(2016): 151–160, 2015.

[59] Aslak Einbu. Co2sim (flytskjema simulator for CO_2 absorp-

sjons prosesser). From https://www.sintef.no/programvare/co2sim-flytskjema-simulator-for-co2-absorpsjons-pr/, 2021.

[60] M. Duss. Packing pressure drop prediction at low operating pressure: Is there anything new? Technical report, Sulzer Chemtech Ltd., 2013.

[61] A. Peeters, A.P.C Faaij, and W.C. Turkenburg. Techno-economic analysis of natural gas combined cycleswith post-combustion CO_2 absorption, including a detailed evaluation of the development potential. *International Journal of Greenhouse Gas Control*, 1(2007):396–417, 2007.

[62] S.K. Saha, G.P. Celata, and S.G. Kandlikar. Thermofluid dynamics of boiling in microchannels. *Advances in Heat Transfer*, 43(2011):77–226, 2011.

[63] X. Zhang, K. Fu, Z. Liang, Z. Yang, W. Rongwong, and Y. Na. Experimental studies of regeneration heat duty for CO_2 desorption from aqueous deta solution in a randomly packed column. *Energy Procedia*, 63(2014):1497 – 1503, 2014.

[64] I. M. Bernhardsen and H. K. Knuutila. A review of potential amine solvents for co2 absorption process: Absorption capacity, cyclic capacity and pka. *International Journal of Greenhouse Gas Control*, 61(2017):27–48, 2017.

[65] M.G. Avili, J.K. Sabet, and S.M. Ghoreishi. Experimental characterization of a random packing with high specificsurface area in a small diameter cryogenic distillation column. *Progress in Nuclear Energy*, 106(2018):417–424, 2018.

[66] Y. Zhang, J.L. Kanga, S. Fulk, and G. Rochelle. Modeling amine aerosol growth at realistic pilot plant conditions. *Energy Procedia*, 114(2017):1045–1060, 2017.

Appendix A

Validation of Simulation Model

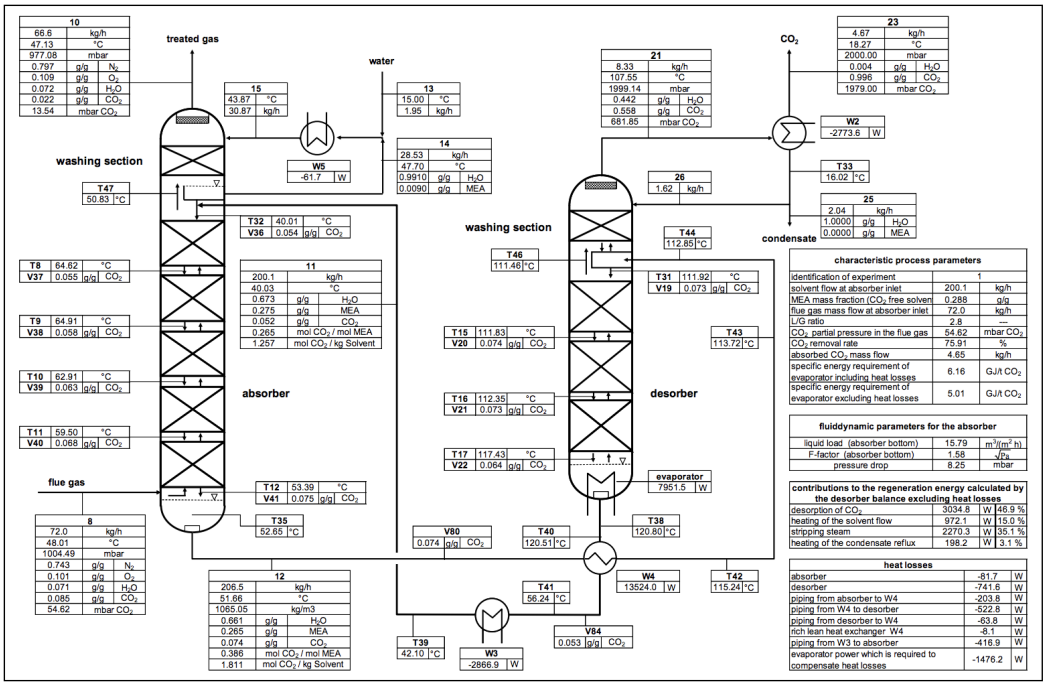

Figure A.1: Flow sheet of the plant used in Notz et al.[4]

Figure A.1 show a flow sheet of the plant used in Notz et al.[4] The absorber column have five packing sections with a water wash on top. The absorber was simulated without the water wash. The packing material is Sulzer Mellapak 250 Y^{TM}. The absorber have a packing height of 4.2 m, and a 0.125 m diameter. The desober have three packing sections, and a water wash

on top. The packing height of the desorber is 2.52 m, with a 0.125 m diameter. The rich flow leaving the absorber enters a flash vessel where it is heated. The flash vessel is located directly above the desorber packing inside the desorber column. The lean flow leaving the desorber is cooled down before it is sent back to the absorber column.

A.1 Data for the Absorber Validation

The results presented for the absorber validation is a summery of the results found in a project that was done during fall 2020 in the subject TKP4580 at NTNU.

The ratio between the simulated and experimental CO_2 absorption rate was calculated. If the ratio is one, the simulated absorption rate is equal to the experimental. The results are listed in Table A.1. This ratio was plotted against the lean loading, vol% of CO_2 in the flue gas, temperature in the flue gas and temperature of lean flow to find systematic errors. The average deviation of the absorption rate was found to be 5.37%. Figure A.2 shows the results for run 1-47. It can be observed that the simulation model predicts the experimental data well, as all deviations are under 20%. The results were both under- and over-predicted. Other parameters in both inlet streams were investigated. Temperature, flow rate and CO_2 content in the flue gas and lean flow were investigated to see if there were any trends for why some results were over- and under-predicted. Nothing stood out as a reason for this prediction.

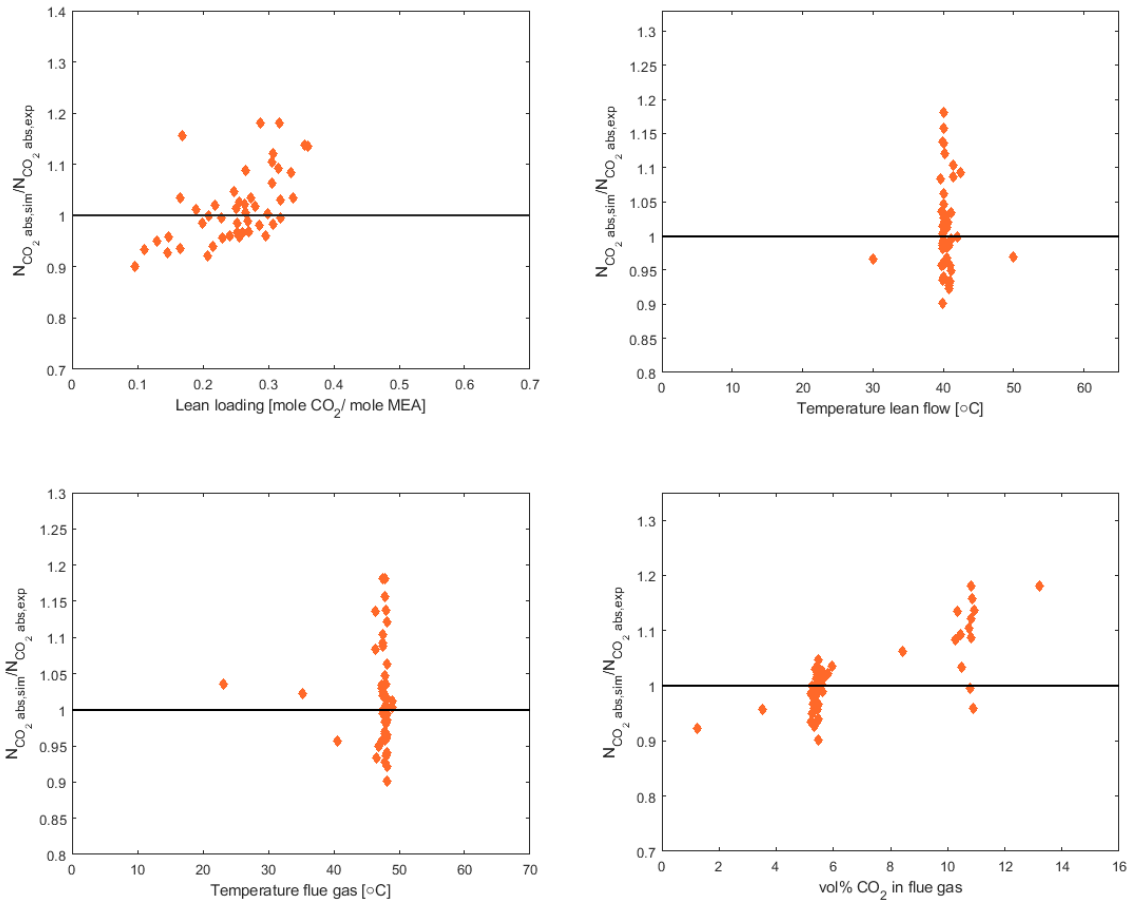

Figure A.2: Plots of ratio between simulated and experimental absorption rate plotted against lean loading, temperature in lean solvent, temperature in flue gas and volume percentage of CO_2 in the flue gas

The experimental data also provided six temperature measurements in the column. These were plotted against the temperature profile from the simulation.

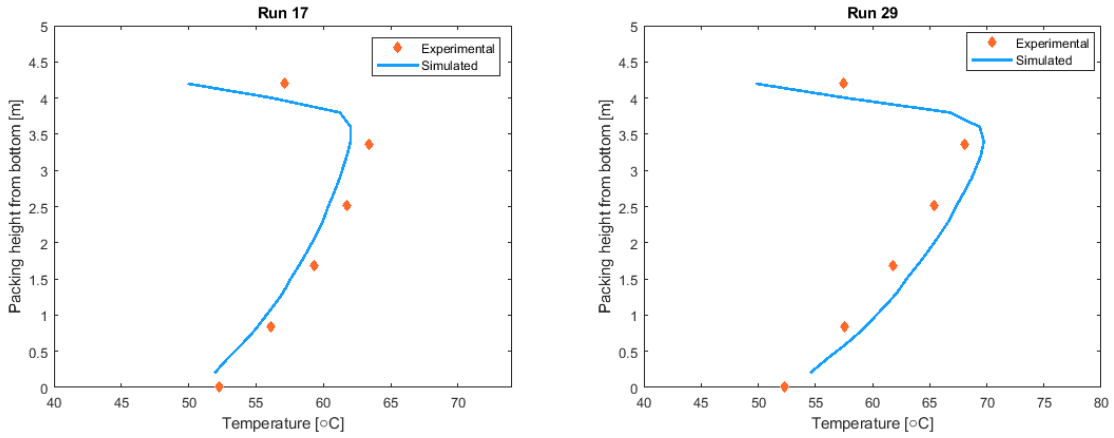

Figure A.3: Temperature profile for simulated and experimental data for run 17 and 29 in validation of the absorber column with experimental data from Notz et al. Blue line shows the simulated temperature and orange diamond shows experimental temperature

Figure A.3 shows the temperature profiles for run 17 and 29. The results from the simulation showed that the prediction was quite accurate. Some small deviations were found. These deviations were both under- and over-predictions. All the simulations had a lower temperature at the top of the column. Notz et al. did not provide a good description of exactly where the measurement points were at the top of the column. This deviation at the top could therefore be a result of different measurement points between simulation and experimental data.

Table A.1: Lean loading, rich loading, absorbed CO_2, percentage deviation and ratio between simulated and experimental absorption rate

	Lean loading	Rich loading		Absorbed CO_2		x_{Abs,CO_2}	$N_{CO_2,abs,sim}/N_{CO_2,abs,exp}$
	$[^{molCO_2}/_{mol\ MEA}]$	$[^{molCO_2}/_{mol\ MEA}]$		[kg/h]		[%]	-
Run	Exp	Exp	Sim	Exp	Sim	-	-
1	0.265	0.386	0.380	4.65	4.68	0.66	1.01
2	0.308	0.464	0.480	6.11	6.85	12.10	1.12
3	0.230	0.308	0.310	3.35	3.21	-4.29	0.96
4	0.268	0.397	0.388	4.83	4.78	-1.02	0.99
5	0.306	0.446	0.454	5.65	6.00	6.27	1.06

6	0.317	0.464	0.495	6.24	7.37	18.13	1.18
7	0.356	0.478	0.491	4.82	5.48	13.76	1.14
8	0.228	0.444	0.440	9.06	9.01	-0.54	0.99
9	0.147	0.393	0.384	10.56	10.12	-4.13	0.96
10	0.299	0.402	0.410	4.34	4.36	0.39	1.00
11	0.280	0.396	0.399	4.59	4.67	1.73	1.02
12	0.256	0.372	0.377	4.76	4.88	2.57	1.03
13	0.287	0.400	0.409	3.53	3.46	-1.87	0.98
14	0.253	0.369	0.369	5.41	5.33	-1.39	0.99
15	0.241	0.359	0.356	6.34	6.09	-3.90	0.96
16	0.096	0.414	0.369	6.37	5.74	-9.85	0.90
17	0.166	0.371	0.364	6.38	5.97	-6.41	0.94
18	0.215	0.387	0.376	6.43	6.05	-5.94	0.94
19	0.247	0.354	0.347	6.43	6.73	4.71	1.05
20	0.261	0.395	0.387	4.71	4.55	-3.39	0.97
21	0.270	0.400	0.388	4.64	4.50	-3.03	0.97
22	0.263	0.389	0.387	4.80	4.91	2.20	1.02
23	0.274	0.393	0.392	4.73	4.90	3.50	1.04
24	0.251	0.392	0.396	4.57	4.63	1.37	1.01
25	0.166	0.435	0.449	4.19	4.34	3.49	1.03
26	0.288	0.474	0.506	5.89	6.96	18.08	1.18
27	0.169	0.501	0.573	5.03	5.82	15.70	1.16
28	0.266	0.470	0.488	6.63	7.21	8.73	1.09
29	0.306	0.465	0.475	6.64	7.33	10.41	1.10
30	0.316	0.459	0.469	6.67	7.29	9.28	1.09
31	0.338	0.454	0.469	6.71	6.94	3.44	1.03
32	0.335	0.449	0.466	6.61	7.16	8.33	1.08
33	0.360	0.441	0.474	6.60	7.50	13.58	1.14
34	0.146	0.417	0.403	4.44	4.12	-7.28	0.93
35	0.208	0.411	0.412	4.55	4.20	-7.77	0.92

36	0.252	0.393	0.401	4.46	4.31	-3.26	0.97
37	0.296	0.398	0.401	4.41	4.23	-4.06	0.96
38	0.308	0.385	0.396	4.50	4.42	-1.67	0.98
39	0.319	0.400	0.403	4.48	4.61	2.96	1.03
40	0.111	0.297	0.276	5.27	4.92	-6.61	0.93
41	0.130	0.297	0.279	5.27	5.00	-5.05	0.95
42	0.190	0.310	0.301	5.26	5.32	1.19	1.01
43	0.200	0.318	0.312	4.98	4.91	-1.39	0.99
44	0.209	0.314	0.306	5.01	5.00	-0.14	1.00
45	0.219	0.324	0.314	5.18	5.28	1.96	1.02
46	0.318	0.417	0.417	4.01	3.99	-0.47	1.00
47	0.255	0.366	0.371	4.86	4.65	-4.26	0.96

Table A.1 shows the lean loading in the experimental data. It also includes rich loading and absorbed CO_2 in [kg/h] for simulation and experimental data, the percentage deviation and ratio between simulated and experimental absorption rate.

A.2 Data for the Desorber Validation

The results presented for the desorber validation is a summery of the results found in a project that was done during fall 2020 in the subject TKP4580 at NTNU.

The ratio between the simulated and experimental desorption rate was calculated. The results from these simulation are listed in Table A.2. The ratio between the desorption rates was plotted against the rich loading, rich solvent flow, reboiler duty and temperature of the rich solvent. Figure A.4 shows the results of these plots. The average deviation in desorption rate was found to be 14.30%.

Figure A.4 shows that all the simulations were under-predicted. The deviation between sim-

ulated and experimental desorption rate varies from -1.1% to -40%. Run 19 and 44 stands out with the highest deviation of 36% and 40% respectively. By examining the data for these runs nothing stood out as the reason for why these two had higher deviations than the other simulations. Several runs were performed at similar conditions, like run 1, 4 and 12. Even then, the deviation between simulation and experimental desorption rate varies from -2% to -15%.

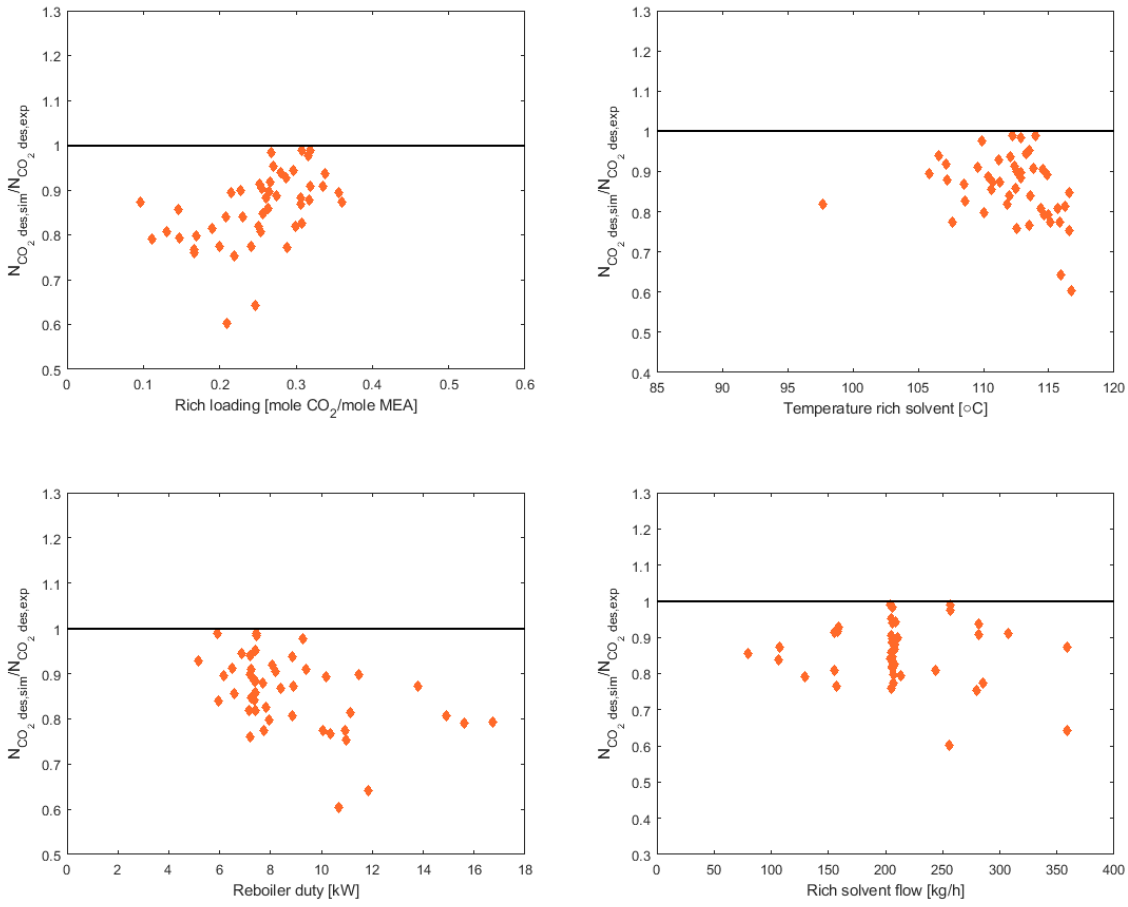

Figure A.4: Plots of ratio between simulated and experimental desorption rate plotted against rich loading, temperature in rich solvent flow, reboiler duty and rich solvent flow

The experimental data also provided temperature measurements for the liquid phase in the desorber column. These were plotted against the temperature profiles from the simulation. This can be seen in Figure A.5

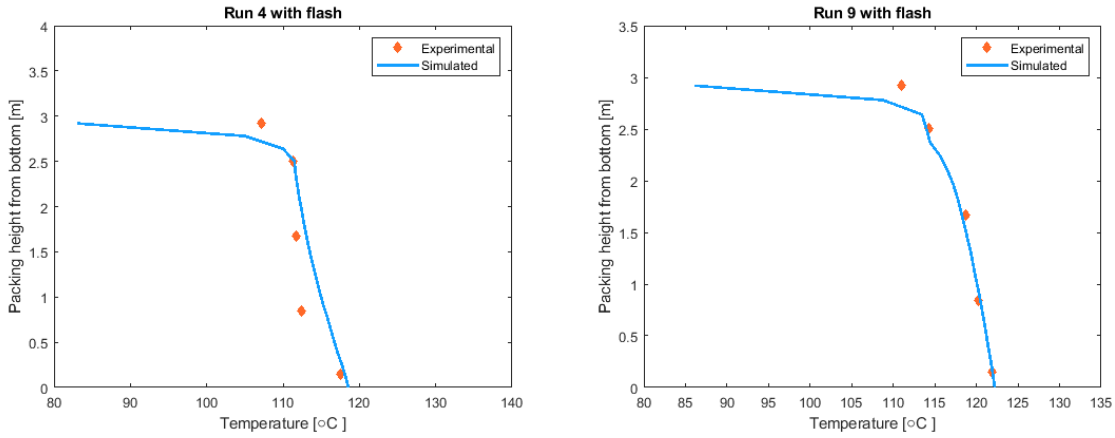

Figure A.5: Temperature profile for simulated and experimental data for run 4 and 9 in validation of the desorber column with experimental data from Notz et al. Blue line shows the simulated temperature and orange diamond shows experimental temperature

Figure A.5 shows the temperature profiles for run 4 and 9. The simulated results gave a good prediction of the experimental temperatures. The deviation was below 1°C, which is a small deviation.

Table A.2: Lean loading, rich loading, desorbed CO_2, percentage deviation and ratio between simulated and experimental desorption rate

	Lean loading		Rich loading	Desorbed CO_2		x_{Des,CO_2}	$N_{CO_2,des,sim}/N_{CO_2,des,exp}$
	$[^{molCO_2}/_{mol\ MEA}]$		$[^{molCO_2}/_{mol\ MEA}]$	[kg/h]		[%]	-
Run	Exp	Sim	Exp	Exp	Sim	-	-
1	0.265	0.278	0.386	4.88	4.38	-10.20	0.90
2	0.308	0.333	0.464	6.48	5.35	-17.40	0.83
3	0.230	0.249	0.308	3.07	2.58	-15.9	0.84
4	0.268	0.276	0.397	4.88	4.80	-1.70	0.98
5	0.306	0.322	0.446	5.76	5.09	-11.70	0.88
6	0.317	0.337	0.464	6.08	5.34	-12.10	0.88
7	0.356	0.367	0.478	4.74	4.24	-10.50	0.90
8	0.228	0.247	0.444	9.15	8.22	-10.10	0.90

9	0.147	0.196	0.393	10.67	8.47	-20.70	0.79
10	0.299	0.318	0.402	4.28	3.50	-18.00	0.82
11	0.280	0.287	0.396	4.65	4.37	-6.00	0.94
12	0.256	0.279	0.372	4.63	3.92	-15.30	0.85
13	0.287	0.287	0.400	3.41	3.16	-7.20	0.93
14	0.253	0.277	0.369	5.19	4.19	-19.20	0.81
15	0.241	0.271	0.359	6.34	4.90	-22.70	0.77
16	0.096	0.138	0.414	6.57	5.73	-12.70	0.87
17	0.166	0.216	0.371	6.20	4.75	-23.40	0.77
18	0.215	0.233	0.387	6.32	5.65	-10.70	0.89
19	0.247	0.278	0.354	6.86	4.40	-35.80	0.64
20	0.261	0.273	0.395	4.98	4.39	-11.70	0.88
21	0.270	0.274	0.400	4.99	4.76	-4.80	0.95
22	0.263	0.279	0.389	4.59	3.94	-14.20	0.86
23	0.274	0.284	0.393	4.42	3.92	-11.30	0.89
24	0.251	0.286	0.392	3.95	3.23	-18.20	0.82
25	0.166	0.227	0.435	4.18	3.17	-24.10	0.76
26	0.288	0.326	0.474	5.93	4.58	-22.70	0.77
27	0.169	0.268	0.501	5.04	4.02	-20.30	0.80
28	0.266	0.291	0.470	6.75	6.19	-8.20	0.92
29	0.306	0.327	0.465	6.94	6.02	-13.20	0.87
30	0.316	0.330	0.459	6.29	6.14	-2.40	0.98
31	0.338	0.346	0.454	6.05	5.67	-6.30	0.94
32	0.335	0.351	0.449	6.33	5.75	-9.10	0.91
33	0.360	0.371	0.441	5.96	5.20	-12.70	0.87
34	0.146	0.186	0.417	4.46	3.82	-14.40	0.86
35	0.208	0.233	0.411	4.68	3.93	-16.10	0.84
36	0.252	0.263	0.393	4.31	3.93	-8.80	0.91
37	0.296	0.294	0.398	4.44	4.19	-5.60	0.94
38	0.308	0.309	0.385	4.27	4.22	-1.10	0.99

39	0.319	0.318	0.400	4.39	3.98	-9.20	0.91
40	0.111	0.151	0.297	5.44	4.30	-20.90	0.79
41	0.130	0.165	0.297	5.42	4.38	-19.20	0.81
42	0.190	0.216	0.310	5.18	4.21	-18.70	0.81
43	0.200	0.230	0.318	5.09	3.95	-22.50	0.78
44	0.209	0.241	0.314	5.13	3.09	-39.70	0.60
45	0.219	0.249	0.324	5.65	4.25	-24.70	0.75
46	0.318	0.322	0.417	3.75	3.71	-1.20	0.99
47	0.255	0.265	0.366	4.57	4.13	-9.60	0.90

Table A.2 shows the rich loading in the experimental data. It also includes lean loading and desorbed CO_2 in [kg/h] for simulation and experimental data, the percentage deviation and ratio between simulated and experimental desorption rate.

A.3 Validation with the e-NRTL Termo Package

The simulations described above were performed with the Astarita thermo package in CO2SIM. The mist model uses the e-NRTL model. Some extra simulations were performed with the e-NRTL model in CO2SIM to assess whether the results changed. Only the absorber results are included. Figure A.6 shows the temperature profile for the experimental data and the CO2SIM simulation of the absorber simulation with the e-NRTL thermo package.

As Figure A.6 show, the temperature profiles from the CO2SIM simulation were in good agreement with the experimental data.

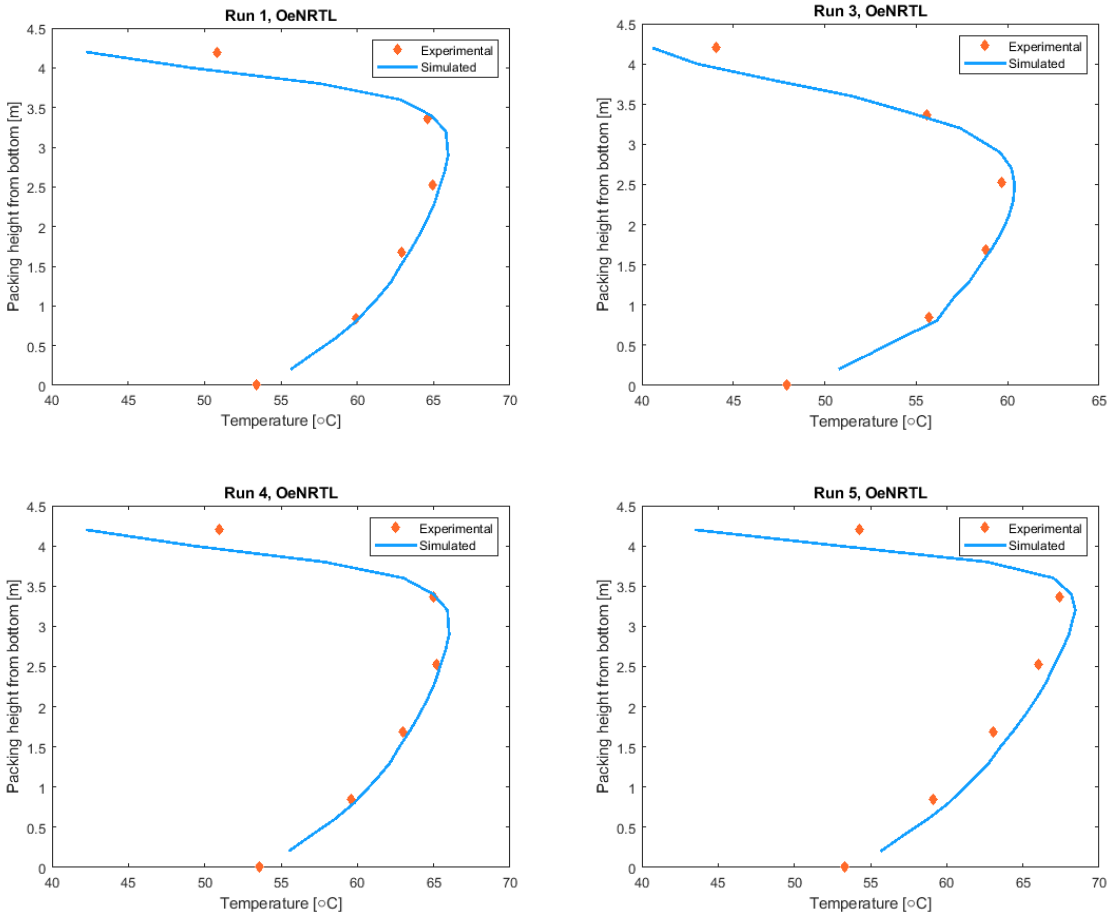

Figure A.6: Temperature profile for experimental data and simulation of the absorber with the e-NRTL termo package. Orange diamonds represent the experimental temperature, blue line is the simulation temperature

Table A.3: Percentage deviation in absorption rate for simulation 1, 3, 4 and 5 with two different termo packages, e-NRTL and Astarita

	$x_{\mathrm{Abs,CO_2}}$	
Run	OeNRTL	Astarita
1	0.68	0.66
3	-4.69	-4.29
4	-2.38	-1.20
5	3.97	6.27

Table A.3 show the percentage deviation in absorption rate for simulation 1, 3, 4 and 5 with the termo packages e-NRTL and Astarita. Only 4 cases are included, as the trend were the same for the other cases validated. As the table show, the results were in good agreement with each other.

A.4 Conclusion of the Validation

The validation was performed with two different thermo packages, Astarita and e-NRTL. The percentage deviation in absorption rate for both thermo packages was in good agreement with each other and the experimental data. The temperature profiles also gave a good representation of the experimental data. It was concluded that the deviations between simulated data and experimental data were acceptable, and that the model could be used for further modeling.

Appendix B

Sensitivity Analysis of the Water wash

A sensitivity analysis of the water wash were performed in order to evaluate how large the circulation flow and mole fraction of MEA should be. The first analysis was performed at a constant fraction of MEA. The weight percentage of MEA was set to be 1.31wt%. The liquid flow was then varied from 73.9 $\mathrm{kg\,s^{-1}}$ to 455.8 $\mathrm{kg\,s^{-1}}$. The results can be found in Table B.1.

Table B.1 shows that the gas-phase MEA emissions decrease as the liquid flow increases. The emissions eventually stabilizes at approximately 202.6$\mathrm{kg\,s^{-1}}$.

The second analysis was performed at a constant liquid flow rate. The weight percentage of MEA into the water wash was then varied. The results can be found in Table B.2. It can be observed that the gas-phase emissions of MEA increase as the wt% of MEA into the water was increases.

Table B.1: Gas-phase MEA emissions for the sensitivity analysis of the water wash at a constant weight percentage of MEA and varying liquid flow rate

Liquid flow rate $[\mathrm{kg\,s^{-1}}]$	MEA into water wash [wt%]	Gas-phase emission [ppm]
73.9	1.31	7.033
76.0	1.31	6.980
80.2	1.31	6.871
83.6	1.31	6.768
88.6	1.31	6.600
101.3	1.31	6.079
126.6	1.31	5.318
141.8	1.31	3.777
151.9	1.31	2.685
177.2	1.31	2.630
202.6	1.31	2.601
253.2	1.31	2.590
354.5	1.31	2.590
405.1	1.31	2.590
455.8	1.31	2.590

Table B.2: Gas-phase MEA emissions for the sensitivity analysis of the water wash at a constant liquid flow rate and varying weight percentage of MEA

Liquid flow rate $[\mathrm{kg\,s^{-1}}]$	MEA into water wash [wt%]	Gas-phase emission [ppm]
80.2	0.54	3.230
80.2	0.57	3.387
80.2	0.67	3.859
80.2	0.83	4.332
80.2	0.84	4.648
80.2	1.01	5.106
80.2	1.10	5.914
80.2	1.31	6.871
80.2	1.41	7.353
80.2	1.50	7.834
80.2	1.62	8.314
80.2	1.73	8.956
80.2	1.82	9.441

Appendix C

Additional Data from Simulations

C.1 Temperature Profiles for case 15 and 18

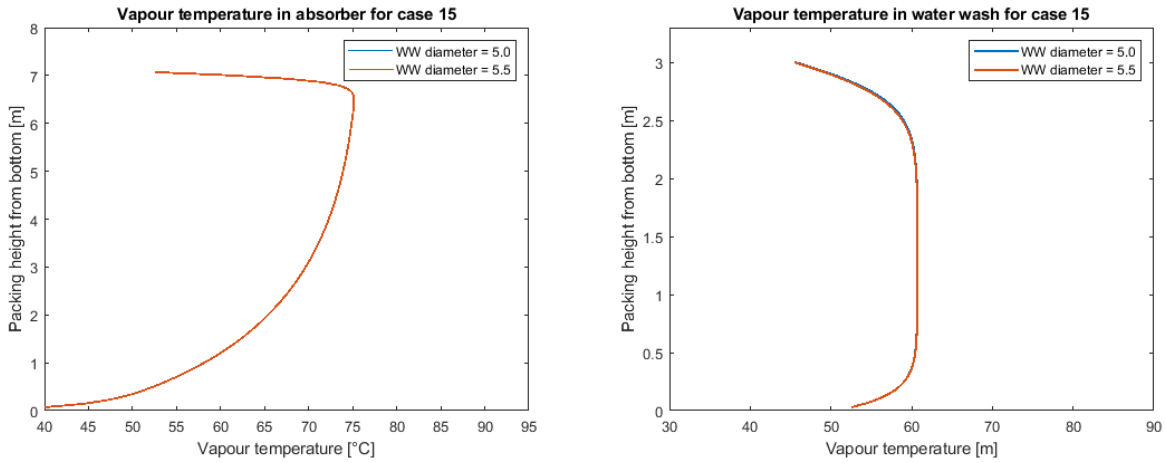

Figure C.1: (a) Vapour temperature in the absorber for case 15 with a water wash diameter of 5.5m and 5m (b) Vapour temperature in the water wash for case 15 with a water wash diameter of 5.5m and 5m

Figure C.1 shows the vapour temperature in the absorber and water wash for case 15 at a water wash diameter of 5.5m and 5.0m. Figure C.2 shows the vapour temperature in the absorber and water wash for case 18 at a water wash diameter of 7.0m and 5.0m.

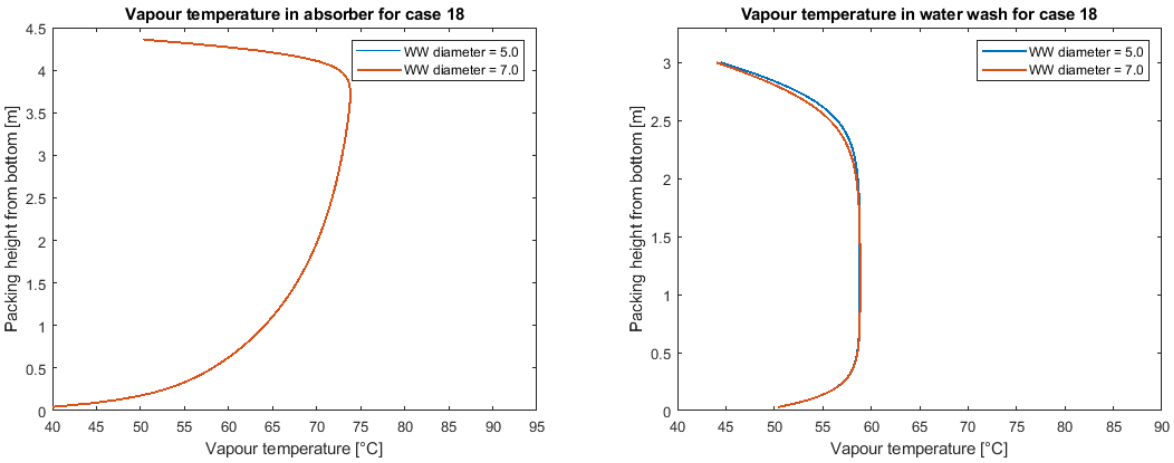

Figure C.2: (a) Vapour temperature in the absorber for case 18 with a water wash diameter of 7.0m and 5m (b) Vapour temperature in the water wash for case 18 with a water wash diameter of 7.0m and 5m

C.2 Liquid-phase Profiles used in the Mist Model

The mist model require the liquid-phase profiles for temperature and composition of MEA and water. The results from CO2SIM are used. The liquid-phase results for the cases modeled with the mist model is shown in this section.

Figure C.3 shows the liquid temperature and mole fraction of H_2O and MEA in the absorber and water wash for case 15 and 18. These were used for the results found in Section 5.7 and 5.8.

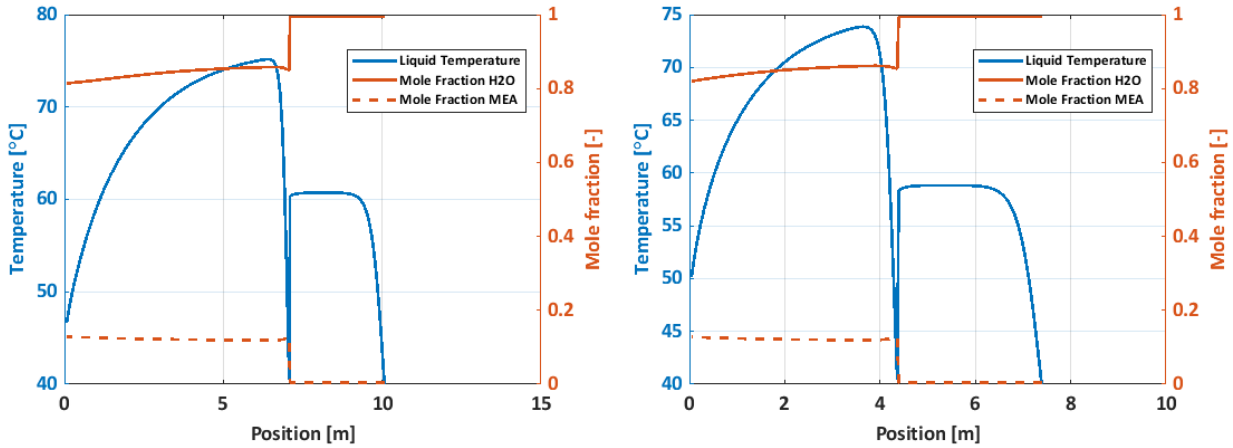

Figure C.3: (a) Liquid temperature, mole fraction of H_2O and MEA for case 15 from CO2SIM (b) Liquid temperature, mole fraction of H_2O and MEA for case 18 from CO2SIM

Figure C.4 shows the liquid temperature and mole fraction of H_2O and MEA in the absorber and water wash for case 15 and 18 where the diameter in the water wash were the same as the absorber. These were used for the results found in Section 5.9.

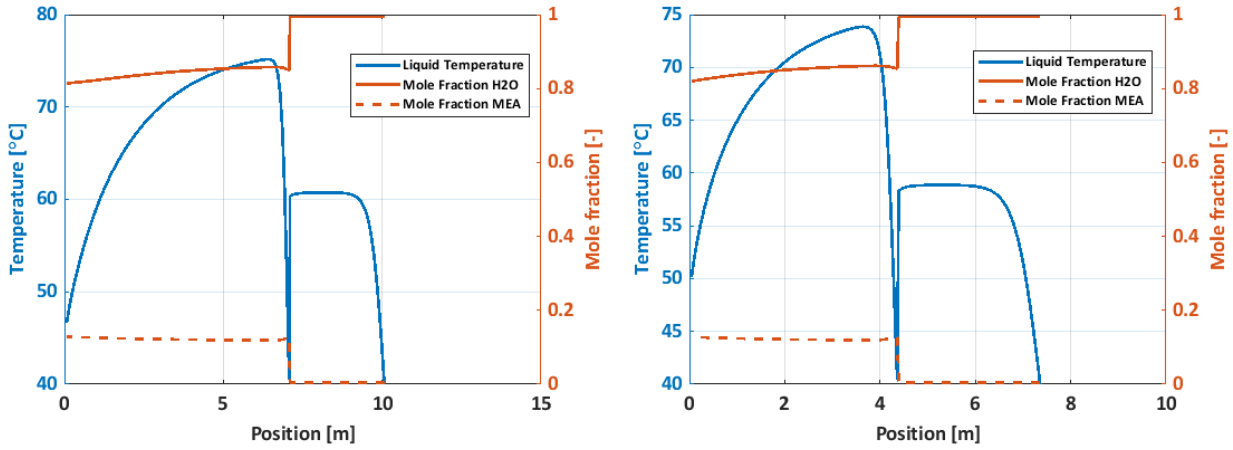

Figure C.4: (a) Liquid temperature, mole fraction of H_2O and MEA for case 15 where the diameter was adjusted to be the same in the absorber and water wash (b) Liquid temperature, mole fraction of H_2O and MEA for case 18 where the diameter was adjusted to be the same in the absorber and water wash

Figure C.5 (a) shows the liquid temperature and mole fraction of H_2O and MEA in the absorber and water wash for case 15 where the liquid flow rate was increased, and the L/G ratio was 3.51 kg/kg. This was used for the results in Section 5.10. Figure C.5 (b) showd the liquid temperature and mole fraction of H_2O and MEA in the absorber and water wash for the isotherm case. This was used for the results in Section 5.11

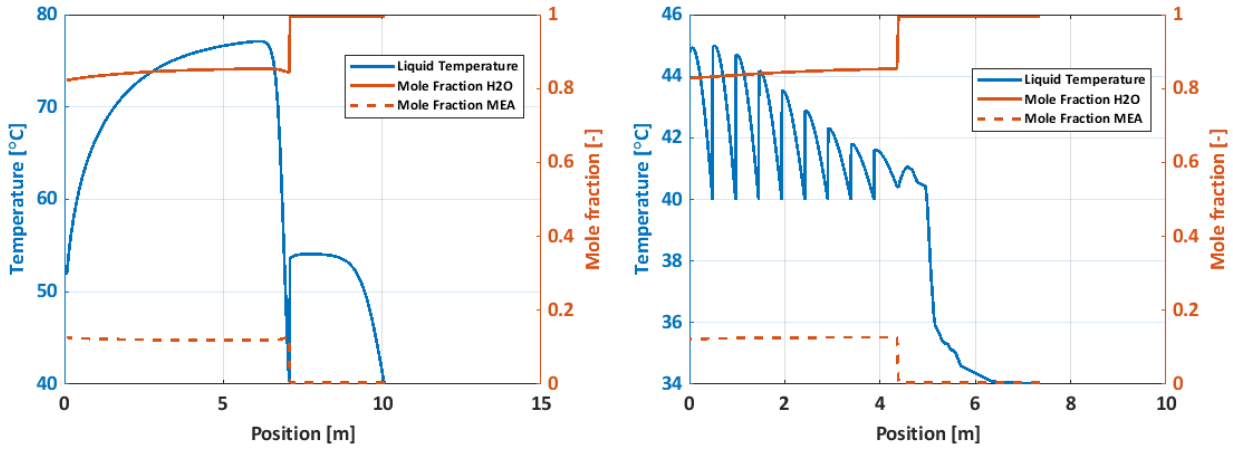

Figure C.5: (a) Liquid temperature, mole fraction of H_2O and MEA for case 15 where the L/G ratio was increased to 3.51 kg/kg (b) Liquid temperature, mole fraction of H_2O and MEA for the isotherm case

C.3 Simulation Data for Base Case and Case 1-18

A summery of the composition, flow rate and temperature in the base case and case 1-18 are shown in Table C.1. The table shows the flue gas and lean flow into the absorber, the rich flow and the gas flow at the top of the absorber. The liquid flow into the water wash and treated gas is also included. The flow sheet can be found in Section 4.3 in Figure 4.1

Table C.1: Flue gas, lean flow, rich flow, gas flow at the top of the absorber, liquid flow into the water wash and treated gas for the base case and case 1-18 with the total flow rate, composition, temperature and pressure

	Stream	CO_2	H_2O	MEA	N_2	Flow	T	P
	-	[wt%]	[wt%]	[wt%]	[wt%]	[$kg\,s^{-1}$]	°C	kPa
Base case	Flue gas	15.8	4.4	0	79.9	48.0	40	105
	Lean flow	4.5	63.3	32.3	0	101.3	40	105
	Rich flow	11.0	57.5	31.5	0	103.4	43	105
	Top abs.	1.5	14.7	0.21	83.6	45.9	54	105
	Liq. WW	0.5	98.2	1.3	0	80.2	40	105
	Treated gas	1.6	8.9	0.002	89.5	42.9	46	105
Case 1	Flue gas	15.8	4.4	0	79.9	48.0	40	105
	Lean flow	4.5	63.3	32.3	0	101.3	40	105
	Rich flow	11.0	57.5	31.5	0	103.4	43	105
	Top abs.	1.5	14.7	0.21	83.6	45.9	54	105
	Liq. WW	0.5	98.2	1.3	0	80.2	40	105
	Treated gas	1.6	8.9	0.002	89.5	42.9	46	105
Case 2	Flue gas	15.8	4.4	0	79.9	48.0	40	105
	Lean flow	4.5	63.3	32.3	0	101.3	40	105
	Rich flow	11.0	57.5	31.5	0	103.4	43	105
	Top abs.	1.5	14.7	0.21	83.6	45.9	54	105
	Liq. WW	0.5	98.2	1.3	0	80.2	40	105
	Treated gas	1.6	8.9	0.002	89.5	42.9	46	105

	Flue gas	15.8	4.4	0	79.9	48.0	40	105
	Lean flow	4.5	63.3	32.3	0	101.3	40	105
	Rich flow	11.0	57.5	31.5	0	103.4	43	105
Case 3	Top abs.	1.5	14.7	0.21	83.6	45.9	54	105
	Liq. WW	0.5	98.2	1.3	0	80.2	40	105
	Treated gas	1.6	8.9	0.002	89.5	42.9	46	105
	Flue gas	15.8	4.4	0	79.9	48.0	40	105
	Lean flow	4.5	63.3	32.3	0	101.3	40	105
	Rich flow	11.0	57.5	31.5	0	103.4	43	105
Case 4	Top abs.	1.5	14.7	0.21	83.6	45.9	54	105
	Liq. WW	0.5	98.2	1.3	0	80.2	40	105
	Treated gas	1.6	8.9	0.002	89.5	42.9	46	105
	Flue gas	15.8	4.4	0	79.9	48.0	40	105
	Lean flow	4.5	63.3	32.3	0	101.3	40	105
	Rich flow	11.0	57.5	31.5	0	103.4	43	105
Case 5	Top abs.	1.7	14.6	0.20	83.6	45.9	54	105
	Liq. WW	0.5	98.2	1.3	0	80.2	40	105
	Treated gas	1.8	8.8	0.002	89.5	42.9	46	105
	Flue gas	15.8	4.4	0	79.9	48.0	40	105
	Lean flow	5.6	62.3	32.0	0	128.3	40	105
	Rich flow	10.7	57.9	31.4	0	130.7	44	105
Case 6	Top abs.	1.7	14.0	0.21	84.1	45.6	52	105
	Liq. WW	0.5	98.2	1.3	0	80.2	40	105
	Treated gas	1.7	8.4	0.002	89.9	42.7	46	105
	Flue gas	15.8	4.4	0	79.9	48.0	40	105
	Lean flow	5.6	62.3	32.0	0	124.9	40	105
	Rich flow	10.7	57.9	31.4	0	130.7	45	105
Case 7	Top abs.	1.7	14.0	0.21	84.1	45.6	46	105
	Liq. WW	0.5	98.2	1.3	0	80.2	40	105

	Treated gas	1.7	8.4	0.002	89.8	42.7	46	105
	Flue gas	15.8	4.4	0	79.9	48.0	40	105
	Lean flow	5.6	62.3	32.0	0	127.3	40	105
	Rich flow	10.7	57.9	31.4	0	130.7	45	105
Case 8	Top abs.	1.7	14.0	0.21	84.1	45.6	51	105
	Liq. WW	0.5	98.2	1.3	0	80.2	40	105
	Treated gas	1.7	8.4	0.002	89.8	42.7	46	105
	Flue gas	15.8	4.4	0	79.9	48.0	40	105
	Lean flow	5.6	62.3	32.0	0	128.3	40	105
	Rich flow	10.7	57.9	31.4	0	130.7	44.6	105
Case 9	Top abs.	1.7	14.0	0.21	84.1	45.6	51	105
	Liq. WW	0.5	98.2	1.3	0	80.2	40	105
	Treated gas	1.7	8.4	0.002	89.8	42.7	46	105
	Flue gas	15.8	4.4	0	79.9	48.0	40	105
	Lean flow	3.7	63.9	32.4	0	86.8	40	105
	Rich flow	11.1	57.3	31.6	0	88.6	43	105
Case 5b	Top abs.	2.1	14.7	0.20	83.1	46.0	56	105
	Liq. WW	0.5	98.2	1.3	0	80.2	40	105
	Treated gas	2.2	9.0	0.002	88.9	43.2	47	105
	Flue gas	15.8	4.4	0	79.9	48.0	40	105
	Lean flow	3.7	63.9	32.4	0	86.8	40	105
	Rich flow	11.1	57.2	31.6	0	88.6	43	105
Case 6b	Top abs.	2.0	14.7	0.2	83.1	46.0	56	105
	Liq. WW	0.5	98.2	1.3	0	80.2	40	105
	Treated gas	2.1	9.0	0.002	88.9	42.9	47	105
	Flue gas	15.8	4.4	0	79.9	48.0	40	105
	Lean flow	3.7	63.9	32.4	0	86.8	40	105
	Rich flow	11.1	57.2	31.6	0	88.5	43	105
Case 7b	Top abs.	1.9	14.8	0.2	83.1	46.0	55	105
	Liq. WW	0.5	98.2	1.3	0	80.2	40	105

	Treated gas	2.0	9.0	0.002	88.9	43.1	47	105
	Flue gas	15.8	4.4	0	79.9	48.0	40	105
	Lean flow	3.7	63.9	32.4	0	86.8	40	105
	Rich flow	11.2	57.2	31.6	0	88.4	43	105
Case 8b	Top abs.	1.8	14.9	0.2	83.0	46.1	55	105
	Liq. WW	0.5	98.2	1.3	0	80.2	40	105
	Treated gas	1.9	9.0	0.002	88.9	43.1	47	105
	Flue gas	15.8	4.4	0	79.9	48.0	40	105
	Lean flow	3.7	63.9	32.4	0	86.8	40	105
	Rich flow	11.3	57.1	31.6	0	88.4	43	105
Case 9b	Top abs.	1.8	14.9	0.2	83.0	46.1	55	105
	Liq. WW	0.5	98.2	1.3	0	80.2	40	105
	Treated gas	1.9	9.1	0.002	89.0	43.0	47	105
	Flue gas	15.8	4.4	0	79.9	48.0	40	105
	Lean flow	5.5	62.4	32.1	0	128.3	40	105
	Rich flow	10.7	58.0	31.4	0	130.7	45	105
Case 10	Top abs.	1.7	14.0	0.21	84.1	45.6	52	105
	Liq. WW	0.5	98.2	1.3	0	80.2	40	105
	Treated gas	1.8	8.4	0.002	89.9	42.7	46	105
	Flue gas	15.8	4.4	0	79.9	48.0	40	105
	Lean flow	5.5	62.5	32.1	0	128.3	40	105
	Rich flow	10.6	58.0	31.4	0	130.8	45	105
Case 11	Top abs.	1.6	13.8	0.21	84.4	45.6	52	105
	Liq. WW	0.5	98.2	1.3	0	80.2	40	105
	Treated gas	1.7	8.4	0.002	89.9	42.7	46	105
	Flue gas	15.8	4.4	0	79.9	48.0	40	105
	Lean flow	5.5	62.5	32.1	0	128.3	40	105
	Rich flow	10.6	58.0	31.4	0	130.8	45	105
Case 12	Top abs.	1.7	13.9	0.20	84.3	45.5	51	105
	Liq. WW	0.5	98.2	1.3	0	80.2	40	105

	Treated gas	1.7	8.3	0.002	90.0	42.63	45	105
	Flue gas	15.8	4.4	0	79.9	48.0	40	105
	Lean flow	5.4	62.5	32.1	0	128.3	40	105
	Rich flow	10.5	58.1	31.4	0	130.8	46	105
Case 13	Top abs.	1.7	13.8	0.20	84.4	45.4	51	105
	Liq. WW	0.5	98.2	1.3	0	80.2	40	105
	Treated gas	1.7	8.2	0.002	90.0	42.6	45	105
	Flue gas	15.8	4.4	0	79.9	48.0	40	105
	Lean flow	3.7	63.9	32.4	0	86.8	40	105
	Rich flow	11.1	57.3	31.6	0	88.6	43	105
Case 10b	Top abs.	2.1	14.6	0.2	83.1	45.9	55	105
	Liq. WW	0.5	98.2	1.3	0	80.2	40	105
	Treated gas	2.3	8.9	0.002	88.8	43.3	47	105
	Flue gas	15.8	4.4	0	79.9	48.0	40	105
	Lean flow	3.7	63.9	32.4	0	86.8	40	105
	Rich flow	11.0	57.3	31.6	0	88.6	43	105
Case 11b	Top abs.	2.2	14.5	0.2	83.0	45.0	55	105
	Liq. WW	0.5	98.2	1.3	0	80.2	40	105
	Treated gas	2.3	8.9	0.002	88.9	43.3	47	105
	Flue gas	15.8	4.4	0	79.9	48.0	40	105
	Lean flow	3.7	63.9	32.4	0	86.8	40	105
	Rich flow	11.0	57.3	31.6	0	88.6	43	105
Case 12b	Top abs.	2.3	14.5	0.2	83.1	45.9	55	105
	Liq. WW	0.5	98.2	1.3	0	80.2	40	105
	Treated gas	2.4	8.8	0.002	88.8	43.3	47	105
	Flue gas	15.8	4.4	0	79.9	48.0	40	105
	Lean flow	3.7	63.9	32.4	0	86.8	40	105
	Rich flow	10.9	57.4	31.6	0	88.6	43	105
Case 13b	Top abs.	2.4	14.4	0.2	83.1	45.9	55	105
	Liq. WW	0.5	98.2	1.3	0	80.2	40	105

	Treated gas	2.5	8.7	0.002	88.8	43.3	47	105
	Flue gas	15.8	4.4	0	79.9	48.0	40	105
	Lean flow	4.4	63.3	32.3	0	114.0	40	105
	Rich flow	10.1	58.4	31.5	0	116.5	46	105
Case 14	Top abs.	1.7	13.9	0.20	84.3	45.5	53	105
	Liq. WW	0.5	98.2	1.3	0	80.2	40	105
	Treated gas	1.8	8.3	0.002	90	42.7	46	105
	Flue gas	15.8	4.4	0	79.9	48.0	40	105
	Lean flow	4.2	63.5	32.3	0	113.9	40	105
	Rich flow	10.0	58.5	31.5	0	116.6	47	105
Case 15	Top abs.	1.7	13.6	0.20	84.6	45.4	53	105
	Liq. WW	0.5	98.2	1.3	0	80.2	40	105
	Treated gas	1.7	8.2	0.002	90.0	42.6	46	105
	Flue gas	15.8	4.4	0	79.9	48.0	40	105
	Lean flow	4.1	63.6	32.3	0	113.7	40	105
	Rich flow	10.0	58.7	31.5	0	116.6	48	105
Case 16	Top abs.	1.7	13.2	0.20	85.0	45.2	52	105
	Liq. WW	0.5	98.2	1.3	0	80.2	40	105
	Treated gas	1.8	7.8	0.002	90.3	42.44	46	105
	Flue gas	15.8	4.4	0	79.9	48.0	40	105
	Lean flow	3.8	63.8	32.4	0	113.5	40	105
	Rich flow	9.5	59.0	31.5	0	116.7	49	105
Case 17	Top abs.	1.7	12.8	0.2	86.4	44.9	51	105
	Liq. WW	0.5	98.2	1.3	0	80.2	40	105
	Treated gas	1.8	7.6	0.002	90.7	42.3	45	105
	Flue gas	15.8	4.4	0	79.9	48.0	40	105
	Lean flow	3.4	64.1	32.5	0	113.3	40	105
	Rich flow	9.2	59.4	31.5	0	116.6	50	105
Case 18	Top abs.	1.7	12.4	0.2	85.8	44.7	50	105
	Liq. WW	0.5	98.2	1.3	0	80.2	40	105

Treated gas	1.8	7.3	0.002	90.9	42.2	44	105

Susanna Sprauten Uhre

Simulation of the MEA Emissions and Energy Consumption in an Absorption-Based Carbon Capture Plant

NTNU
Kunnskap for en bedre verden